博士論文

A Study on Fullerene Derivatives as n-Type Semiconductor Materials for Organic Thin Film Devices

（有機薄膜デバイス用 n 型半導体材料としての
フラーレン誘導体に関する研究）

安部　陽子

Abstracts

I described work on the development of fullerene derivatives as n-type semiconductor materials for organic thin film devices in this thesis.

Morphology control of the interface of the electron donor and acceptor is one of the most crucial parameter to maximize the device performance of organic solar cells. I found that thermal annealing of a p-i-n organic photovoltaic device containing a crystalline benzoporphyrin donor and a newly developed electron accepting fullerene derivative enhanced its performance when the fullerene derivative exhibits an amorphous mesophase at proper temperature. Optimization of the electronic property of materials and the structure of molecular aggregates is also indispensable for high-performance devices. Recent studies on polymer and small-molecule organic solar cells, as well as tandem cells, increase requirement for low-LUMO acceptor materials because the bandgaps of donors become narrower and the HOMO levels of donors are lowered. 56π-electron fullerene derivatives have been focused as high-performance acceptor materials, but it is in large part due to their high-LUMO levels and only a few low-LUMO acceptor materials have been reported. I developed soluble low-LUMO 56π-electron fullerene derivatives bearing cyano groups and 56π-electron hydrofullerene derivatives, for control of the electronic level and the structure of molecular aggregates, respectively. Also I performed high throughput preparation of dihydromethano[60]fullerene $C_{61}H_2$, which is an important starting material for synthesis of 56π-electron fullerene derivatives, without the chromatographic process. Finally I discovered that a process of the formation of the stable fullerene radicals which

act as dopant for the fullerene solid in thin film, resulted in enhancement the electron mobility of organic FET.

Contents

Chapter 1 General Introduction

1.1 Introduction - 1-
1.2 Organic Thin Film Solar Cells - 3-
1.3 Organic FETs - 9-
1.4 Purpose of Study -11-
1.5 References and Notes -11-

Chapter 2 An Amorphous Mesophase Generated by Thermal Annealing for High-Performance Organic Photovoltaic Devices

2.1 Introduction -14-
2.2 Synthesis of SIMEF-Ph, An -16-
2.3 Thermal Properties of SIMEF-Ph, An -17-
2.4 SCLC Measurements of SIMEF-Ph, An -20-
2.5 OPV Device Performances of SIMEF-Ph, An -22-
2.6 Conclusion -26-
2.7 Experimental Section -27-
2.8 References and Notes -51-

Chapter 3 1,8-Diazabibicycloundecene-mediated Separation of Singly bonded Fullerene Dimer and Application to Facile Preparation of $C_{61}H_2$

3.1 Introduction -55-
3.2 Separation of Singly Bonded Dimer from the Mixture with C_{60} -57-
3.3 Synthesis of $C_{61}H_2$ from the Singly Bonded Dimer-DBU Complex -61-
3.4 Conclusion -63-
3.5 Experimental Section -63-
3.6 References and Notes -65-

Chapter 4 Low-LUMO 56π-Electron Fullerene Acceptors Bearing Electron-withdrawing Cyano Groups for Small-Molecule Organic Solar Cells

4.1 Introduction -66-
4.2 Synthesis of 56π-Electron Low-LUMO Fullerenes -68-
4.3 Electrochemical Properties of 56π-Electron Low-LUMO Fullerenes -70-

4.4 OPV Device Performances of 56π-Electron Low-LUMO Fullerenes -73-
4.5 Conclusion -76-
4.6 Experimental Section -77-
4.7 References and Notes -82-

Chapter 5 56π-Electron Hydrofullerene Derivatives as Electron Acceptors for Organic Solar Cells
5.1 Introduction -85-
5.2 Synthesis of 56π-Electron Hydrofullerene Derivatives -87-
5.3 Electrochemical Properties of 56π-Electron Hydrofullerene Derivative -89-
5.4 OPV Device Performances of 56π-Electron Hydrofullerene Derivative -90-
5.5 Conclusion -93-
5.6 Experimental Section -93-
5.7 References and Notes -98-

Chapter 6 Mobility of Long-lived Fullerene Radical in Solid State and Nonlinear Temperature Dependence
6.1 Introduction -101-
6.2 Synthesis and Electrochemical Property of the Singly Bonded Fullerene Dimer -102-
6.3 Crystal Structure of the Singly Bonded Fullerene Dimer -104-
6.4 ESR Study of the Singly Bonded Fullerene Dimer -106-
6.5 FET Device Performances of the Singly Bonded Fullerene Dimer -109-
6.6 Conclusion -111-
6.7 Experimental Section -112-
6.8 References and Notes -122-

Chapter 7 Conclusion -124-

List of publications -127-

Chapter 1

General Introduction

1.1 Introduction

The remarkable development of electronics in the 20th century has been supported by devices made from inorganic materials such as silicon and compound semiconductors. In the 21st century, an important issue is how electronics can be used more naturally and efficiently. For example, wearable electronics and rollable displays for portable electronics could provide a means toward these ends. Making such electronics a reality, however, will require an approach completely different from the conventional approaches.

Manufacturing large-area devices using inorganic materials is currently difficult and expensive because complicated processing steps and large-scale vacuum devices are used. In addition, most inorganic devices are made from a very hard silicon crystal, which does not allow for flexibility. In contrast, many organic materials can be used to produce electronic circuits through a simple process, such as ink printing in air, because organic materials can be dissolved in organic solvents to make the ink. In addition, organic materials can be used to form high-quality thin films, even on heat-sensitive plastic substrates. Organic materials are light and soft, and are better suited for materials worn on the human body. Even though organic materials had traditionally been considered poor electrical conductors, the discovery of organic conductors such as conductive polymers and acenes opened up new possibilities.

Buckminsterfullerene (C_{60}, [60]fullerene) (Figure 1) is a promising candidate

for use in organic electronics and has been extensively studied in the past few decades. The possibility of its existence had been suggested by Eiji Osawa of Toyohashi University of Technology in 1970,[1] and then found by Richard Smalley, Robert Curl, James Heath, Sean O'Brien, and Harold Kroto at Rice University in 1985.[2] The soccer-ball shape (I_h-symmetry) of [60]fullerene—with 60 vertices, 12 pentagonal faces, 20 hexagonal faces, and a spherically distorted π-conjugated system—gives the molecule unique properties such as high electron affinity, small reorganization energy, and good charge transport ability.[3] Despite the many interesting features of fullerene, its industrial application has been hindered by low solubility in organic solvents. Recently, various addition reactions to fullerene have been developed for preparing fullerene derivatives that are soluble in organic solvents and applicable to organic thin film devices.

This thesis is focused on the development of fullerene derivatives suitable for application in organic thin film devices such as organic solar cells and organic field-effect transistors (FETs). This chapter presents a brief review of these two types of organic devices, with emphasis on the progress of organic semiconductors.

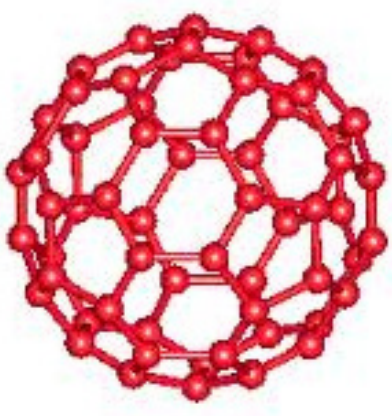

Figure 1. Structure of [60]fullerene

1.2 Organic Thin Film Solar Cells

In recent years, environmental and energy problems have worsened on a global scale. Organic thin film solar cells have been garnered widespread attention as a new energy source. Such cells can be made flexible and portable because of their sheet-like form and light weight, and they are expected to be used in next-generation solar cells (Figure 2).[4] Further, the cells can be fabricated by a coating process, which reduces the manufacturing cost to approximately one-third that of today's mainstream silicon solar cells. In 1986, a prototype of an organic thin film solar cell was reported by C.W. Tang of Eastman Kodak Company.[5] A pn-heterojunction with an organic electron donor (organic p-type semiconductor) and an organic electron acceptor (organic n-type semiconductor) was first created using copper phthalocyanine (CuPc) as donor and 3,4,9,10-perylenetetracarboxylic bis(benzimidazole) (PTCBI) as acceptor (Figures 3 and 4). The power conversion efficiency (PCE) of the pn-heterojunction cell reached 1%; this value is markedly higher than that of Schottky-type organic thin film solar cells, which use only a single layer of organic semiconductor.[6] At that time, [60]fullerene was unavailable, because it had been discovered just a year before and had not yet been isolated.[2] In 1991, Hiramoto et al. reported a pin-junction device having a donor-acceptor mixture layer (i-layer) between the donor layer (p-layer) and the acceptor layer (n-layer); the i-layer was prepared by co-deposition of the donor and acceptor materials. A bulk heterojunction layer was formed by mixing the electron donor and electron acceptor throughout a single layer (Figure 3), but the PCE remained around 1%.[7] That work provided the first glimpse of the utility of the bulk heterojunction in organic thin film solar cells. In 1992, shortly after the isolation and synthesis of fullerenes has become possible,[8] Sariciftci et al. reported ultrafast charge

transfer to C_{60} from 2-methoxy-5-(2-ethylhexyloxy)polyphenylenevinylene (MEH-PPV) (Figure 4), an electron-donating conductive polymer.[9] However, the PCE of organic thin film solar cells did not progress beyond 1% because fullerenes had a problem, namely, poor solubility in organic solvents.

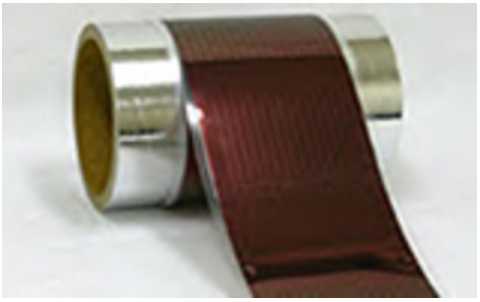

Figure 2. An organic thin film solar cell

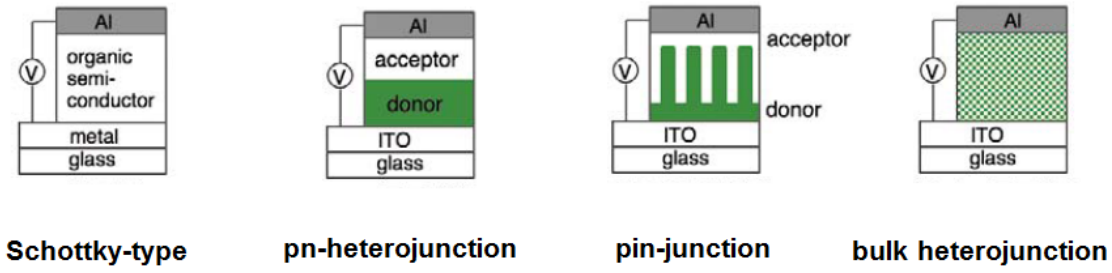

Figure 3. Various structures of organic thin film solar cells

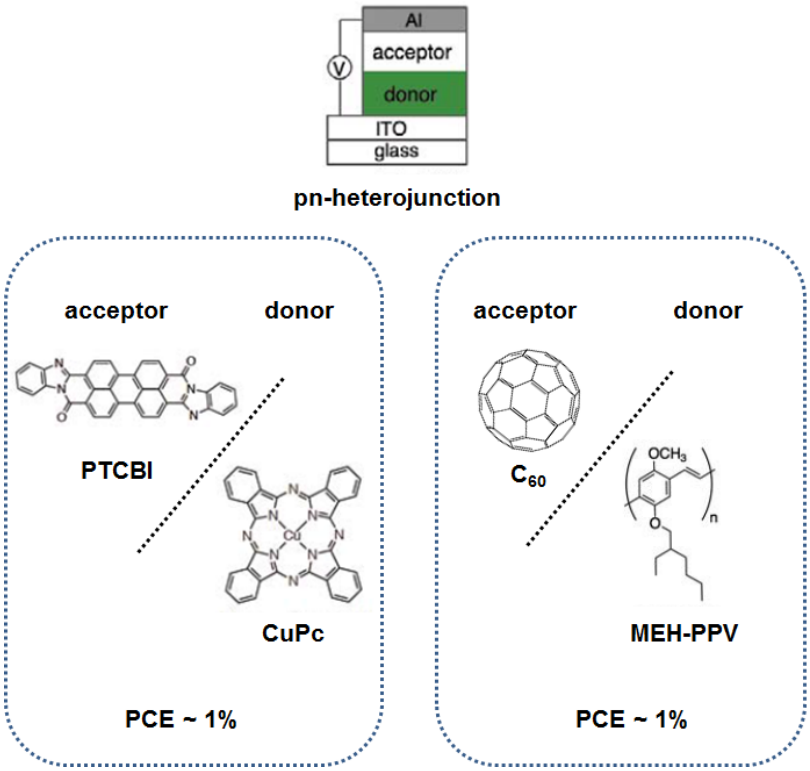

Figure 4. Typical donor and acceptor materials for pn-heterojunction organic thin film solar cells and PCE values

In 1995, Heeger et al. reported the use of bulk heterojunction layer formed with a soluble fullerene derivatives and a conductive polymer.[10] In the same year, Hummelen et al. developed a soluble fullerene, phenyl-C61-butyric acid methyl ester (PCBM),[11] and blended MEH-PPV and PCBM in a 1:4 ratio. At this optimized ratio, PCE of 1.5% was achieved (Figure 5).

Around this time, polythiophene came to be used instead of PPV in the electron donor. In 2002, Brabec et al. reported that a combination of PCBM and poly-3-hexyl thiophene (P3HT) (Figure 5) gave PCE of 2.8%.[12] Intensive research conducted around the world revealed that device performance depends strongly on post-deposition processing of the device[13-15] and on the regioselectivity of polythiophene.[16] Giving

PCE near 5%, the combination of P3HT and PCBM became the standard material for organic solar cells.

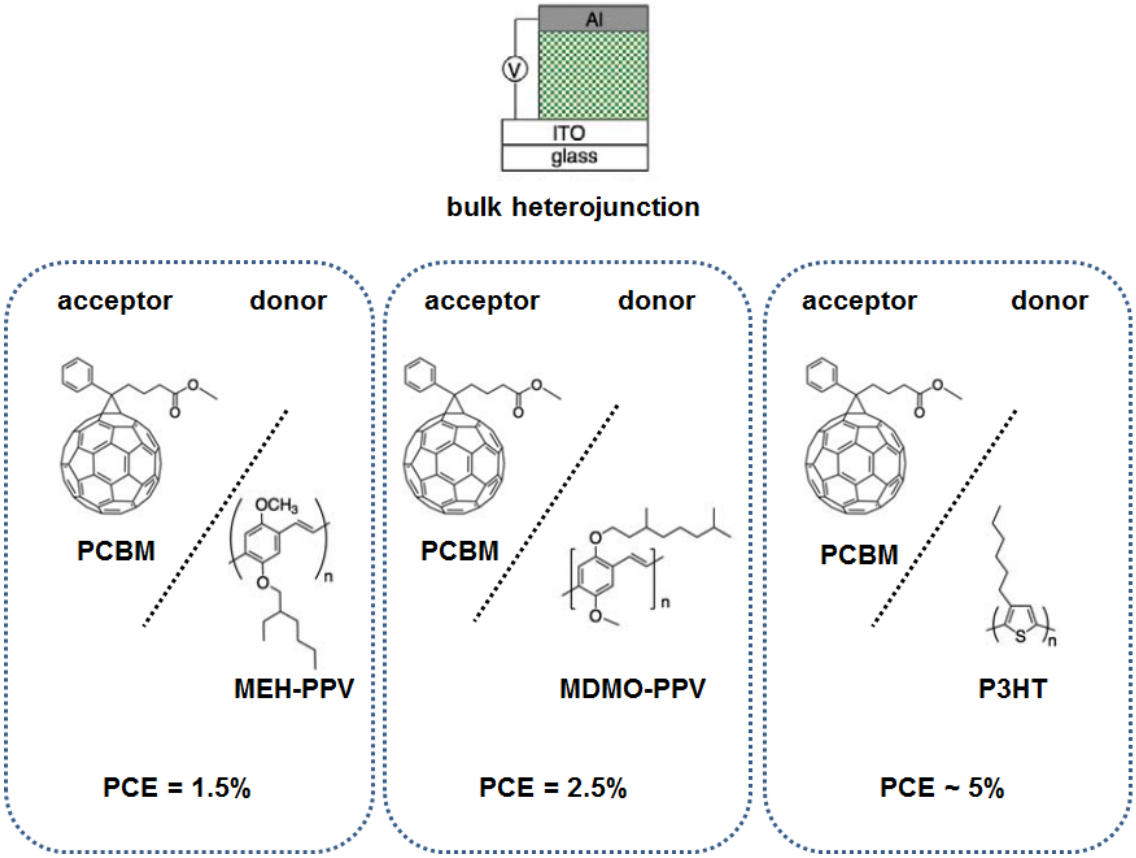

Figure 5. Typical donor and acceptor materials for the bulk heterojunction organic thin film solar cell and the PCE values

After 2006, the PCE has further improved with the development of new materials. Low-bandgap polymers have been developed, which have both electron-donating and electron-accepting sites in their main chain (Figure 6).[17-19] They exhibit long-wavelength absorption due to charge transfer within the molecule. In addition, indene-C_{60} bisadduct (ICBA) with further reduced 56π-electron conjugated system has been developed (Figure 6).[20-23] Compared with PCBM, ICBA has a higher

LUMO level and tends to give a higher open-circuit voltage. Through these efforts, PCE has now surpassed 10%. This value is comparable to the conversion efficiency of amorphous silicon solar cells, but falls just short of the conversion efficiency of polycrystalline or single-crystalline silicon solar cells.

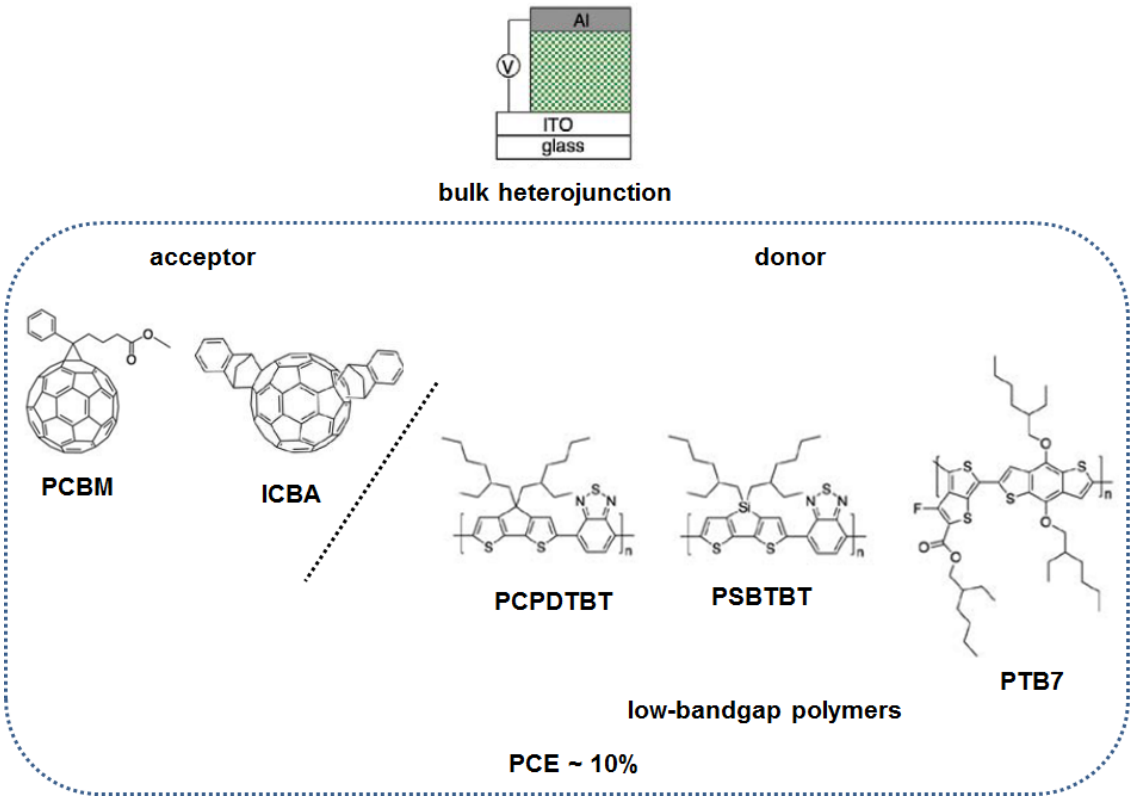

Figure 6. Typical donor and acceptor materials for high-performance bulk heterojunction organic thin film solar cells and PCE value

The photoconversion mechanism of organic solar cells can be explained by the energy diagram shown in Figure 7. In organic thin film solar cells, the films are typically deposited on a transparent conductive electrode, usually composed of indium tin oxide (ITO). Active layers consist of an electron-rich organic semiconductor (i.e., the electron donor) that absorbs light and generates electron-hole pairs (excitons) and an

electron-deficient organic material (i.e., the electron acceptor) that separates and transports the generated charges. In the charge-separated state, there is a vacancy (hole) in the HOMO of the electron donor and an electron in the LUMO of the electron acceptor. The donor is a radical cation, and the acceptor is a radical anion. The open-circuit voltage of the organic thin film solar cells tends to improve as the energy gap widens between the LUMO of the electron acceptor and the HOMO of the electron donor. In contrast, efficient charge separation hardly occurs when the LUMO level of the electron acceptor and the LUMO level of the electron donor are too close. The preferable size of the energy gap of both LUMO level is about 0.2 to 0.3 eV. On the one hand, the hole in the HOMO of the donor flows toward ITO, moving upward in the energy diagram without encountering any barrier. On the other hand, the electron in the LUMO of the acceptor flows toward the aluminum electrode. In other words, upon excitation by sunlight, the electron moves inside the device from the ITO electrode (which has a large work function) to the aluminum electrode (which has a small work function). As a result, an electric current is produced.

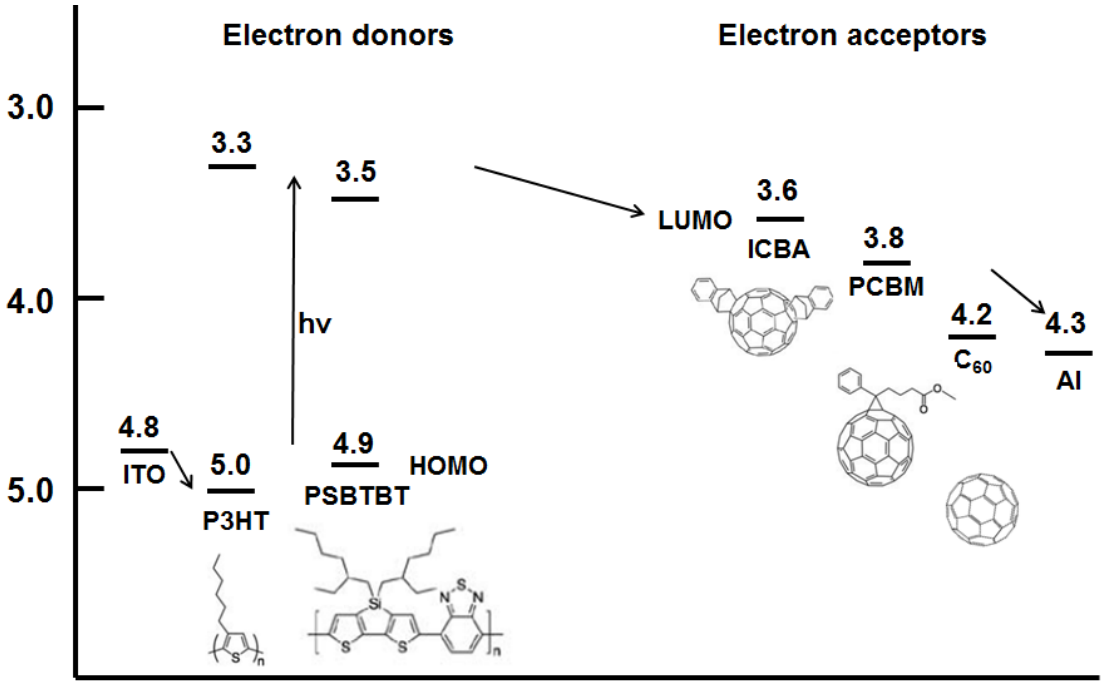

Figure 7. Energy diagram of the organic thin film solar cells

There is still a lot of room to improve the PCE of organic solar cells through the development of materials. Compared with organic donor materials, organic acceptor materials are available in much less variety, making it difficult to properly match the donor and acceptor in terms of solubility and energy levels. One effective strategy might be to develop a fullerene derivative that suitably matches with the donor material.

1.3 Organic FETs

An organic transistor is a current switching device with an organic semiconductor material. In recent years, applications of organic FETs has been actively investigated worldwide because their performance has been dramatically improved and their carrier mobility exceeds that of amorphous silicon FETs. The study of organic transistor dates back to the 1950s, and the semiconducting character of organic

materials under an applied voltage is known.[24] Yet organic materials have traditional been thought of as insulators, since the stability and resistance of organic films are very different from those of typical inorganic semiconductors. However, organic transistors became the object of intense study in the early 1980s with the development of organic solar cells. The year 1983 saw the first report of an organic FET, which used polyacetylene in the active layer.[25] In 1984, Kudo et al. reported an organic FET using merocyanine dye and achieved carrier mobility of about 10^{-5} to 10^{-7} $cm^2V^{-1}s^{-1}$.[26] After considerable efforts at material development, the carrier mobility of an organic FET using pentacene (Figure 8) surpassed 1 $cm^2V^{-1}s^{-1}$.[27] Furthermore, carrier mobility has been approaching 50 $cm^2V^{-1}s^{-1}$ with the use of single-crystalline rubrene (Figure 8).[28] Organic FETs now have sufficient performance that can be put to practical use.

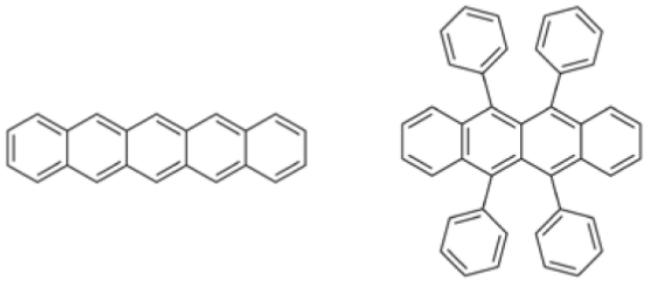

Figure 8. Typical p-type organic materials for organic thin film FETs

It is worth noting that the characteristics of an organic FET (p-channel or n-channel) are determined by the characteristics of the materials that constitute the active layer. Compared with of p-type organic semiconductor materials, n-type organic semiconductor materials for use in FETs are not available in sufficient variety.

1.4 Purpose of Study

Organic thin film devices are very promising in terms of flexibility and manufacturing cost, but still have problems in terms of durability and conversion efficiency in comparison with conventional inorganic devices. To improve their performances, the optimization of both the electronic property of materials and the structure of molecular aggregates play a crucial role. For organic solar cells, not only the structure of each of material in the device, but morphology control of the interface of the electron donor and the electron acceptor is center of the discussion. Accordingly, in the research presented in this thesis, I investigated organic solar cells using various fullerene derivatives that are sufficiently soluble in common organic solvents and I examined the effects of the physical properties and morphology of electron acceptor materials on device characteristics. First I focused on the control of the interfacial morphology of a donor-acceptor mixture layer with 58π-electron fullerene derivatives, and then, explored the possibility of control of the electronic property and the molecular morphology of 56π-electron fullerene derivatives, which are becoming standard acceptor materials for high-performance organic solar cells, with introduction of appropriate substituents on fullerene core. Also, I developed an organic FET using a fullerene dimer, which is a minimum unit of fullerene polymers, as the n-type organic semiconductor. Through this work, relatively high electron mobility was obtained and a unique function was observed that is not found in conventional acceptor materials.

1.5 References and Notes

(1) E. Osawa, *Kagaku* **1970**, *25*, 854.

(2) H. W. Kroto, J. R. Heath, S. C. O'Brien, R. F. Curl, R. E. Smalley, *Nature* **1985**, *318*,162.

(3) A. Hirsch, M. Brettreich, *Fullerenes*, *Wiley-VCH*, *Weinheim* **2008**, 1–48.

(4) http://www.mitsubishichem-hd.co.jp/csr/kaiteki/index.html

(5) C. W. Tang, *Appl. Phys. Lett*. **1986**, *48*, 183.

(6) D. Kearns, M. Calvin, *J. Chem. Phys*. **1958**, *29*, 950.

(7) M. Hiramoto, H. Fujiwara, M. Yokoyama, *Appl. Phys. Lett*. **1991**, *58*, 1062.

(8) W. Kretschmer, L. Lamb, K. Fostiropoulos, D. Huffman, *Nature* **1990**, *347*, 354.

(9) N. S. Sariciftci, L. Smilowitz, A. J. Heeger, F. Wudl, *Science* **1992**, *285*, 1474.

(10) G. Yu, J. Gao, J, C. Hummelen, F. Wudl, A. J. Heeger, *Science* **1995***, 270*, 1789.

(11) J. C. Hummelen, B. W. Knight, F. LePeq, F. Wudl, J. Yao, C. L. Wilkins, *J. Org. Chem.* **1995***, 60*,532.

(12) P. Schilinsky, C. Waldauf, C. J. Brabec, *Appl. Phys. Lett.* **2002***, 81*, 3885.

(13) F. Padinger, F. R. S. Rittberger, N. S. Sariciftci, *Adv. Funct. Mater.* **2003***, 13,* 85.

(14) G. Li, V. Shrotriya, J. Huang, Y. Yao, T. Moriarty, K. Emery, Y. Yang, *Nat. Mater.* **2005***, 4*, 864.

(15) M. Reyes-Reyes, K. Kim, D. L. Carroll, *Appl. Phys. Lett.* **2005***, 87*, 83506.

(16) Y. Kim, S. Cook, S. M. Tuladhar, S. A. Choulis, J. Nelson, J. R. Durrant, D. D. C. Bradley, M.Giles, I. McCulloch, C.-S. Ha, M. Ree, *Nat. Mater.* **2006***, 5*, 197.

(17) D. Mulbacher, M. Scharber, M. Morana, Z. Zhu, D. Waller, R. Gaudiana, C. Brabec, *Adv.Mater.* **2006***, 18*, 2884.

(18) J. Peet, J. Y. Kim, N. E. Coates, W. L. Ma, D. Moses, A. J. Heeger, G. C. Bazan, *Nat. Mater.* **2007***, 6*,497.

(19) J. Hou, H.-Y. Chen, S. Zhang, G. Li, Y. Yang, *J. Am. Chem. Soc.* **2008***, 130*, 16144.

(20) Y. He, H.-Y. Chen, J. Hou, Y. Li, *J. Am. Chem. Soc.* **2010***, 132*, 1377.

(21) Y. He, G. Zhao, B. Peng, Y. Li, *Adv. Funct. Mater.* **2010***, 20*, 3383.

(22) G. Zhao, Y. He, Y. Li, *Adv. Mater.* **2010***, 22*, 4355.

(23) Y.-J. Cheng, C.-H. Hsieh, Y. He, C.-S. Hsu, Y. Li, *J. Am. Chem. Soc.* **2010***, 132*, 17381.

(24) H. Akamatsu, H. Inokuchi, Y. Matsunaga, *Nature*, **1954**, *173*,168

(25) F. Ebisawa, T. Kurokawa, S. Nara, *J. Appl. Phys.* **1983**, *54*, 3255.

(26) K. Kudo, M. Yamashina, T. Moriizumi, *Jpn. J. Appl. Phys*. **1984**, *23*, 130.

(27) T. W. Kelley, L. D. Boardman, T. D. Dunbar, D. V. Muyres, M. J. Pellerite, T. P. Smith, *J. Phys.Chem*. *B*, **2003**, *107*, 5877.

(28) J. Takeya, M. Yamagishi, Y. Tominari, R. Hirahara, Y. Nakazawa, T. Nishikawa, T. Kawase, T. Shimoda, S. Ogawa, *Appl. Phys. Lett*. **2007**, *90*, 102120.

Chapter 2

An Amorphous Mesophase Generated by Thermal Annealing for High-Performance Organic Photovoltaic Devices[†]

2.1 Introduction

Printable thin-film organic photovoltaic devices (OPV) using organofullerene acceptors are attracting tremendous attention with regard to energy and chemical resources issues,[1,2] and also because of a record performance of 10% power conversion efficiency (PCE) reported recently by Mitsubishi Chemical.[3,4] Device fabrication often calls for an annealing process, in which the device is exposed to heat or solvent vapor during fabrication to improve its performance.[5,6] Possible origins of the beneficial effects of thermal and solvent annealing are the removal and introduction of solvent in the active layer, respectively.[7-19] However, the molecular understanding of such effects remains unclear, because the active layer of OPV devices are generally ill-defined to carry out detailed studies. We have considered that a p-i-n device (Figure 1),[20–22] by using benzoporphyrin donor (BP; green)[22–24] and silylmethyl[60]fullerene acceptor (SIMEF; blue), is suitable for molecular-level studies of annealing, because the highly insoluble and thermally stable BP is entirely phase-separated from the fullerene layer.[22] For this study, I developed new fullerene derivatives, (*o*-anisylsilylmethyl)(phenylsilylmethyl)[60]fullerene (**2**, SIMEF-Ph, *o*-An)) and its congeners **3** and **4** (SIMEF-Ph, *m*- and *p*-An), and studied their crystal structures,

thermotropic properties and photovoltaic performance. I found that heat-driven desolvation of the active layer containing co-crystals of **2** creates a new amorphous mesophase that maximizes the short circuit current density (J_{SC}) values as well as the overall device performance. Heating of benzene-containing devices, on the other hand, resulted in a molten phase of **2** and lowing of the fill factor (FF). The active layer made of pristine crystals of **2–4** was found to be inferior. This counterintuitive result suggests that the amorphous mesophase of the fullerene can maximize the BP/fullerene interfacial contact and hence the charge carrier generation that appears to be the performance-limiting factor of our p-i-n device, and the molten phase destroys the fullerene/buffer interface and increases the shunt resistance (R_{sh}).

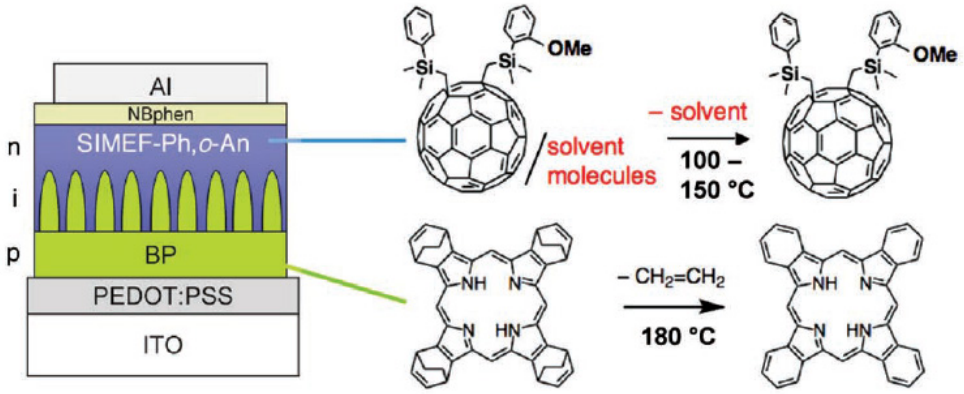

Figure 1. Schematic illustration of solution-processable small-molecule-based p-i-n OPV devices containing SIMEF-Ph, *o*-An (**2**) and BP, and the desolvation process of the fullerene upon heating at 10-150 °C. The thickness of the p-i-n active layer is approximately 140nm and the size of each BP column (green in the i layer) is approximately 25nm in diameter and 80nm in height.

2.2 Synthesis of SIMEF-Ph, An

To study the effects of heat-induced desolvation of the active layer, I screened our fullerene derivatives[25] to find that the new SIMEF compound **2** is a suitable substrate because of its ability to co-crystallize with a wide variety of aromatic solvents. On the other hand, the *m*- and *p*-An isomers **3** and **4** form only solvent-free crystals. These molecules were synthesized as reported for a simpler analog (Scheme 1).[26] A mono-silylmethylfullerene **1** was obtained in 86% isolated yield by the reaction of [60]fullerene in 1,2-dichlorobenzene with 3 equiv of a dimethylphenylsilylmethyl Grignard reagent in the presence of 30 equiv of N,N-dimethylformamide (DMF). The second silylmethyl bearing an *o*-, *m*-, or *p*-methoxy group was then introduced by treatment of **1** with t-BuOK and an appropriate halide. The reactions were regioselective, giving the desired 1,4-di(organo)[60]fullerenes without any regioisomers.

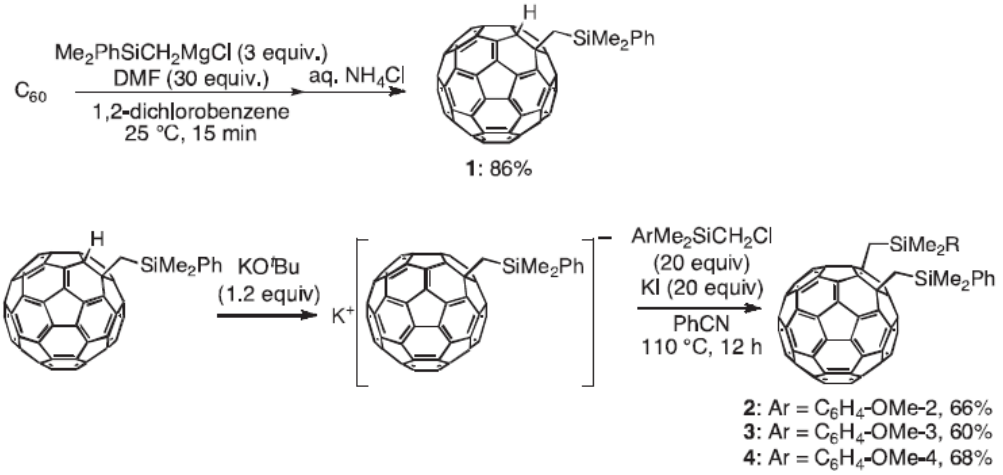

Scheme 1. Synthesis of SIMEF-Ph, An **2**-**4** via **1**

2.3 Thermal Properties of SIMEF-Ph, An

I found that **2** co-crystallizes with a variety of solvents such as toluene, chlorobenzene, and benzene as well as pyridine and CS_2 (unsuitable for device fabrication and hence not studied further) (Figure 2). Single-crystal X-ray structures (see the Experimental Section) were determined for **2**•toluene and **2**•chlorobenzene, and were used as reference standards for the analysis of variable-temperature X-ray diffraction (VT-XRD) data.

I evaluated the thermal properties of co-crystalline of **2**•solvent by differential scanning calorimetry (DSC) and VT-XRD (Figure 2). The pristine crystals of **2**, **3** and **4** show simple thermal behavior. The crystals of **2** melt at 225 °C and decompose at 365 °C. Those of **3** and **4** are amorphous at room temperature, and crystallize at 108 °C and 140 °C, respectively (Figure 2d; see also the Experimental Section). On the other hand, co-crystals of **2**•toluene lose solvent at 111±14 °C with a large endothermicy (42.3 J g^{-1} endothermic). This temperature is the same as the boiling point of toluene (111 °C), indicating that the solvent molecules are very loosely bound in the crystal lattice. During the desolvation, they form an amorphous mesophase that show no defined XRD peaks (at 130 °C in Figure 2a), form solvent-free crystals at 153 °C and go to an isotropic phase at 224 °C with the endothermic as large as 30.0 J g^{-1}. Crystals of **2**• chlorobenzene lose solvent at 102±12 °C (30.2 J g^{-1} endothermic). This temperature is 29 °C lower than the boiling point of CB (131 °C), suggesting that the desolvation relaxes the crystal lattice. During the desolvation, they also form an amorphous mesophase (at 110 °C in Figure 2b), immediately form solvent-free crystals at 127 °C and go to an isotropic phase at 223 °C with the endothermic loss of 30.0 J g^{-1}. The

crystals of **2**•benzene lose solvent at 131±14 °C with very large endothermicity of 44.4 J g^{-1}, suggesting a large structural change. This temperature is 51 °C higher than the boiling point of benzene (80 °C). The desolvation, results in liquidification to create a liquid containing crystals (as observed by optical microscope; see the Experimental Section), which goes to a homogeneous isotropic phase at 220 °C with the very small endothermic of 0.5 J g^{-1}. I surmise that the benzene molecules are tightly bound in the crystal lattice and that, once lost, the lattice is entirely destroyed and recrystallization is difficult. Thus, the endothermicity of the desolvation, and the difference between the boiling point of the included solvent and the desolvation temperature exhibit a good correlation to the phase behavior, and also to the annealing temperature dependence of the OPV device performance (vide infra).

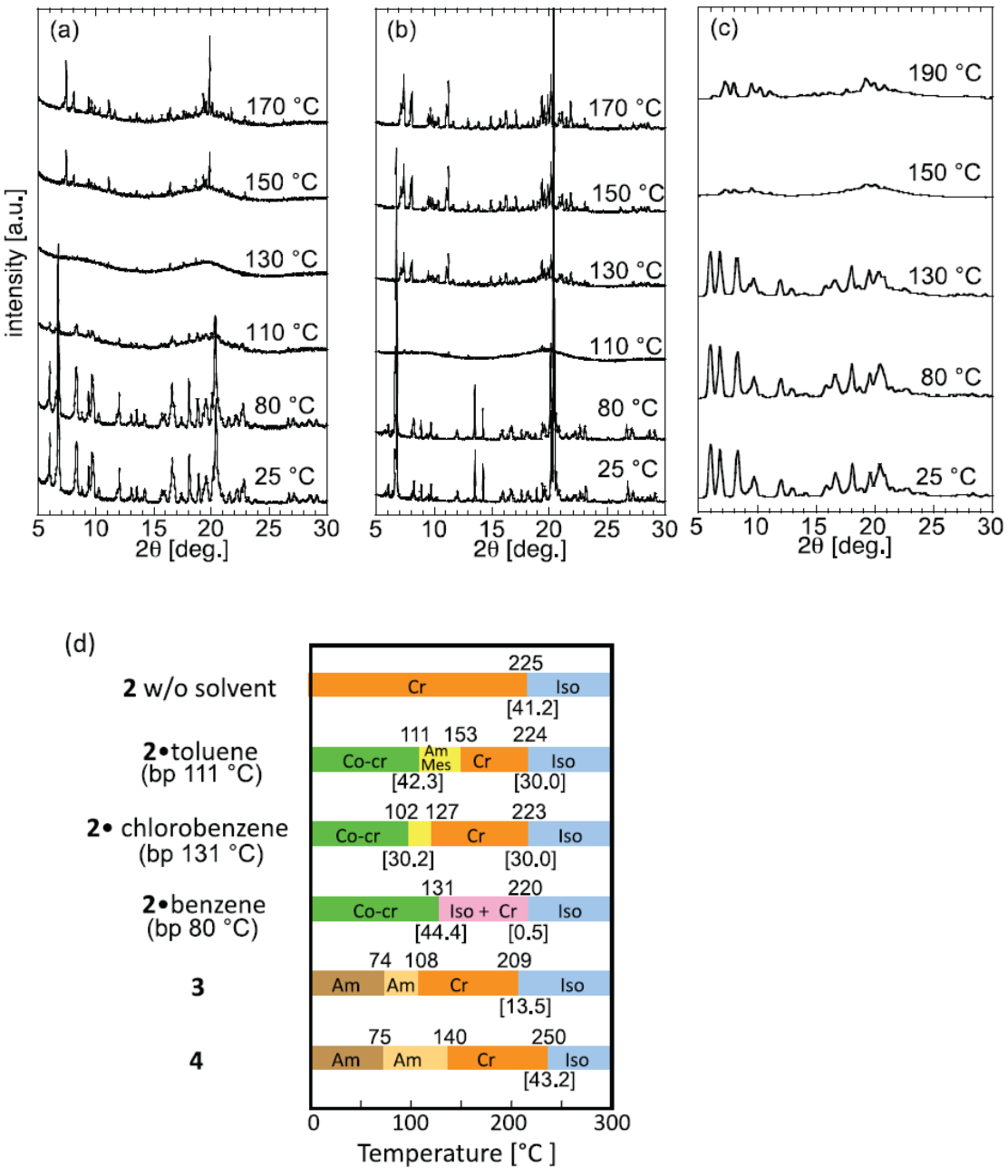

Figure 2. VT-XRD patterns of **2**•toluene (a), **2**•chlorobenzene (b), and **2**•benzene (c) at 25–190 °C. All samples were prepared by drop-casting of **2** in the respective solvent on glass. The XRD of **2**• toluene (a) and **2**•chlorobenzene (b) were obtained from the

sample mounted on the sample holder, and the XRD of **2**•benzene (c) was obtained from capillary powder sample because of difficulties in measuring of molten phase. d) Thermal properties of **2** – **4**, and solvent co-crystals of **2**. The boiling point of each solvent is denoted as bp. Co-cr = co-crystalline phase, Am Mes = amorphous mesophase, Cr = crystalline phase, Iso = isotropic phase. The endothermicity data for each phase change is shown in brackets (J g^{-1}).

2.4 SCLC Measurements of SIMEF-Ph, An

I next measured the dark current density of thin films of **2**•solvent in electron-only devices (glass/Al/**2**•solvent/LiF/Al) for different annealing temperatures, which is limited by space charge, and electric field-dependence of the electron mobility ($\mu_e = \mu_{e0}e^{\gamma\sqrt{E}}$, where E is electric field, μ_{e0} the zero-field electron mobility, and γ the electric-field coefficient), and can be estimated by the advanced equation of space charge limited current.[27-31] The μ_{e0} of **2** formed by toluene, chlorobenzene, and benzene showed an expected temperature dependence; that is, high μ_{e0} in a crystalline phase and low μ_{e0} in an amorphous mesophase (Figure 3).

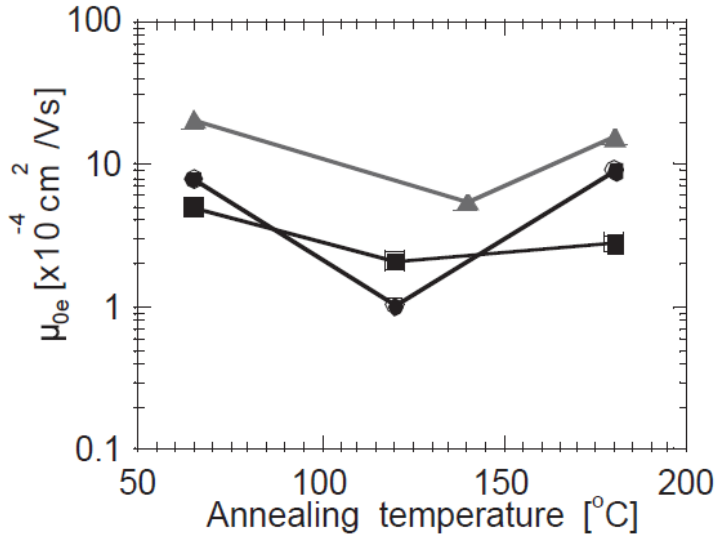

Figure 3. Zero-field electron mobilities of **2**•solvent co-crystals as a function of pre-annealing temperature before complete fabrication of devices. Active layer of **2**•solvent formed by drop-casting from toluene (circles), chlorobenzene (squares), and benzene (triangles) solutions. The mobilities were calculated from the SCLC current measured using the electron-only device configuration (glass/Al/**2**•solvent/LiF/Al).

The thin films of **2**•solvent were formed by drop-casting from toluene, chlorobenzene, and benzene solutions ot the aluminium-deposited glass substrate, and were thermally annealed at the phase change temperature of co-crystal before deposition of LiF/Al top electrode. The thin film of **2**•toluene annealed at 65 °C showed a μ_{e0}7.8 × 10^{-4} $cm^2V^{-1}s^{-1}$, which decreased to 1.0 × 10^{-4} $cm^2V^{-1}s^{-1}$ for 120 °C-annealed film, and increased to 9.1 × 10^{-4} $cm^2V^{-1}s^{-1}$ for 180 °C-annealed film. Similarly, the μ_{e0} of **2** drop-cast from a chlorobenzene solution (5.0 × 10^{-4} $cm^2V^{-1}s^{-1}$ for 65 °C-annealed) decreased for 120 °C-annealed film, and increased for 180 °C-annealed film. The thin film of **2**

obtained by drop-casting from a benzene solution showed the highest μ_{e0} of 2.1×10^{-3} $cm^2V^{-1}s^{-1}$ for 65 °C-annealed film, which decreased for 140 °C-annealed film, and slightly increased for 180 °C- annealed film. I may consider that the highest mobility of the benzene-based device is relevant to the highest stability of the **2**•benzene co-crystals described above.

2.5 OPV Device Performances of SIMEF-Ph, An

The performance of the p-i-n photovoltaic devices fabricated by using toluene, chlorobenzene, and benzene solutions of **2** showed a marked dependence on the annealing temperature (Figure 4), but in a sense entirely opposite from the mobility data. Thus, I made three observations. For the devices made with toluene and chlorobenzene as a processing solvent, I found marked increases of both PCE and J_{SC} only when the fullerene is in its amorphous state; that is, upon medium-temperature annealing of the devices (Figure 4a, b). For the devices processed with benzene, I found the decrease of PCE and FF upon high-temperature annealing of the devices (Figure 4c). For all devices, I found that the open-circuit voltage (V_{OC}) is insensitive to the annealing temperature (Figure 4d).

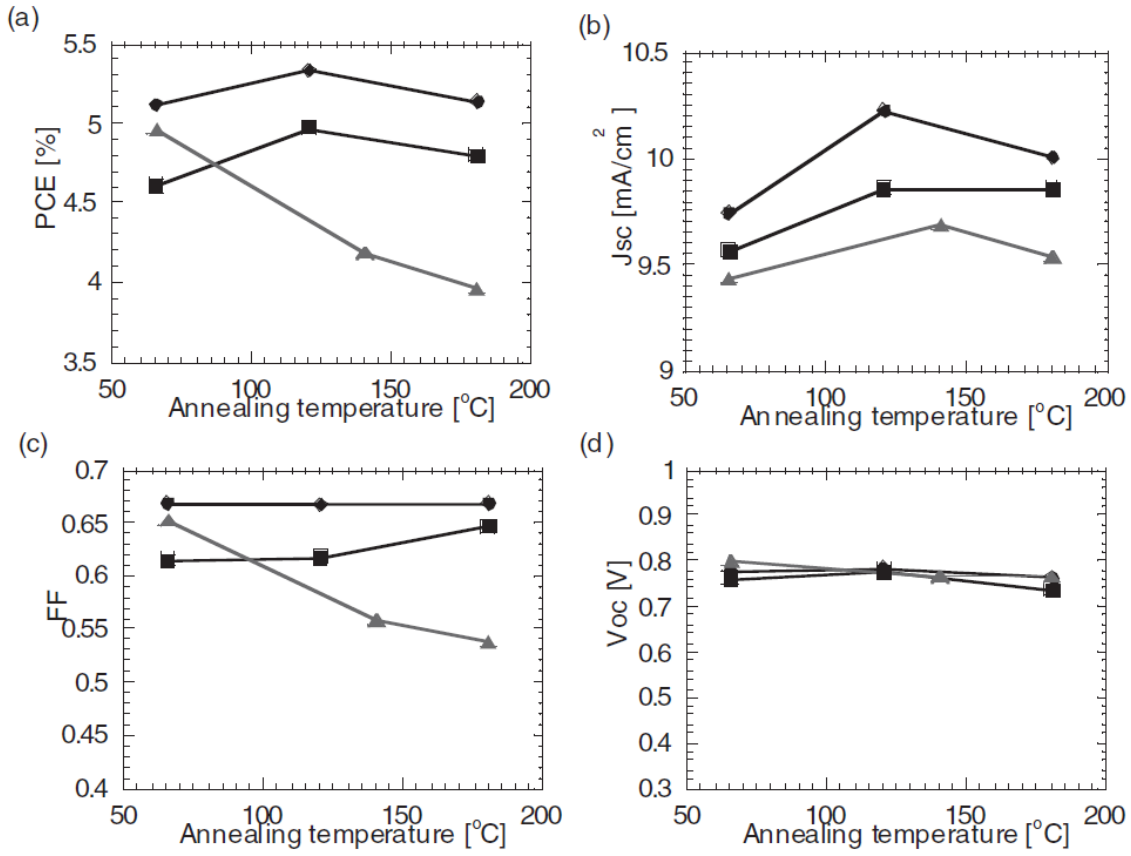

Figure 4. Photovoltaic performances of p-i-n OPV devices (device A-C) using **2**·toluene (circles), and **2**·chlorobenzene (squares), and **2**·benzene (triangles) as an n-layer: a) Power conversion efficiency, b) short-circuit current density, c) fill factor(FF), and, d) open-circuit voltage as a function of pre-annealing temperature.

I used a device configuration of glass/ITO/PEDOT:PSS/BP/BP:**2**/**2**•solvent/2,9-bis(naphthalene-2-yl)-4,7-diphenyl-1,10-phenanthoroline (NBphen; as cathode buffer layer)/Al as I previously reported.[(22)] To study solvent effects, I first fabricated the p-i structure, and coated a 25–30 nm of **2** as an n-layer that was dissolved in toluene, chlorobenzene, and benzene (devices are

denoted as device A, B and C, respectively). Note that this procedure warrants the deposition of **2** containing three different solvents (blue in Figure 1) on the same BP columnar structure standing on the BP p-layer (green in Figure 1). To induce desolvation and a morphology change of the fullerene containing film, I heated the device approximately at the phase-change temperature of the **2**•solvent co-crystals (Figure 2d) before deposition of NBphen and Al layers. The data were compared with those for devices annealed at 65 and 180 °C.

The PCE value of device A (5.1% for device annealed at 65 °C) increased to 5.4% at 120 °C (111 °C-153 °C causes amorphasization; Figure 2d). This improvement is due to the significant increase of J_{SC}, while V_{OC} and FF remained unchanged (Figure 4b-d). The PCE dropped to 5.1 % at 180 °C mainly due to the decrease of J_{SC}. The PCE and J_{SC} values of device B (4.6% at 65 °C) also increased to 5.0% at 120 °C (107 °C-127 °C causes amorphasization), then dropped to 4.7% at 180°C. The FF of device B gradually increased from 0.61 (65 °C) to 0.64 (120 °C) and 0.65 (180 °C). The device made with benzene was exceptional, the PCE of device C (4.9% at 65 °C) dropped largely to 4.2% at 140 °C, and 4.0% at 180 °C (131 °C-220 °C causes liquidification). This PCE drop is due to the marked decrease of FF, while J_{SC} slightly increased and V_{OC} remained unchanged.

Improvement of the J_{SC} value of devices A and B at the amorphousization temperature is unexpected and remarkable in light of the low electron mobility of the amorphous mesophase (Figure 3), indicating that J_{SC} is not limited by the electrons mobility in the mesophase but rather increased by improved carrier generation efficiency at the donor/acceptor interface. This is illustrated by the cartoon in Figure 5.

The contact between crystalline BP and fullerene•solvent crystallite (nm-sized ordered fullerene molecules) improves by conversion into an amorphous solid, and deteriorates again after recrystallization of fullerene. This result also suggests that electron mobility of the fullerene film is high enough to make other processes limiting the device performance.

The large drop of the PCE of the device C made with benzene occurred upon annealing at high temperatures. It is due to the drop of FF, which in turn was caused mainly by the increase of R_{sh} (see the Experimental Section, Table 3). I thus consider that the liquidification of the fullerene layer occurred through loss of the tightly bound benzene molecules, and that hence I could not form good contact between the fullerene n-layer and the buffer and the Al layers.[32]

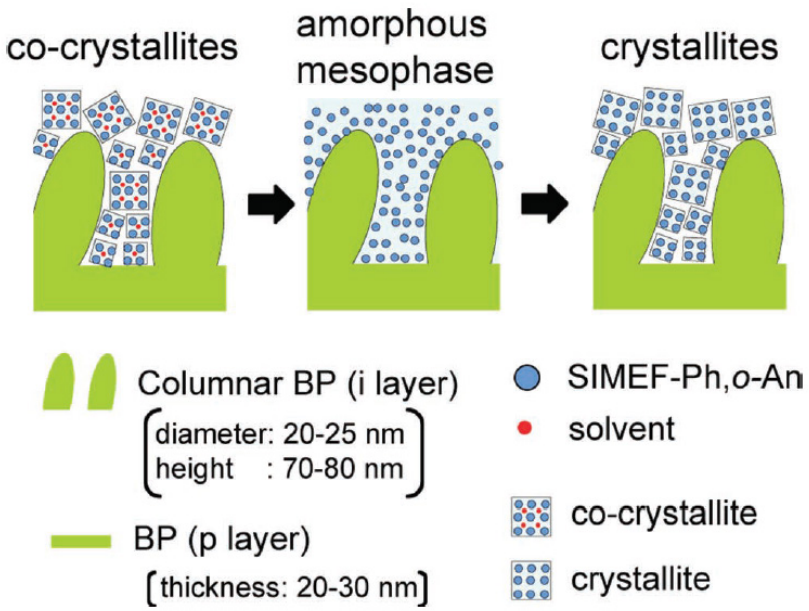

Figure 5. Schematic illustration of the phase transition behavior of SIMEF-Ph, *o*-An upon heating within a p-i-n structure.

My conjecture that amorphous mesophase gave the best PCE was supported further by comparison of p-i-n OPV devices based on **3** and **4** (see the Experimental Section for the data). The compounds **3** and **4** form glass phases at room temperature and form a crystalline phase at high temperature (Figure 2d). I fabricated p-i-n devices with a configuration of glass/ITO/PEDOT:PSS/BP/BP: **3** or **4**/**3** or **4**/ di(benzo[b]phosphole sulfide (DBPSB; as cathode buffer layer)/Al (denoted devices D and E).[33] The PCE value of device D (using **3**) and E (**4**) decreased greatly above 120 °C (from 3.9% to 2.9% and from 4.3% to 3.8%, respectively) due to a decrease in the FF value (from 0.62 to 0.50 and from 0.61 to 0.55, respectively). Parenthetically, the higher V_{OC} values of the devices made using **2** and **4** rather than **3** are due to the higher LUMO levels of the former (LUMO of **2**, **3** and **4** = 3.72, 3.74 and 3.70 eV, see the Experimental Section). The difference of the LUMO levels can be ascribed to better electron donation by the *o*- and *p*-methoxy groups compared with the *m*-methoxy group.

2.6 Conclusion

In summary, by using a new SIMEF compound **2** that forms solvent co-crystals and loses the solvent molecules upon heating around 100 °C, I have constructed a model OPV device suitable for in situ and ex situ studies on the effects of the desolvation of the n-type fullenrene material and the resulting the phase changes on the device performance. To maximize the overall device performance, one needs to optimize three parameters; the structure of each of material in the device, the structure of the molecular aggregates, and the hierarchical ordering of such aggregates. The case that I described

above illustrates that thermal annealing serves to control the second and the third parameters. Thermal annealing above 100 °C forms a partially desolvated amorphous mesophase sandwiched between the BP donor and the cathode buffer layer; this amorphous fullerene layer improves the J_{SC} value and the overall device performance through improvement of the interfacial contact and, hence, the carrier generation at the donor-acceptor interface. This statement raises the question of whether less-than-1-nm scale fullerene derivatives can ever form fully developed crystals in the tens of nm-size space available within the active layer (Figure 5). Such small molecular aggregates are generally called embryos[34] or crystallites and are considered to have properties that are dissimilar to the corresponding fully developed crystals. Nonetheless, I consider that the phase behavior and the physical properties observed for μm-thin films of fullerene molecules provide useful hints to analyze and design OPV devices. Finally, I suggest that studies on the phase behavior of organic semiconductors in the presence of suitably chosen additives (including solvent) will be a fruitful effort in organic electronics research.[35]

2.7 Experimental Section

2.7.1 Synthesis

General Considerations. All reactions dealing with air- or moisture-sensitive compounds were carried out using standard Schlenk technique or a glove box under an argon or nitrogen atmosphere. HPLC analyses were performed on a Shimadzu LC-10A system equipped with SPD-M10A diode array detector and a Buckyprep column

(Nacalai Tesque Inc., 4.6 mm ID x 250 mm). Preparative HPLC was performed on a Buckyprep column (20mm ID × 250 mm) using toluene/2-isopropanol (10/0 – 4/6) as eluent (flow rate 5–15 mL/min, detected at 350 nm with an UV spectrophotometric detector, Shimadzu SPD-6A) and an RP-FULLERENE column (Nomura Chemical, 20 mm ID × 250 mm) using toluene/acetonitrile (7/3 – 4/6) as eluent (flow rate 5–12 mL/min, detected at 350 nm with an UV spectrophotometric detector, Shimadzu SPD-6A). Flash silica gel column chromatography was performed on silica gel 60N (Kanto Chemical, spherical and neutral, 140-325 mesh) as described by Still.[36] Gel permeation column chromatography was performed on a Japan Analytical Industry LC-9201 (eluent: toluene) with JAIGEL 2H and 3H polystyrene column. NMR spectra were measured with a JEOL EX-400 (400 MHz) or a JEOL ECA-500 (500 MHz) spectrometer. Spectra are reported in parts per million from internal tetramethylsilane (d 0.00 ppm) for ^{1}H NMR, from solvent carbon (e.g. d 77.00 ppm for chloroform) for ^{13}C NMR. High-resolution mass spectra were measured by APCI using a time-of-flight mass analyzer on a JEOL JMS-T100LC (AccuTOF) spectrometer. $PhMe_2SiCH_2MgCl$, $(C_4H_9)Me_2SiCH_2SiCl$, and $(C_{12}H_{25})Me_2SiCH_2SiCl$ were prepared according to the literatures,[37] and titrated before use. PCBM was purchased from Frontier Carbon Corporation and used as received. Other materials were purchased from Tokyo Chemical Industry Co., Sigma-Aldrich Co., Kanto Chemical Co., Inc., Wako Pure Chemical Industries, or other commercial suppliers and used after appropriate purification before use.

Synthesis of 1-(dimethylphenylsilylmethyl)-1,9-dihydro(C_{60}-I_h)[5,6]fullerene, $C_{60}(CH_2SiMe_2Ph)H$ (1). To a solution of C_{60} (2.00 g, 2.78 mmol) in

1,2-dichlorobenzene (500 mL) containing *N*,*N*-dimethylformamide (6.45 mL, 83.3 mmol) was added a THF solution of $PhMe_2SiCH_2MgCl$ (9.80 mL, 0.850 M, 8.33 mmol) at 25 °C. Color of the solution immediately changed from purple to dark green. After stirring for 10 min, saturated aqueous NH_4Cl solution (1.0 mL) was added to terminate the reaction. The resulting dark red solution was subjected to vacuum distillation to remove 1,2-dichlorobenzene. The residue containing small amount of 1,2-dichlorobenzene (ca. 0.5~3 mL) was dissolved in toluene (200 mL), and passed through a pad of silica gel to remove magnesium salts. The toluene solution was evaporated to obtain concentrated solution (ca. 5~10 mL) containing the product, which was reprecipitated by addition of methanol (ca. 100~200 mL) to obtain brown powder. Purification of the product was carried out with preparative HPLC separation (Buckyprep column, eluent: toluene/2-propanol = 7/3) to obtain the title compound (1.99 g, 2.28 mmol, 82% isolated yield, analytically pure). ^{1}H NMR (500 MHz, $CDCl_3$): δ 0.89 (s, 6H, $SiCH_3$), 3.16 (s, 2H, CH_2), 6.39 (s, 1H, $C_{60}H$), 7.44–7.46 (m, 3H, Ph), 7.88–7.90 (m, 2H, Ph); ^{13}C NMR (125 MHz, $CDCl_3$): δ –0.75 (2C, $SiCH_3$), 38.03 (1C, CH_2), 61.57 (1C, $C_{60}H$), 62.23 (1C, $C_{60}CH_2$), 128.19 (2C, Ph), 129.68 (1C, Ph), 134.16 (2C, Ph), 134.89 (2C, C_{60}), 136.57 (2C, C_{60}), 138.22 (1C, Ph), 140.05 (2C, C_{60}), 140.20 (2C, C_{60}), 141.63 (2C, C_{60}), 141.64 (2C, C_{60}), 141.94 (2C, C_{60}), 141.97 (2C, C_{60}), 142.03 (2C, C_{60}), 142.06 (2C, C_{60}), 142.54 (2C+2C, C_{60}), 143.27 (2C, C_{60}), 144.66 (2C, C_{60}), 144.71 (2C, C_{60}), 145.28 (2C, C_{60}), 145.36 (2C, C_{60}), 145.39 (2C+2C, C_{60}), 145.64 (2C, C_{60}), 145.88 (2C, C_{60}), 146.18 (2C, C_{60}), 146.22 (2C, C_{60}), 146.30 (2C, C_{60}), 146.41 (2C, C_{60}), 149.92 (2C, C_{60}), 147.35 (1C, C_{60}), 147.49 (1C, C_{60}), 154.05 (2C, C_{60}), 157.86 (2C, C_{60}); APCI-HRMS (–): *m*/*z* calcd for $C_{69}H_{13}Si$ ($M–H^+$), 869.0787; found, 869.0743.

Synthesis of 1-(dimethylphenylsilylmethyl)-7-{dimethyl(2-methoxyphenyl)silylmethyl}-1,7-dihydro(C_{60}-I_h)[5,6]fullerene, $C_{60}(CH_2SiMe_2Ph)\{CH_2SiMe_2(o\text{-}An)\}$ (2). To a solution of **1** (1.02 g, 1.17 mmol) in benzonitrile was added a THF solution of KO^{t}Bu (1.41 mL, 1.0 M, 1.41 mmol) at 25 °C. A dark green solution of potassium salt of $C_{60}(CH_2SiMe_2Ph)^-$ was obtained immediately. After stirring for 10 min, *o*-$AnMe_2SiCH_2Cl$ (5.03g, 23.4 mmol) and potassium iodide were added to the solution. Then, the reaction mixture was stirred for 17 h at 110 °C. The resulting dark red solution was treated with 1.0 mL of saturated aqueous NH_4Cl solution, and then vacuum distillation was performed to remove benzonitrile. The residue containing small amount of benzonitrile (ca. 0.5~2 mL) was dissolved in toluene (100 mL), and passed through a pad of silica gel to remove potassium salts. The toluene solution was evaporated to obtain concentrated solution (ca. 2~5 mL) containing the product, which was reprecipitated by addition of methanol (ca. 50~100 mL) to obtain dark brown powder. Purification of the product was performed by silica gel column chromatography (eluent: CS_2/hexane = 1/1), giving analytically pure product. An OPV-grade material was prepared by preparative HPLC separation (Buckyprep column, eluents: toluene/2-propanol = 7/3) to obtain >99.9% pure product **2** (0.810 g, 0.772 mmol, 66% isolated yield) as black crystals. ^{1}H NMR (500 MHz, $CDCl_3/CS_2$): δ 0.60 (s, 3H, $SiCH_3$), 0.63 (s, 3H, $SiCH_3$), 0.70 (s, 3H, $SiCH_3$), 0.73 (s, 3H, $SiCH_3$), 2.67 (d, 1H, ^2J = 14.3 Hz, CH_2), 2.72 (d, 1H, ^2J = 14.3 Hz, CH_2), 2.81 (d, 1H, ^2J = 14.3 Hz, CH_2), 2.84 (d, 1H, ^2J = 14.3 Hz, CH_2), 3.78 (s, 3H, OCH_3), 6.71 (d, 1H, C_6H_4), 6.89 (t, 1H, C_6H_4), 7.30–7.35 (m, 1H, C_6H_4), 7.36–7.40 (m, 3H, Ph), 7.44–7.47 (m, 1H, C_6H_4), 7.70–7.72 (m, 2H, Ph); ^{13}C NMR (125 MHz, $CDCl_3/CS_2$): δ –0.92 (1C, $SiCH_3$), –0.89 (1C, $SiCH_3$), –0.72 (1C, $SiCH_3$), –0.66 (1C, $SiCH_3$), 31.56 (1C,

CH_2), 32.56 (1C, CH_2), 54.77 (1C, OCH_3), 55.65 (1C, $C_{60}CH_2$), 56.00 (1C, $C_{60}CH_2$), 109.23 (1C, C_6H_4), 120.62 (1C, C_6H_4), 125.43 (1C, C_6H_4), 127.84 (2C, Ph), 129.37 (2C, Ph), 131.56 (1C, C_6H_4), 137.89 (1C, C_6H_4), 133.90 (2C, Ph), 135.78 (1C, C_6H_4), 138.16 (1C, C_{60}), 138.22 (1C, C_{60}), 138.38 (1C, C_{60}), 138.73 (1C, C_{60}), 140.42 (1C, C_{60}), 141.20 (1C, C_{60}), 141.52 (1C, C_{60}), 141.76 (1C, C_{60}), 142.29 (1C, C_{60}), 142.36 (1C, C_{60}), 142.40 (1C, C_{60}), 142.45 (1C, C_{60}), 142.47 (1C, C_{60}), 142.60 (1C, C_{60}), 142.64 (1C, C_{60}), 142.88 (1C, C_{60}), 142.90 (1C, C_{60}), 143.03 (2C, C_{60}), 143.05 (1C, C_{60}), 143.15 (1C, C_{60}), 143.17 (1C, C_{60}), 143.32 (1C, C_{60}), 143.39 (1C, C_{60}), 143.73 (1C, C_{60}), 143.76 (1C, C_{60}), 143.98 (1C, C_{60}), 144.00 (1C, C_{60}), 144.04 (1C, C_{60}), 144.06 (1C, C_{60}), 144.27 (1C, C_{60}), 144.30 (1C, C_{60}), 144.33 (1C, C_{60}), 144.48 (1C, C_{60}), 144.52 (1C, C_{60}), 144.53 (1C, C_{60}), 144.66 (1C, C_{60}), 144.73 (1C, C_{60}), 144.90 (1C, C_{60}), 145.19 (1C, C_{60}), 145.21 (1C, C_{60}), 146.55 (2C, C_{60}), 146.56 (1C, C_{60}), 146.72 (1C, C_{60}), 146.74 (1C, C_{60}), 146.75 (1C, C_{60}), 146.88 (1C, C_{60}), 146.89 (1C, C_{60}), 147.19 (1C, C_{60}), 147.24 (1C, C_{60}), 147.44 (1C, C_{60}), 147.73 (1C, C_{60}), 147.82 (1C, C_{60}), 148.29 (1C, C_{60}), 148.33 (1C, C_{60}), 153.21 (1C, C_{60}), 153.51 (1C, C_{60}), 157.34 (1C, C_{60}), 157.50 (1C, C_{60}), 164.23 (1C, $COCH_3$); APCI-HRMS (–): *m*/*z* calcd for $C_{79}H_{28}OSi_2$ ($M–H^+$), 1048.1679; found, 1048.1656.

Synthesis of 1-(dimethylphenylsilylmethyl)-7-{dimethyl(3-methoxyphenyl)silylmethyl}-1,7-dihydro(C_{60}-I_h)[5,6]fullerene, $C_{60}(CH_2SiMe_2Ph)\{(CH_2SiMe_2(m\text{-}An)\}$ (3). Synthesis of **3** was performed by employing the procedure of **2** described above using chloromethyldimethyl-3-methoxyphenylsilane with potassium iodide as a reactant. The reaction mixture was stirred for 17 hrs at 110 °C to produce di-adduct **3** in 60% yield as >99.9% pure brown crystals by purification with silica gel column chromatography

preparative and preparative HPLC separation (Buckyprep 20 mm ID x 250 mm, toluene/2-isopropanol = 7/3, and RP fullerene 20 mm ID x 250 mm, toluene/acetonitrile = 7/3). ^{1}H NMR (500 MHz, $CDCl_3/CS_2$): δ 0.66–0.68 (m, 12H, $SiCH_3$), 2.61 (d, 1H, ^{2}J = 14.6 Hz, CH_2), 2.62 (d, 1H, ^{2}J = 14.6 Hz, CH_2), 2.75 (d, 1H, ^{2}J = 14.6 Hz, CH_2), 2.77 (d, 1H, ^{2}J = 14.6 Hz, CH_2), 3.80 (s, 3H, OCH_3), 6.89–6.91 (m, 1H, C_6H_4), 7.14–7.17 (m, 1H, C_6H_4), 7.26–7.28 (m, 2H, C_6H_4), 7.36–7.37 (m, 3H, Ph), 7.68–7.70 (m, 2H, Ph); ^{13}C NMR (125 MHz, $CDCl_3/CS_2$): δ –1.02 (1C, $SiCH_3$), –1.00 (1C, $SiCH_3$), –0.96 (1C, $SiCH_3$), –0.94 (1C, $SiCH_3$), 32.50 (2C, CH_2), 54.88 (1C, OCH_3), 55.63 (1C, $C_{60}CH_2$), 55.65 (1C, $C_{60}CH_2$), 114.50 (1C, C_6H_4), 119.68 (1C, C_6H_4), 126.21 (1C, C_6H_4), 127.84 (2C, Ph), 128.12 (2C, C_6H_4), 129.37 (2C, Ph), 133.91 (2C, Ph), 138.06 (2C, C_{60}), 138.15 (2C, C_{60}), 138.47 (1C, C_{60}), 138.49 (1C, C_{60}), 139.62 (1C, C_{60}), 140.58 (1C, C_{60}), 141.51 (1C, C_{60}), 141.54 (1C, C_{60}), 141.77 (1C, C_{60}), 142.36 (2C, C_{60}), 142.48 (1C, C_{60}), 142.49 (1C, C_{60}), 142.69 (2C, C_{60}), 142.94 (2C, C_{60}), 143.07 (2C, C_{60}), 143.26 (1C, C_{60}), 143.42 (1C, C_{60}), 143.43 (1C, C_{60}), 143.79 (1C, C_{60}), 144.05 (2C, C_{60}), 144.07 (2C, C_{60}), 144.29 (2C, C_{60}), 144.31 (1C, C_{60}), 144.53 (2C, C_{60}), 144.63 (1C, C_{60}), 144.64 (1C, C_{60}), 144.90 (2C, C_{60}), 145.26 (2C, C_{60}), 146.61 (2C, C_{60}), 146.75 (2C, C_{60}), 146.93 (2C, C_{60}), 146.98 (1C, C_{60}), 147.00 (1C, C_{60}), 147.18 (2C, C_{60}), 147.70 (2C, C_{60}), 148.36 (2C, C_{60}), 153.17 (1C, C_{60}), 153.21 (1C, C_{60}), 157.23 (1C, C_{60}), 157.29 (1C, C_{60}), 158.89 (1C, $COCH_3$); APCI-HRMS (–): *m*/*z* calcd for $C_{79}H_{28}OSi_2$ ($M–H^+$), 1048.1679; found, 1048.1647.

Synthesis of 1-(dimethylphenylsilylmethyl)-7-{dimethyl(4-methoxyphenyl)silylmethyl}-1,7-dihydro(C_{60}-I_h)[5,6]fullerene, $C_{60}(CH_2SiMe_2Ph)\{CH_2SiMe_2(p\text{-An})\}$ (4). Synthesis of **4**

was performed by employing the procedure of **2** described above using chloromethyldimethyl-4-methoxyphenylsilane with potassium iodide as a reactant. The reaction mixture was stirred for 17 hrs at 110 °C to produce di-adduct **4** in 68% yield as >99.9% pure brown crystals by purification with silica gel column chromatography preparative and HPLC separation (Buckyprep 20 mm ID x 250 mm, toluene/2-isopropanol = 7/3, and RP fullerene 20 mm ID x 250 mm, toluene/acetonitrile = 7/3). ^{1}H NMR (500 MHz, $CDCl_3/CS_2$): δ 0.63 (s, 3H, $SiCH_3$), 0.64 (s, 3H, $SiCH_3$), 0.66 (s, 3H, $SiCH_3$), 0.70 (s, 3H, $SiCH_3$), 2.58 (d, 1H, ^{2}J = 14.3 Hz, CH_2), 2.61 (d, 1H, ^{2}J = 14.3 Hz, CH_2), 2.73 (d, 1H, ^{2}J = 14.3 Hz, CH_2), 2.75 (d, 1H, ^{2}J = 14.3 Hz, CH_2), 3.77 (s, 3H, OCH_3), 6.85–6.87 (m, 2H, C_6H_4), 7.33–7.34 (m, 3H, Ph), 7.55–7.57 (m, 2H, C_6H_4), 7.65–7.66 (m, 2H, Ph); ^{13}C NMR (125 MHz, $CDCl_3/CS_2$): δ –0.99 (1C, $SiCH_3$), –0.93 (1C, $SiCH_3$), –0.81 (1C, $SiCH_3$), –0.73 (1C, $SiCH_3$), 32.52 (1C, CH_2), 32.82 (1C, CH_2), 54.81 (1C, OCH_3), 55.66 (1C, $C_{60}CH_2$), 55.73 (1C, $C_{60}CH_2$), 113.63 (2C, C_6H_4), 127.84 (2C, Ph), 128.80 (1C, C_6H_4), 129.37 (2C, Ph), 133.90 (2C, Ph), 135.39 (2C, C_6H_4), 138.09 (2C, C_{60}), 138.15 (2C, C_{60}), 138.16 (1C, C_{60}), 138.48 (1C, C_{60}), 138.52 (1C, C_{60}), 140.57 (1C, C_{60}), 141.52 (1C, C_{60}), 141.54 (2C, C_{60}), 141.77 (2C, C_{60}), 142.36 (2C, C_{60}), 142.37 (1C, C_{60}), 142.48 (1C, C_{60}), 142.50 (1C, C_{60}), 142.69 (2C, C_{60}), 142.94 (1C, C_{60}), 143.07 (2C, C_{60}), 143.26 (2C, C_{60}), 143.42 (1C, C_{60}), 143.45 (1C, C_{60}), 143.79 (1C, C_{60}), 143.81 (1C, C_{60}), 144.05 (1C, C_{60}), 144.07 (2C, C_{60}), 144.29 (2C, C_{60}), 144.33 (1C, C_{60}), 144.54 (2C, C_{60}), 144.63 (1C, C_{60}), 144.66 (1C, C_{60}), 144.89 (1C, C_{60}), 144.90 (1C, C_{60}), 145.26 (2C, C_{60}), 146.62 (1C, C_{60}), 146.76 (1C, C_{60}), 146.93 (2C, C_{60}), 147.10 (1C, C_{60}), 147.20 (1C, C_{60}), 147.21 (1C, C_{60}), 147.72 (2C, C_{60}), 148.36 (1C, C_{60}), 148.37 (1C, C_{60}), 153.21 (1C, C_{60}), 153.26 (1C, C_{60}), 157.30 (1C, C_{60}), 157.38 (1C, C_{60}),

160.59 (1C, *C*$COCH_3$); APCI-HRMS (–): *m*/*z* calcd for $C_{79}H_{28}OSi_2$ ($M–H^+$), 1048.1679; found, 1048.1724.

2.7.2 Electrochemical Properties

Cyclic voltammetry (CV) of **2**–**4** was performed using HOKUTO DENKO HZ-5000 voltammetric analyzer. All measurements were carried out in a one-compartment cell under Ar gas, equipped with a glassy-carbon working electrode, a platinum wire counter electrode, and an Ag/Ag^+ reference electrode. Measurements were performed in THF solution containing tetrabutylammonium perchlorate (0.1 M) as a supporting electrolyte at 25 °C with a scan rate of 0.1 V/s. All potentials were corrected against Fc/Fc^+.

All compounds were electrochemically stable up to three-electron reduction. The values of their reversible half-wave reduction potentials and estimated LUMO levels are listed in Table S1. Compounds **2**, **3** and **4** have first reduction potentials at $E_{1/2}$ = –1.08, –1.06 and –1.10 V (vs. Fc/Fc^+, in THF), respectively.

Table 1. Reduction Potentials for **2**–**4**[a]

compound	$E_{1/2}^{red1}$/V	$E_{1/2}^{red2}$/V	$E_{1/2}^{red3}$/V	LUMO level [b]
2	–1.08	–1.66	–2.25	–3.72
3	–1.06	–1.63	–2.22	–3.74
4	–1.10	–1.68	–2.27	–3.70

[a] Potential in volts vs ferrocene/ferrocenium measured with cyclic voltammetry in THF containing $Bu_4N^+ClO_4^-$ (0.1 M) as a supporting electrolyte. Glassy-carbon, platinum wire, and Ag/Ag^+ electrodes were used as working, counter, and reference electrodes, respectively. [b] The values from the vacuum level were estimated using the following equation; LUMO = –($E_{1/2}^{red1}$ + 4.80).

a)

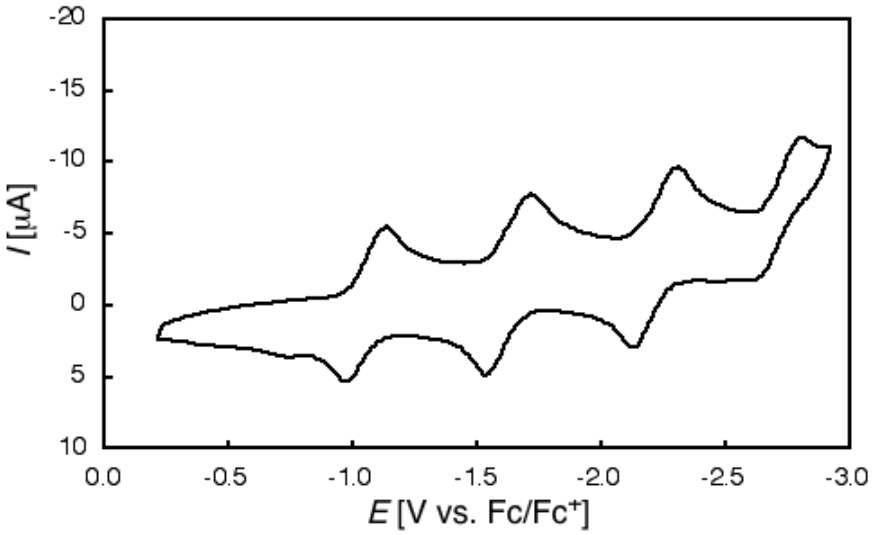

b)

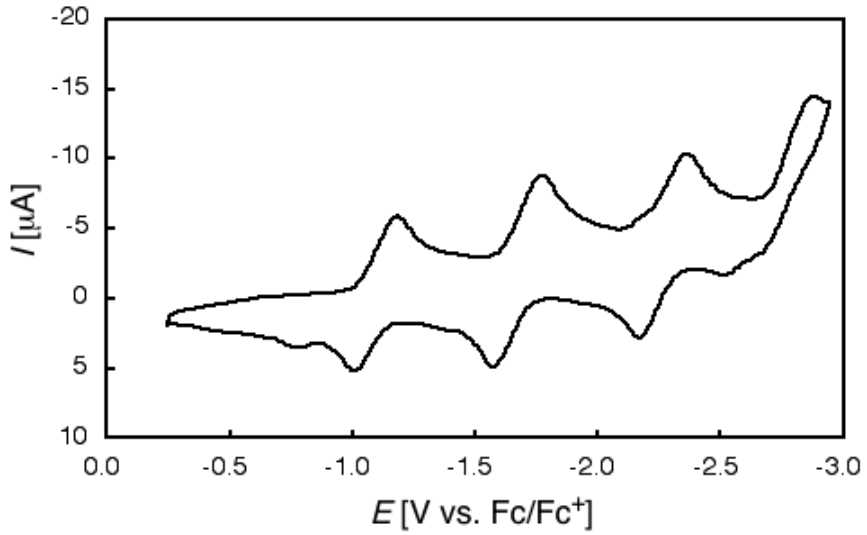

Figure 6. Cyclic voltammogram of **3** (a) and **4** (b) in THF at 25 °C.

2.7.3 Differential Scanning Calorimetry Analysis

Differential scanning calorimetry (DSC) was performed on a NETZSCH thermal analyzer (DSC 204/F1). Samples (~5 mg) were placed in aluminum pans and heated at 10 °C/min, under nitrogen.

a)

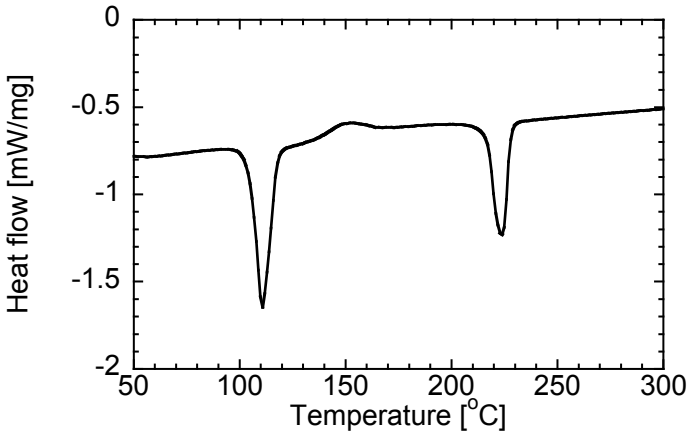

b)

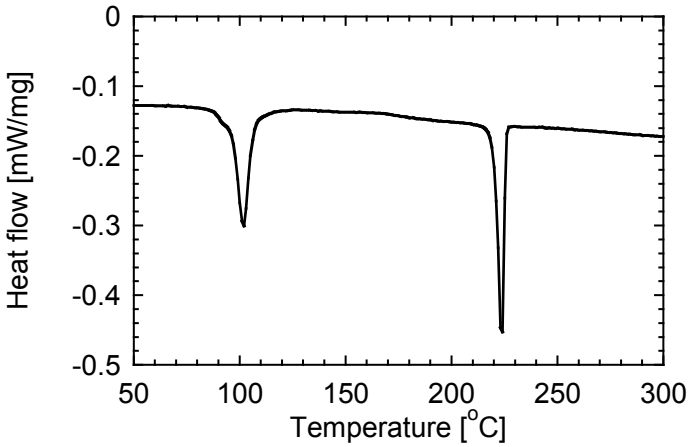

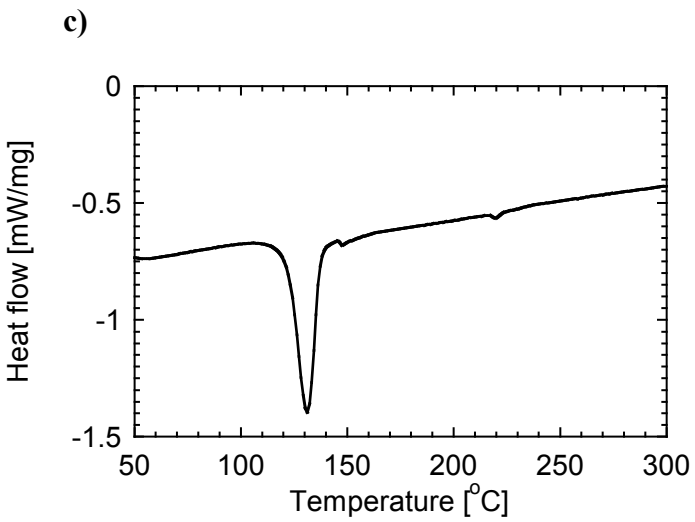

Figure 7. DSC data for co-crystals of **2** with solvent molecule. DSC data for **2**•toluene (a), **2**•CB (b), and **2**•benzene (c).

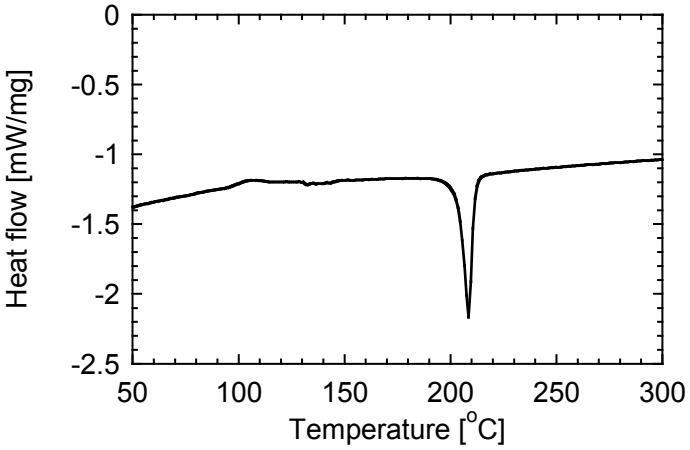

Figure 8. DSC data for **3**.

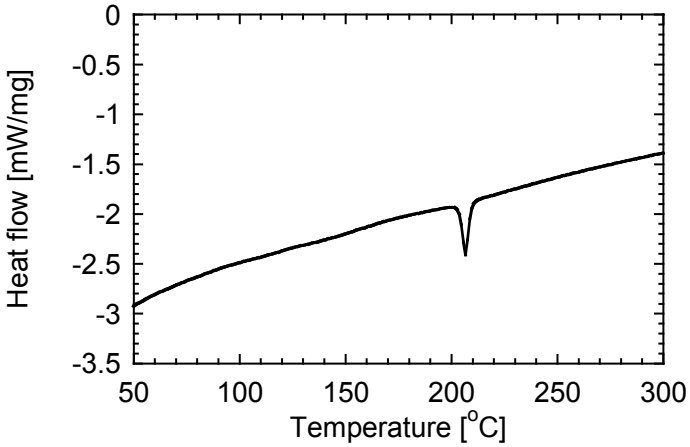

Figure 9. DSC data for **4**.

2.7.4 X-Ray Diffraction Studies

Single-crystal X-ray structural analyses of 2–4. Crystal of **2** was obtained by slow diffusion of 2-propanol that was layered on a toluene solution of the compound. In the same manner, crystals of **3** and **4** were obtained by slow diffusion of ethanol into a CS_2 (**3**) or *para*-xylene (**4**) solution of the compound. Crystals of compounds **3** and **4** did not contain solvent molecules in their crystal packing.

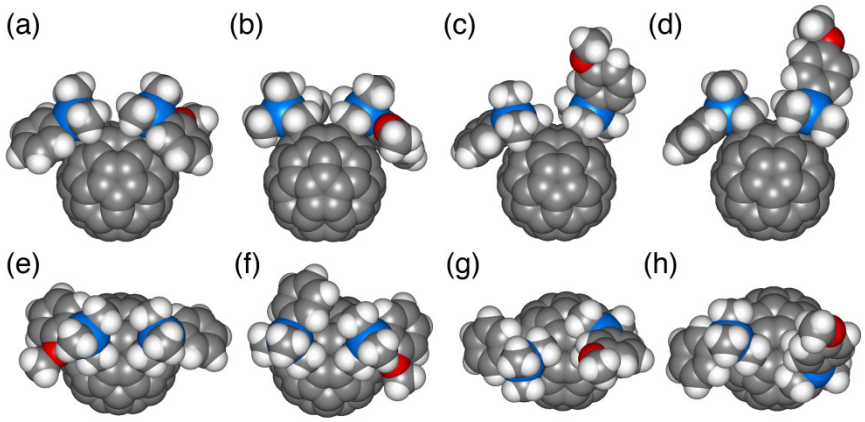

Figure 10. Crystallographic structures of **2**–**4**. (a) Side view of CPK model of **2**·toluene. (b) Side view of CPK model of **2** obtained from anisole solution. (c) Side view of CPK model of **3**. (d) Side view of CPK model of **4**. (e) Top view of CPK model of **2**·toluene. (f) Top view of CPK model of **2** obtained from anisole solution. (g) Top view of CPK model of **3**. (h) Top view of CPK model of **4**.

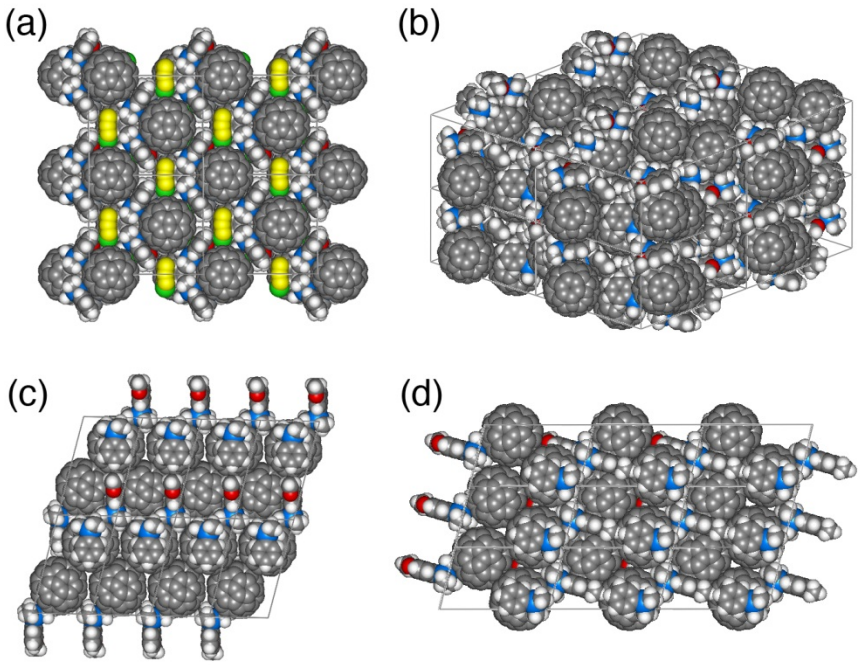

Figure 11. Crystal packing structures of **2**–**4**. (a) Crystal packing of **2**•CB. (b) Crystal packing of **2** obtained from anisole solution. (c) Crystal packing of **3**. (d) Crystal packing of **4**.

Powder X-ray diffraction analysis of 3 and 4. For the benzene co-crystals of **2**, the compound **3** and **4**, XRD was performed on a Rigaku R-AXIS RAPID II imaging plate diffractometer using Cu-Kα radiation. The measurement temperatures were varied using the temperature controller Rigaku CGD-4 under nitrogen. Samples were grinded down and packed into glass capillaries, and annealed for 1 hour at the target temperature before measurement.

a)

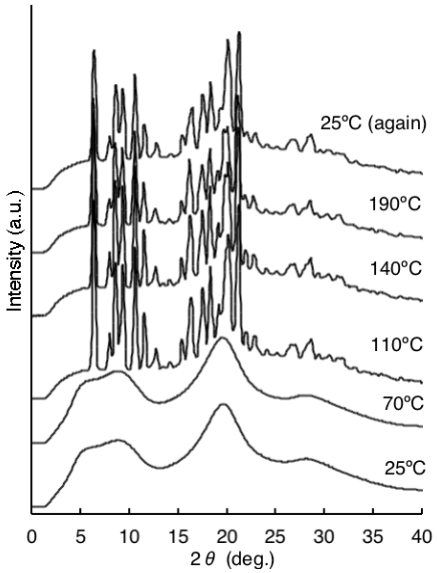

b)

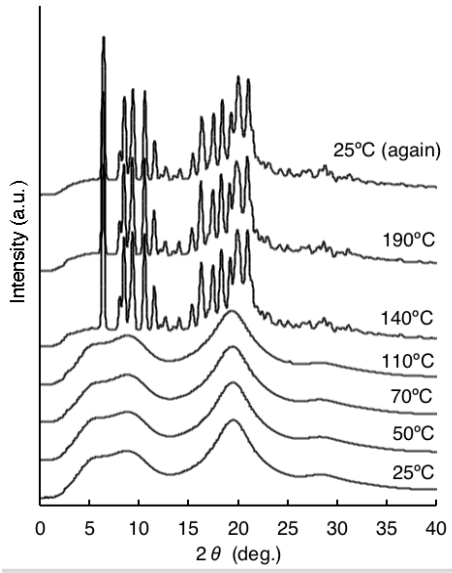

Figure 12. VT-XRD patterns of **3** and **4**. (a) The VT-XRD spectra of **3** at 25 °C, 70 °C, 110 °C, 140 °C, 190 °C and 20 °C (after 190 °C). (b) The VT-XRD spectra of **4** at 20 °C, 50 °C, 70 °C, 110 °C, 140 °C, 190 °C, and 25 °C (after 190 °C).

2.7.5 Electron Mobility

The single layer devices with the configuration of a glass/Al/**2**•solvent/LiF/Al (electron-only device) was fabricated, in which **2**•solvent formed by drop casting of a toluene, CB and benzene solutions on an Al electrode, and the thickness was controlled by changing the concentration of solution (0.7-1.2 wt%). The **2**•solvent film was annealed at a target temperature for 10 min, and then the SCLC devices were completed by vacuum deposition of a 0.5-nm LiF and an 80-nm Al layer. The current density–voltage characteristics under dark condition was recorded using a Keithley 2400 source-measurement unit. Electron mobility was estimated by the fitting curve of space charge limited current (SCLC) as following equation,

$$J_e = \frac{9}{8} \cdot \varepsilon_0 \varepsilon_r \mu_{0e} \exp\left(0.891 \gamma_e \sqrt{\frac{V}{L}}\right) \frac{V^2}{L^3} \qquad (1)$$

where $\varepsilon_0 \varepsilon_r$ is the permittivity of the fullerenes, μ_{0e} is the zero-field mobilty of electron, γ_e is the field activation factor, L is the device thickness and V is the voltage drop across the devices.

Table 2. Electron mobility of the **2**•solvent from the field dependent SCLC

fullerene	phase[a]	Annealing Temp. [°C]	μ_{e0} [cm^2/Vs] [b]	γ [$m/V]^{1/2}$ [b]
	Co-cy	65	7.8×10^{-4}	1.2×10^{-4}
2•toluene	Am Mes	120	1.0×10^{-4}	6.7×10^{-4}
	Cy	180	9.1×10^{-4}	4.3×10^{-4}
	Co-cy	65	5.0×10^{-4}	2.4×10^{-4}
2•CB	Am Mes	120	2.1×10^{-4}	2.5×10^{-4}
	Cy	180	2.3×10^{-4}	4.5×10^{-4}
	Co-cr	65	2.1×10^{-3}	1.9×10^{-4}
2•benzene	Iso + Cr	140	5.6×10^{-4}	4.6×10^{-5}
	Iso + Cy	180	1.6×10^{-3}	0

[a] Co-cr = co-crystalline phase, Am Mes = amorphous mesophase, Cr = crystalline phase, Iso = isotropic phase.

[b] Zero-field mobility and electridc field coefficient using field-dependent mobility model.

a)

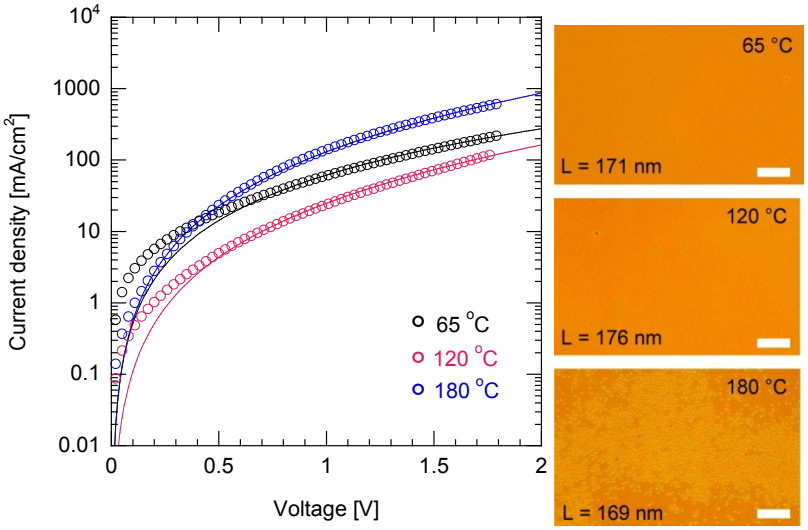
Current density [mA/cm^2]
Voltage [V]
65 °C
120 °C
180 °C
L = 171 nm
L = 176 nm
L = 169 nm

b)

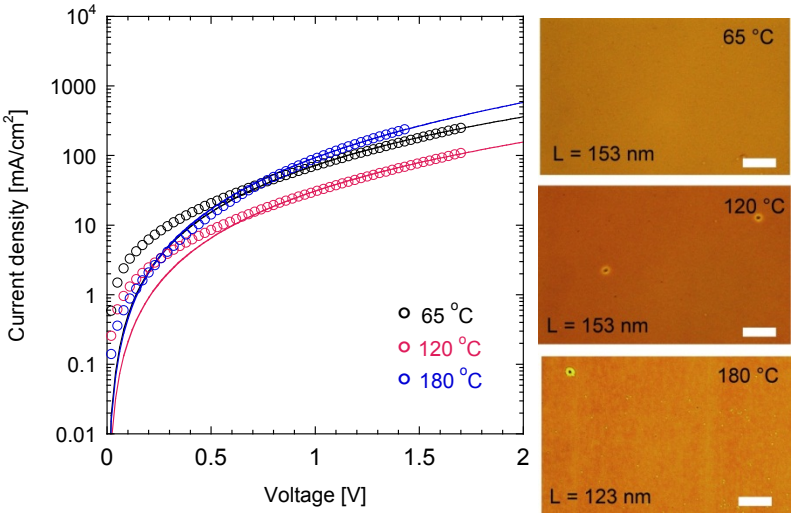
Current density [mA/cm^2]
Voltage [V]
65 °C
120 °C
180 °C
L = 153 nm
L = 153 nm
L = 123 nm

c)

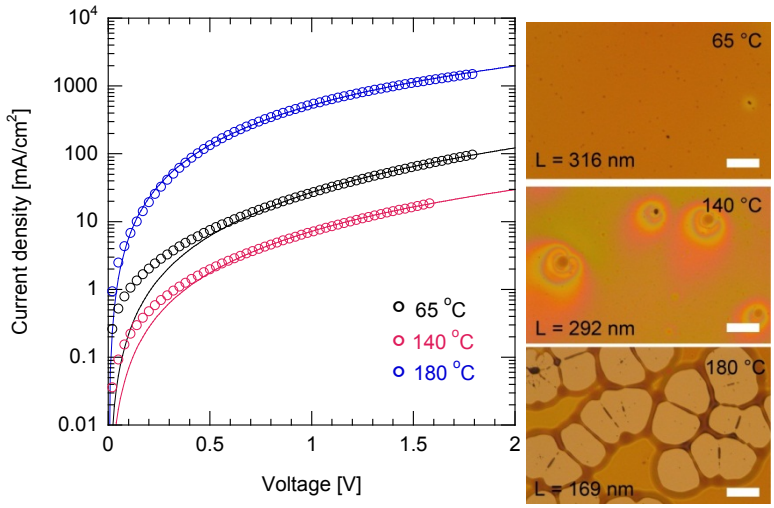

Figure 13. Temperature dependence of J-V characteristics (left) and optical microscope images (right) from electron-only devices composed of **2**•toluene (a), **2**•CB (b), and **2**•benzene (c). (open circle: experimental values, solid line: calculated values, scale bar: 100 μm, L: thickness of fullerene layer).

2.7.6 Device Fabrication and Characteristics

Organic photovoltaic cells having a p-i-n structure were fabricated according to the following procedure. An ITO-coated glass substrate was exposed to UV ozone prior to usage, and was then coated with PEDOT:PSS (CLEVIOS P VP AI4083). The substrate was first heated at 120 °C for 10 min under air and then heated at 180 °C for 3 min in a nitrogen glove box to remove residual water. A 0.5 wt% solution of 1,4:8,11:15,18:22,25-tetraethano-29*H*,31*H*-tetrabenzo[*b*,*g*,*l*,*q*]porphyrin (CP; a precursor of tetrabenzoporphyrin (BP)) in chlorobenzene:chloroform (2:1, weight ratio) was spin coated on the PEDOT:PSS layer. The resulting film was heated at 180 °C for 20 min that converted the soluble CP to insoluble crystalline BP, which serves as a p layer. On top of the BP layer, the i layer was deposited by spin coating (1,500 rpm) a mixture of CP and a fullerene derivative **2–4** (CP, 0.6 wt%; fullerene **2–4**, 1.4 wt%) in a chloroform–chlorobenzene mixture (1:1 ratio). The i layer was heated at 180 °C for 20 min. A 0.7 wt% solution of **2** (in toluene, chlorobenzene or benzene; for devices A to C) or 1.2 wt% solution of **2–4** in toluene (devices D and E) was spin coated (3,000 rpm) as an n layer. After heating this film for 10 min at 65 °C, 120 °C and 180 °C, the device was completed by vacuum deposition of a 7-nm 2,9-bis(naphthalen-2-yl)-4,7-diphenyl-1,10-phenanthroline (NBphen) (or 5-nm di(benzo[b]phosphole sulfide (DBPSB)), and an 80-nm Al layer. The current density–voltage characteristics under AM 1.5 G solar illumination (100 mW/cm^2) was recorded using a Keithley 2400 source-measure unit.

Table 3. Photovoltaic performance of the devices A-C under 100 mW/cm^2 illumination (glass/ITO/PEDOT:PSS/BP/BP:**2**/**2**•solvent/NBPhen/Al)

device (fullerene)	phase[a]	Annealing Temp. [°C]	PCE [%]	J_{SC} [mA/cm^2]	V_{OC} [V]	FF	R_s [Ω·cm^2]	R_{sh} [kΩ·cm^2]
device-A (**2**•toluene)	Co-cy	65	5.1	9.8	0.78	0.67	2.4	1.7
	Am Mes	120	5.4	10.2	0.79	0.67	2.8	1.9
	Cy	180	5.1	10.0	0.77	0.67	1.8	1.7
device-B (**2**•CB)	Co-cy	65	4.6	9.6	0.77	0.61	2.1	1.0
	Am Mes	120	5.0	9.9	0.78	0.64	2.1	1.1
	Cy	180	4.7	9.8	0.74	0.65	1.6	1.5
device-C (**2**•benzene)	Co-cr	65	4.9	9.4	0.80	0.65	2.7	1.3
	Iso + Cy	140	4.2	9.7	0.77	0.56	2.2	0.8
	Iso + Cy	180	4.0	9.6	0.77	0.54	2.2	0.6

[a] Co-cr = co-crystalline phase, Am Mes = amorphous mesophase, Cr = crystalline phase, Iso = isotropic phase.

a)

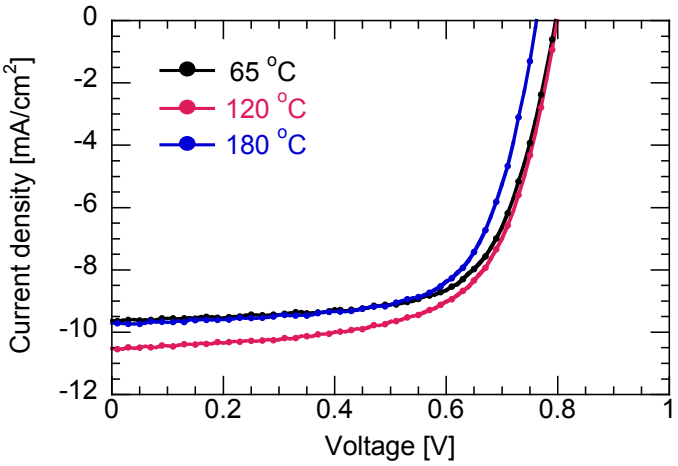

b)

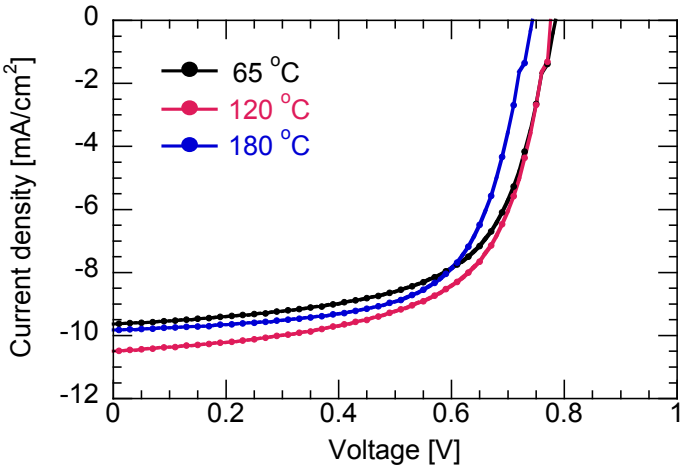

c)

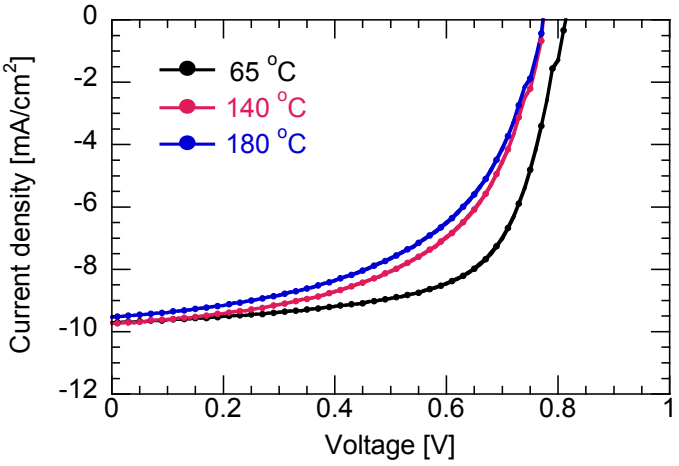

Figure 14. J-V curves of device A (a), device B (b), and device C (c).

Table 4. Photovoltaic performances of device-D, and –E

device (fullerene)	Annealing Temp. [°C]	PCE [%]	J_{SC} [mA/cm^2]	V_{OC} [V]	FF
device-D (**3**)	65	4.0	9.0	0.71	0.62
	120	3.9	8.8	0.71	0.62
	180	2.9	8.6	0.69	0.50
device-E (**4**)	65	4.4	9.6	0.74	0.61
	120	4.3	9.8	0.73	0.61
	180	3.8	9.6	0.73	0.55

a)

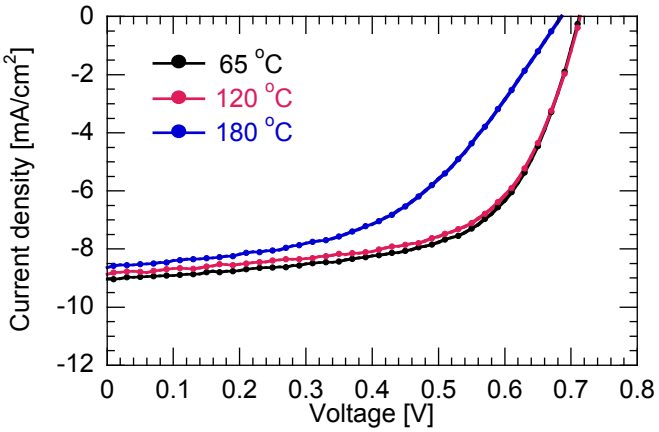

b)

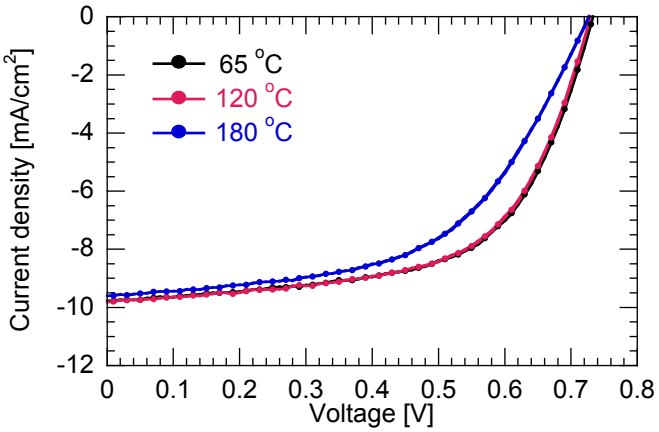

Figure 15. J-V curves of device D (a), and device E (b).

2.8 References and Notes

† This chapter is published on *Adv. Mater.* **2012**, *24*, 3521.

(1) G. Dennler, M. C. Scharber, C. J. Brabec, *Adv. Mater.* **2009**, *21*, 1323.

(2) E. Nakamura, K. Sato, *Nat. Mater.* **2011**, *10*, 158.

(3) R. F. Service, *Science* **2011**, *332*, 293.

(4) M. A. Green, K. Emery, Y. Hishikawa, W. Warta and E. D. Dunlop, *Prog. Photovolt: Res. Appl.* **2012**, *20*, 12.

(5) S. I. Na, S. S. Kim, J. Jo, D. Y. Kim, *Adv. Mater.* **2008**, *20*, 4061.

(6) J. Peet, A. J. Heeger, G. C. Bazan, *Acc. Chem. Res.* **2009**, *42*, 1700.

(7) B. Walker, A. B. Tamayo, X.-D. Dang, P. Zalar, J. H. Seo, A. Garcia. M. Tantiwiwat, T-Q. Nguyen, *Adv. Funct. Mater.* **2009**, *19*, 3063.

(8) H. Hoppe, T. Glatzel, M. Niggemann, W. Schwinger, F. Schaeffler, A. Hinsch, M. Ch, Lux-Steiner, N. S. Sariciftci, *Thin Solid Films* **2006**, *511*, 587.

(9) M. M. Wienk, J. M. Kroon, W. J. H. Verhees, J. Knol, J. C. Hummelen, P. A. van Hal, R. A. J. Janssen, *Angew. Chem. Int. Ed.* **2003**, *42*, 3371.

(10) W. Ma, C. Yang, A. J. Heeger, *Adv. Funct. Mater.* **2005**, *15*, 1617.

(11) G. Li, V. Shrotriya, Y. Yao, J. Huang, Y. Yang, *J. Appl. Phys.* **2005**, *98*, 043704.

(12) V. D. Mihailetchi, H. X. Xie, B. de Boer, L. J. A. Koster, P. W. M. Blom, *Adv. Funct. Mater.* **2006**, *16*, 699.

(13) M. Berggren, G. Gustafsson, O. Inganäs, M. R. Andersson, O. Wennerstrom, T. Herberg, *Appl. Phys. Lett.* **1994**, *65*, 1489.

(14) F. Padinger, R. S. Rittberger, N. S. Sariciftci, *Adv. Funct. Mater.* **2003**, *13*, 85.

(15) G. Li, V. Shrotriya, Y. Yao, J. Huang, Y. Yang, *J. Mater. Chem.* **2007**, *17*, 3126.

(16) G. Li, V. Shrotriya, J. Huang, Y. Yao, T. Moriarty, K. Emery, Y. Yang, *Nat. Mater.* **2005**, *4*, 864.

(17) Y. Zhao, Z. Xie, Y. Qu, Y. H. Geng, L. X. Wang, *Appl. Phys. Lett.* **2007**, *90*, 043504.

(18) C.-W. Chu, H. Yang, W.-J. Hou, J. Huang, G. Li, Y. Yang, *Appl. Phys. Lett.* **2008**, *92*, 103306.

(19) T. A. Bull, L. S. C. Pingree, S. A. Jenekhe, D. S. Ginger, C. K. Luscombe, *ACS Nano*, **2009**, *3*, 627.

(20) M. Hiramoto, H. Fujiwara, M. Yokoyama, *J. Appl. Phys.* **1992**, *72*, 3781.

(21) B. Maenning, J. Drechsel, D. Gebeyehu, P. Simon, F. Kozlowski, A. Werner, F. Li, S. Grundmann, S. Sonntag, M. Koch, K. Leo, M. Pfeiffer, H. Hoppe, D. Meissner, N. S. Sariciftci, I. Riedel, V. Dyakonov, J. Parisi, *Appl. Phys. A.* **2004**, *79*, 1.

(22) Y. Matsuo, Y. Sato, T. Niinomi, I. Soga, H. Tanaka, E. Nakamura, *J. Am. Chem. Soc.* **2009**, *131*, 16048.

(23) S. Y. Ku, C. D. Liman, J. E. Cochran, M. F. Toney, M. L. Chabinyc, C. J. Hawker, *Adv. Mater.* **2011**, *23*, 2289.

(24) M. Guide, X. D. Dang, T. Q. Nguyen, *Adv. Mater.* **2011**, *23*, 2313.

(25) Y. Matsuo, E. Nakamura, *Chem. Rev.* **2008**, *108*, 3016.

(26) Y. Matsuo, A. Iwashita, Y. Abe, C. Z. Li, K. Matsuo, M. Hashiguchi, E. Nakamura, *J. Am. Chem. Soc.* **2008**, *130*, 15429.

(27) V. D. Mihailetchi, J. K. J. van Duren, P. W. M. Blom, J. C. Humme-len, R. A. J. Janssen, J. M. Kroon, M. T. Rispens, W. J. H. Verhees, M. M. Wienk, *Adv. Funct. Mater.* **2003**, *13*, 43.

(28) C. Melzer, E. Koop, V. D. Mihailetchi, P. W. M. Blom, *Adv. Funct. Mater.* **2004**, *14*, 865.

(29) C. Goh, R. J. Kline, M. D. McGehee, E. N. Kadnikova, J. M. J. Frechet, *J. Appl. Phys. Lett.* **2005**, *86*, 122110.

(30) V. D. Mihailetchi, H. Xie, B. de Boer, L. J. A. Koster, P. W. M. Blom, *Adv. Funct. Mater.* **2006**, *16*, 699.

(31) P. N. Murgatroyd, *J. Phys. D* **1970**, *3*, 151.

(32) Y. Zhang, H. L. Yip, O. Acton, S. K. Hau, F. Huang, A. K. Y. Jen, *Chem. Mater.* **2009**, *21*, 2598.

(33) H. Tsuji, K. Sato, Y. Sato, E. Nakamura, *Chem. Asian J.* **2010**, *5*, 1294.

(34) P. G. Vekilov, Crystal Growth & Design, **2010**, *10*, 5007.

(35) C. Müller, T. A. M. Ferenczi, M. Campoy-Quiles, J. M. Frost, D. D. C. Bradley, P. Smith, N. Stingelin-Stutzmann, J. Nelson, *Adv. Mater.* **2008**, *20*, 3510.

(36) W.C. Still, M. Kahn, A. Mitra, *J. Org. Chem*. **1978**, *43*, 2923.

(37) (a) R. A. Andersen, G. Wilkinson, *Inorg. Synth*. **1979**, *19*, 262. (b) M. R. Collier, M. F. Lappert, R. Pearce, *J. Chem. Soc*., *Dalton Trans*. **1973**, 445.

Chapter 3

1,8-Diazabicycloundecene-mediated Separation of Singly Bonded Fullerene Dimer and Application to Facile Preparation of $C_{61}H_2$[†]

3.1 Introduction

Fullerene derivatives are key components in the organic thin-film photovoltaic devices. However, the use of chromatography methods for separation and purification is usually required, and has significant environmental issues due to the use of a large amount of organic solvent. In particular, separation of fullerenes frequently requires high-performance liquid chromatography (HPLC) separation with expensive specially designed columns such as Cosmosil Buckyprep-series columns. A key requirement for achieving low cost and high throughput synthesis of high performance fullerenes is to remove or at least limit the use of chromatographic technique.

Nagata and co-workers have reported a simple and low-cost method for the separation of C_{60} from fullerene mixtures by the aid of 1,8-diazabicyclo[5.4.0]undec-7-ene (DBU).[1,2,3] In this method, C_{70} and higher fullerenes form insoluble charge-transfer complexes with DBU through electron transfer from DBU to the fullerene[4] (Figure 1). Selective complexation is probably attributed to the difference in electron affinity between C_{60} and higher fullerenes. Nagata *et al.* discussed that the difference in the reaction rate constant for the complexation of DBU with C_{60} and that of DBU with C_{70} is about 10 times higher for DBU-C60, even though the electron affinity of C_{70} is only 0.08-eV higher than that of C_{60}. They speculated that

not only the difference in electron affinity but the solubility in the reaction solvent as well as the curvature of the π-conjugated system of fullerenes also affects the reactivity of C_{60} and C_{70} with DBU.

The singly bonded fullerene dimer $[C_{60}(CH_2SiMe_2O^iPr)]_2$[5,6,7] is an important starting material to obtain dihydromethano[60]fullerene $C_{61}H_2$,[5] which is a key intermediate for the synthesis of high-performance organic electron acceptors for the use in organic solar cells, for example $[C_{60}(CH_2)$(Ind), Ind = indene], $[C_{60}(CH_2)$(QM), QM = quinodimethane], and $C_{60}(CH_2)(C(Ph)(CH_2)_3CO_2Me)$ (abbreviated PCBM(CH_2)).[8] Another unique characteristic of $[C_{60}(CH_2SiMe_2O^iPr)]_2$ is its dumbbell structure with a C_{60}–C_{60} single bond bearing large cage fragments at both ends. When this fullerene dimer is prepared as for the starting material for the synthesis of $C_{61}H_2$, residual C_{60} in the reaction mixture should be removed before use, because $C_{61}H_2$ and C_{60} share a similar feature and are hard to separate. With consideration about the unique structure of the fullerene dimer, I anticipate that the separation of the fullerene dimer from the dimer and C_{60} mixtures with the aid of DBU is possible. Herein I report a simple procedure for the separation of fullerene dimer $[C_{60}(CH_2SiMe_2O^iPr)]_2$ with selective complexation with DBU, and the synthesis of dihydromethano[60]fullerene $C_{61}H_2$ using the dimer-DBU complex as a starting material.

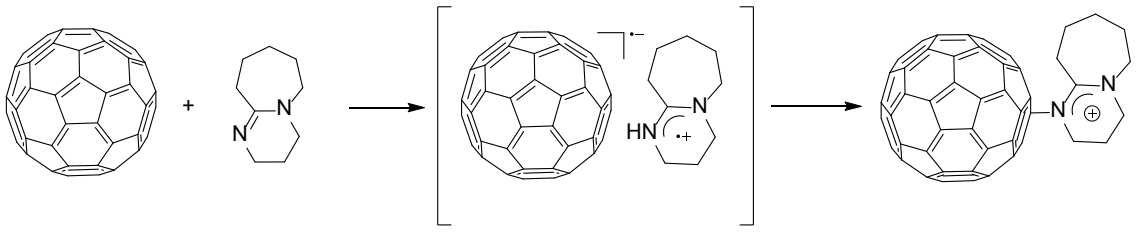

Figure 1. Formation of the charge-transfer complex of fullerene and DBU.

3.2 Separation of Singly Bonded Dimer from the Mixture with C_{60}

A ca. 28:66 mixture (Figure 2a) of C_{60} (52.4 mg, 0.069 mmol) and $[C_{60}(CH_2SiMe_2O^iPr)]_2$ (dimer **1**, 202 mg, 0.117 mmol) was dissolved in 1,2,4-trimethylbenzene (TMB, 15 mL), and the resulting solution was degassed three times. To this solution, DBU (0.25 mL, 9.3 eq.) was added (Scheme 1). A black precipitate was gradually observed, and the content of dimer **1** in the solution phase was reduced accordingly. After 3 h, the precipitate was filtered and washed with TMB, and dried under reduced pressure to obtain black crystals (182.0 mg). It is noteworthy that these crystals were found to be soluble in *o*-dichlorobenzene (ODCB) through decomplexation, which enabled examination of the dimer component by HPLC analysis, and of the ratio of dimer and DBU in the complex by NMR analysis. The component of dimer **1** and C_{60} was 92.9% and 2.8%, respectively (Figure 2b). On the other hand, in the solution phase of the reaction mixture, the ratio of dimer **1** and C_{60} was 6.9% and 78.9%, respectively (Figure 2c). With the NMR analysis of obtained crystals, the ratio of dimer **1** and DBU revealed to 1:1. This result indicated the possibility of separating fullerene and its derivatives without the use of chromatography methods.

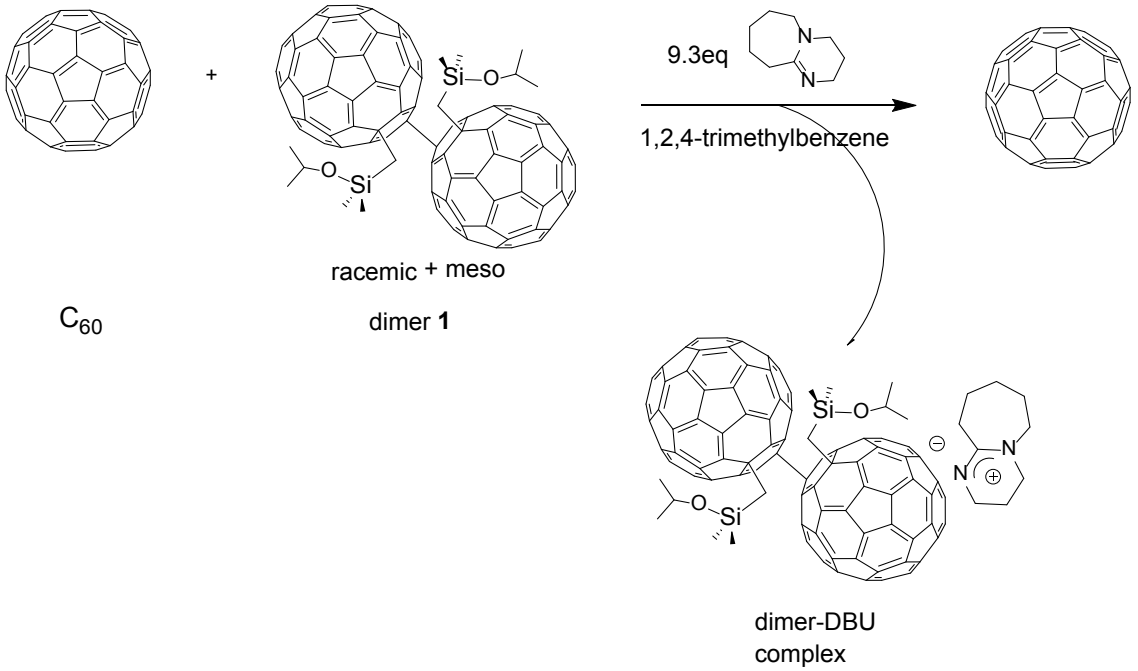

Scheme 1. Separation of singly bonded dimer from the mixture with C_{60}

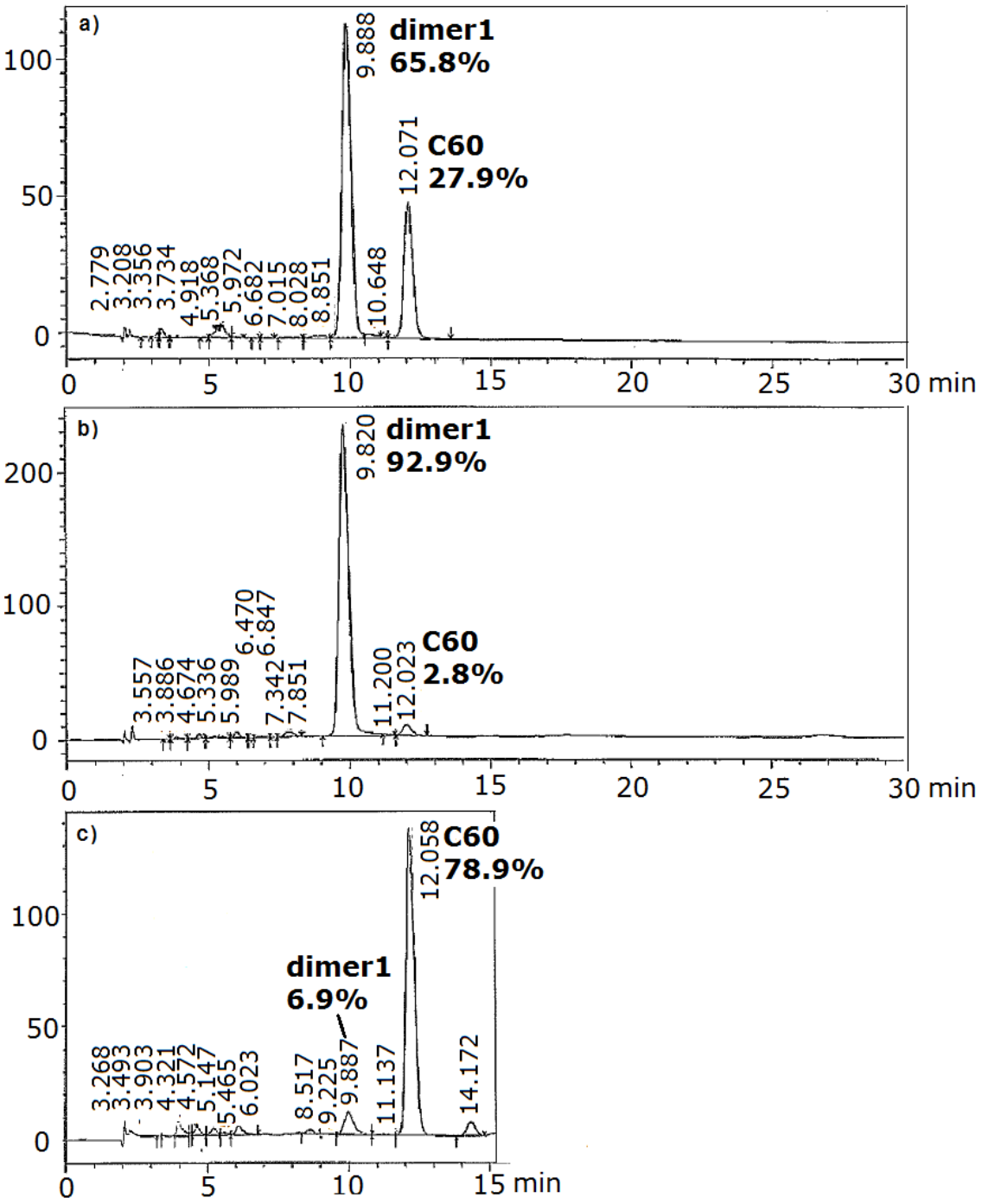

Figure 2. HPLC profiles of the selective complexation of dimer **1** and C_{60}. a) Starting mixture in TMB. b) Crude materials dissolved in ODCB. c) Solution phase from the reaction mixture.

Next, I tried to recover the free dimer from the dimer-DBU complex. The dimer-DBU complex (31.6 mg) was dissolved in ODCB (200 mL), and the resulting solution was degassed three times. After stirring at room temperature for 1 h, the resulting dark red solution was passed through a pad of silica gel to remove dissociated DBU. After volatile components were removed under reduced pressure, the concentrated solution containing the product was reprecipitated by addition of methanol to obtain a dark brown powder (15.5 mg). The resulting powder was dissolved in toluene and was subjected to HPLC analysis. The content ratio of dimer **1** and C_{60} was 94.3% and 4.3%, respectively (Figure 3). The recovery ratio of the free dimer **1** from the dimer-DBU complex was 56%.

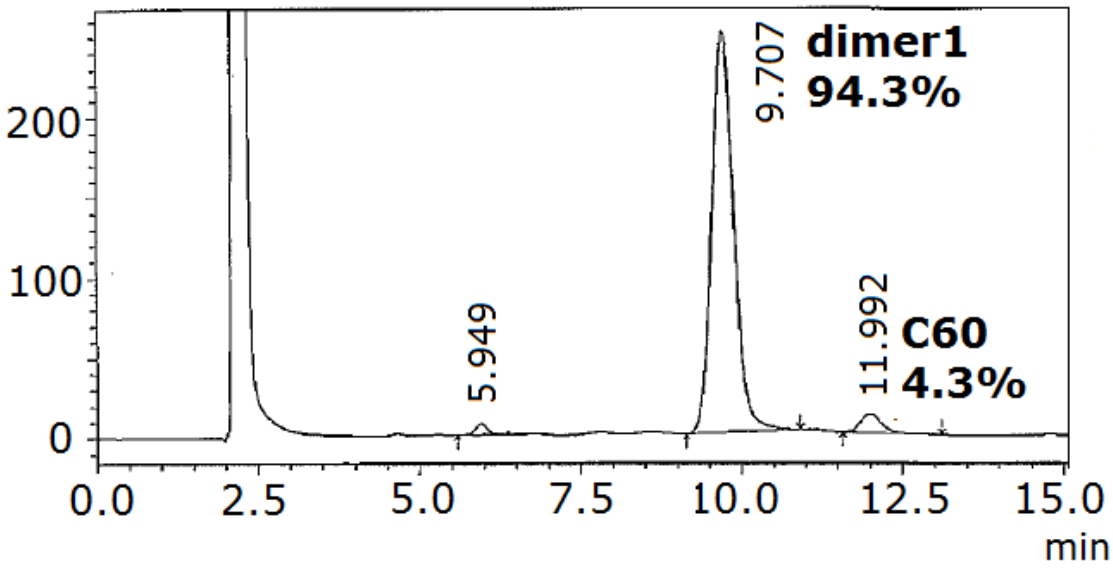

Figure 3. HPLC profile of recovered free-dimer.

In the separation of C_{60} and higher fullerenes reported by Nagata *et al*., water was added to promote the complexation with higher fullerenes and DBU.[2] Note that, in the present study, adding water resulted in reducing the selectivity of the complexation of dimer **1** and C_{60} with DBU, which resulted in the reduction of dimer-recovery from 56% to ca. 0%. In the case of the separation of C_{60} and dimer, it is better to be performed without water.

3.3 Synthesis of $C_{61}H_2$ from the Singly Bonded Dimer-DBU Complex

I also performed synthesis of dihydromethano[60]fullerene ($C_{61}H_2$) from the dimer-DBU complex to demonstrate the application of the dimer-DBU complex for obtaining $C_{61}H_2$ without chromatography methods. After adding ODCB to the dimer-DBU complex (104 mg), copper(II) chloride (146 mg) was added to the solution and the mixture was stirred for 6 h at 180 °C (Scheme 2). The reaction was quenched by adding 50 mL of methanol. The resulting precipitate was collected with filtration and washed with *n*-hexane and methanol, and dried in vacuo to obtain $C_{61}H_2$ as brown crystals (82.9 mg). The HPLC analysis showed that the obtained $C_{61}H_2$ had a purity of 87.4% (Figure 4).

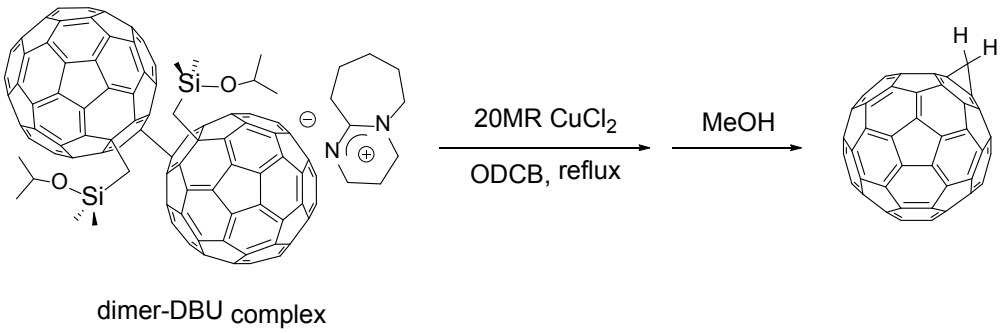

dimer-DBU complex

Scheme 2. Synthesis of dihydromethanofullerene from dimer-DBU complex

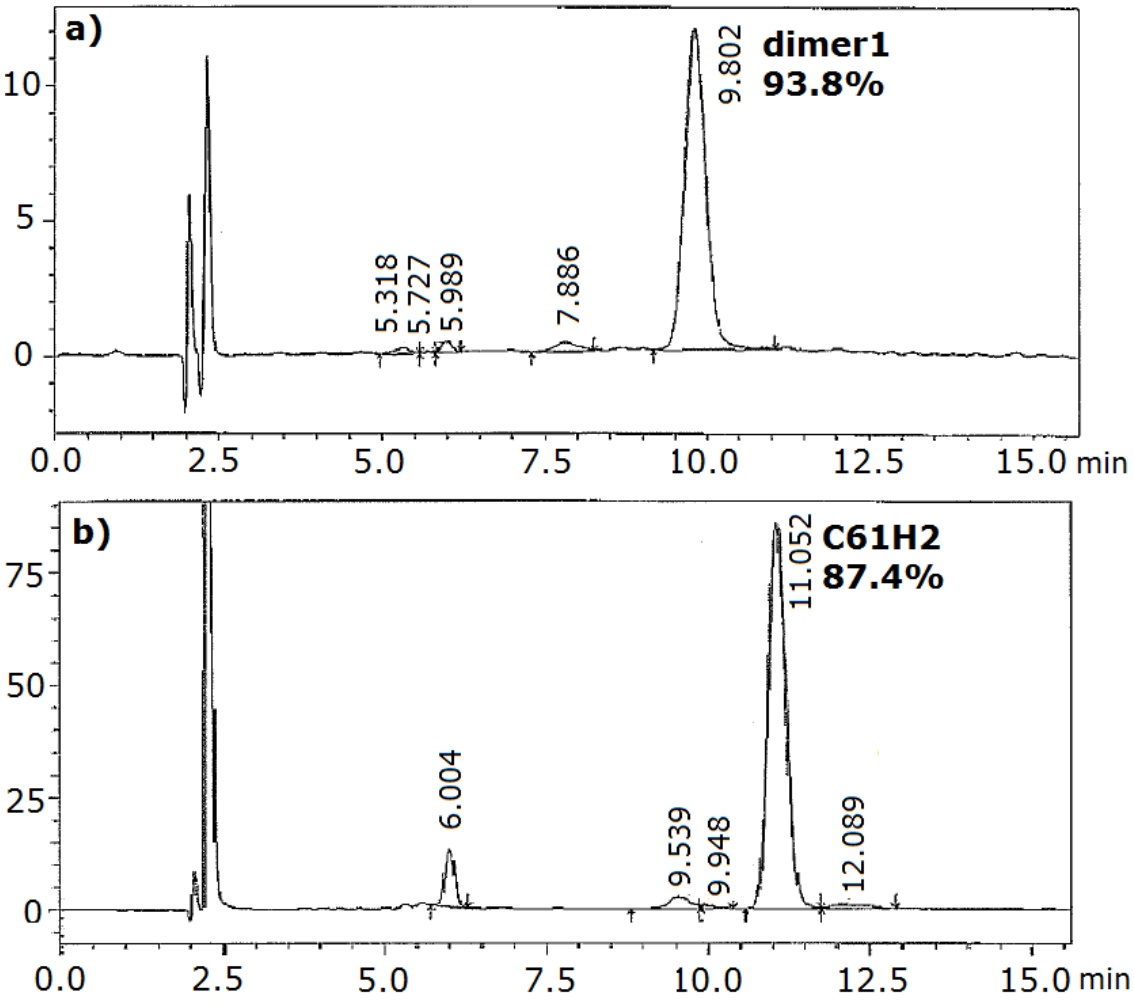

Figure 4. HPLC profiles of synthesis of $C_{61}H_2$. a) Starting mixture in ODCB. b) Crude material dissolved in ODCB.

3.4 Conclusion

I performed the separation of a singly bonded fullerene dimer from a mixture of this dimer and C_{60} using the selective complexation with DBU in TMB. The dimer-DBU complex was found to be desociated into the dimer and DBU in ODCB. A practical method for separating the free-dimer from the dimer-DBU complex could then be realised simply by just dissolving in ODCB and then filtrate through pad of silica gel. Furthermore, the synthesis of the $C_{61}H_2$, which is a key intermediate material in the synthesis of a variety of high-performance electron acceptors for organic thin-film devices,[8] was achieved by using the dimer-DBU complex as the starting material. These results provide a route towards the large scale synthesis of $C_{61}H_2$ without the use of chromatographic purification, that is, make a contribution to enhance efficiency of the development of fullerene derivatives for organic electronic devices.

3.5 Experimental Section

3.5.1 Methods and materials

All reactions dealing with air- or moisture-sensitive compounds were carried out using standard Schlenk technique or a glove box under an argon or nitrogen atmosphere. HPLC analyses were performed on a Shimadzu LC-2010A HT system equipped with SPD-M10A diode array detector and a Buckyprep column (Nacalai Tesque Inc., 4.6 mm ID x 250 mm). NMR spectra were measured with a Bruker AVANCE (400 MHz) spectrometer. Spectra are reported in parts per million from internal tetramethylsilane (δ 0.00 ppm) for ^{1}H NMR. $[C_{60}(CH_2SiMe_2O^iPr)]_2$ was

prepared according to the literature.[5,6,7] [60]Fullerene was purchased from Frontier Carbon Corporation and used as received. Other materials were purchased from Tokyo Chemical Industry Co., Sigma-Aldrich Co., Kanto Chemical Co., Inc., Wako Pure Chemical Industries, or other commercial suppliers and used without further purification.

3.5.2 NMR analysis of singly bonded dimer-DBU complex

I measured ^{1}H NMR spectrum for the dimer-DBU complex dissolved in ODCB-d_4. Assignments of two expected isomers of singly bonded dimer, namely, the *meso* and *racemic* diastereomers, were performed by comparison with the reported spectra.[9] Signals were slightly shifted compared to the free dimer. I ascribe this to weak interaction between the dimer and DBU in ODCB. ^{1}H NMR (400 MHz, ODCB-d_4): δ 0.33 (s, 12H, SiCH_3, *racemic* + *meso*), 0.99 (s, 6H, OCH(CH_3)$_2$, *meso*), 1.00 (s, 6H, OCH(CH_3)$_2$, *meso*) 1.01 (s, 6H, OCH(CH_3)$_2$, *racemic*), 1.02 (s, 6H, OCH(CH_3)$_2$, *racemic*), 1.36–1.66 (m, 10H, DBU), 2.30–2.38 (m, 2H, DBU), 2.51(d, ^2J = 14 Hz, 4H, SiCH_2, *meso*), 2.62 (d, ^2J = 14 Hz, 2H, SiCH_2, *racemic*), 2.76 (d, ^2J = 14 Hz, 2H, SiCH_2, *racemic*), 2.85–2.93 (m, 4H, DBU), 3.10–3.17 (m, 2H, DBU), 3.93–4.06 (m, 2H, OCH(CH$_3$)$_2$).

3.5.3 NMR analysis of recovered free-dimer from dimer-DBU complex

These signals are in good agreement of those from the authentic sample.[5] ^{1}H NMR (400 MHz, ODCB-d_4): δ 0.34 (s, 12H, SiCH_3, *racemic* + *meso*), 0.99 (s, 6H, OCH(CH_3)$_2$, *meso*), 1.00 (s, 6H, OCH(CH_3)$_2$, *meso*) 1.01 (s, 6H, OCH(CH_3)$_2$, *racemic*),

1.02 (s, 6H, OCH(CH_3)$_2$, *racemic*), 2.52 (d, ^2J = 14 Hz, 4H, SiCH_2, *meso*), 2.62 (d, ^2J = 14 Hz, 2H, SiCH_2, *racemic*), 2.78 (d, ^2J = 14Hz, 2H, SiCH_2, *racemic*), 3.93–4.06 (m, 2H, OC*H*(CH_3)$_2$).

3.6 References and Notes

† This chapter is published on *Fullerenes, Nanotubes and Carbon Nanostructures* in press.

(1) K. Nagata, E. Dejima, Y. Kikuchi, M. Hashiguchi, *Chem. Lett.* **2005**, *34*, 178.

(2) K. Nagata, E. Dejima, Y. Kikuchi, M. Hashiguchi, *Org. Process Res. Dev.* **2005**, *9*, 660.

(3) M. Hashiguchi, K. Nagata, K. Tanaka, Y. Matsuo, *Org. Process Res. Dev.* **2012***, 16*, 643.

(4) A. Skiebe, A. Hirsch, H. Klos, B. Gotschy, *Chem. Phys. Lett.* **1994**, *220*, 138.

(5) Y. Zhang, Y. Matsuo, C.-Z. Li, H. Tanaka, E. Nakamura, *J. Am. Chem. Soc.* **2011**, *133*, 8086.

(6) Y. Zhang, Y. Matsuo, E. Nakamura, *Org. Lett.* **2011**, *13*, 6058.

(7) Z. Xiao, Y. Matsuo, M. Maruyama, E. Nakamura, *Org. Lett.* **2013**, *15*, 2176.

(8) Y. Matsuo, J. Kawai, H. Inada, T. Nakagawa, H. Ota, S. Otsubo, E. Nakamura, *Adv. Mater.* **2013**, *25*, 6266.

(9) G. W. Wang, C.-Z.Wang, S.-E. Zhua, Y. Murata, *Chem. Commun.* **2011**, *47*, 6111.

Chapter 4

Low-LUMO 56π-Electron Fullerene Acceptors Bearing Electron-withdrawing Cyano Groups for Small-Molecule Organic Solar Cells[†]

4.1 Introduction

Organic solar cells (OSCs) are being developed as a viable technology for low-cost, environmentally friendly energy production.[(1)] Among them, small-molecule organic solar cells (SMOSCs) are emerging as a promising route to high-efficiency devices, having already achieved a power conversion efficiency (PCE) of >8%.[(2,3,4)] Small-molecule semiconductors offer several advantages over their polymeric counterparts such as more facile synthesis and purification, inherent monodispersity and high tunability, with the latter leading to a diverse range of efficient chromophores.[(5,6,7,8,9,10)] While SMOSCs have increased in efficiency in recent years with the development of various small molecule electron donors, the repertoire of fullerene electron acceptors has been limited. Most reports have used [6,6]-phenyl-C_{61}-butyric acid methyl ester (PCBM) for solution-processed devices and C_{60} for evaporated ones. I have also used soluble 1,4-silylmethylfullerene (SIMEF) [(11)] in tetrabenzoporphyrin-based SMOSCs to form an ideal interpenetrated donor/acceptor interface structure.[(12,13)] As SIMEF has shown, developing new fullerene derivatives is a new direction of research in this field.

On the road towards improved fullerene design, little attention has been devoted to developing low-LUMO fullerenes. Most of the focus has been directed towards obtaining high-LUMO 56π fullerenes, which have been regarded as high-performance

acceptors.[14,15,16,17,18,19,20] However, recent studies on polymer and small-molecule OSCs, as well as tandem OSCs, have started to require low-LUMO fullerenes too. The reason behind these requirements is that as the bandgaps of donors become narrower and the HOMO levels of donors are lowered, fullerene acceptors with lower LUMO levels are generally needed[21] for suitable band energy alignment to induce efficient exciton dissociation. For such purposes, dicyano[60]fullerene, $C_{60}(CN)_2$, reported by Wudl and co-workers,[22] can be regarded as a representative low-LUMO fullerene derivative.[13] The LUMO level of $C_{60}(CN)_2$ is 0.1 eV deeper than that of C_{60} because of its two strong electron-withdrawing cyano groups. However, the low solubility and high crystallinity of $C_{60}(CN)_2$ make it difficult to obtain good quality thin films, which limits its use in solution-processed OSCs. Herein I report the synthesis of soluble low-LUMO fullerenes (Figure 1). In this work, I focused on using these fullerenes in SMOSCs containing chloroindium phthalocyanine (InClPc)[23] as a low bandgap small molecule donor (Figure 2). Respectable PCEs of ~2% were obtained for p-n heterojunction devices, indicating the potential of these new acceptors in OSC research.

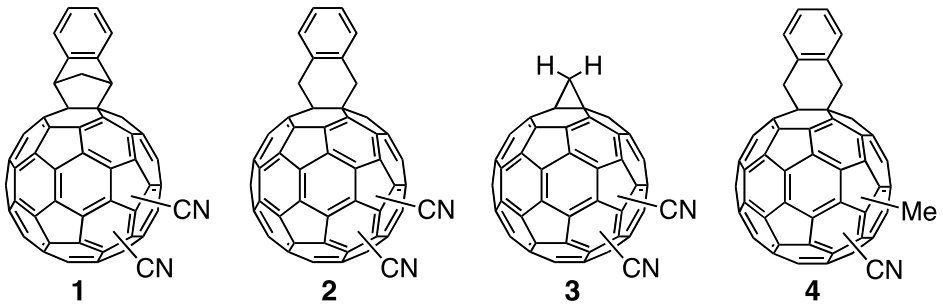

Figure 1. 56π-electron fullerenes bearing cyano groups.

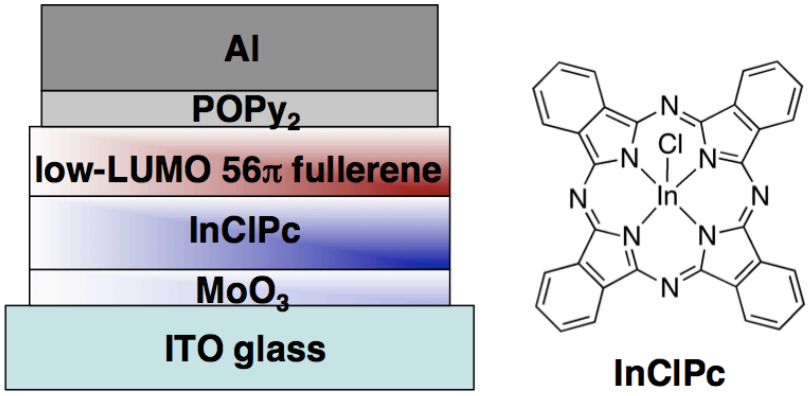

Figure 2. Device configuration and the structure of InClPc.

4.2 Synthesis of 56π-Electron Low-LUMO Fullerenes

I synthesized the 56π-electron fullerene derivatives with low LUMO levels $C_{60}(Ind)(CN)_2$ (**1**), $C_{60}(QM)(CN)_2$ (**2**) and $C_{60}(CH_2)(CN)_2$ (**3**) (Ind = indene; QM = quinodimethane), as well as a methylated compound $C_{60}(QM)(CN)(Me)$ (**4**) (Figure 1, Scheme 1). First, cyano groups were introduced onto 58π-electron fullerenes, including an indene monoadduct ($C_{60}(Ind)$),[15] quinodimethane monoadduct ($C_{60}(QM)$),[24] and dihydromethanofullerene ($C_{60}(CH_2)$).[7] Treatment of a solution of 58π-electron fullerenes in *o*-dichlorobenzene with a solution of sodium cyanide in DMF at ambient temperature immediately afforded intermediate sodium salts of fullerene cyanides, which were reacted *in situ* with electrophilic cyano compounds. Reaction with *p*-toluenesulfonyl cyanide (TsCN) at 100 °C for 8 h produced 56π-electron dicyano fullerene derivatives **1**–**3** in isolated yields of 20–46%. By using methyl trifluoromethanesulfonate (MeOTf) as an electrophile, I also synthesized methylated compound **4** in 6.5% yield. Overall, a favorable feature of this reaction is the ability to control the number of addends. Undesired multiple adducts, which are ordinarily seen in the synthesis of 56π-electron fullerenes,[15] do not form because the first nucleophilic

addition produces a negatively charged fullerene derivative (*e.g.*, $C_{60}(Ind)(CN)^-$), preventing further nucleophilic addition.

Compounds **1**–**4** were soluble in various organic solvents such as toluene, chlorobenzene, and chloroform. The solubilities of **1**–**4** in toluene were 1.4, 1.4, 0.8, and 1.8 wt%, respectively. Solubilizing groups such as Ind and QM along with the fact that the products are regioisomeric mixtures of 56π-electron fullerenes are responsible for this solubility. Compounds **1**–**4** were all stable in air, and showed thermal stability until at least 350 °C according to thermogravimetry–differential thermal analysis under nitrogen gas flow.

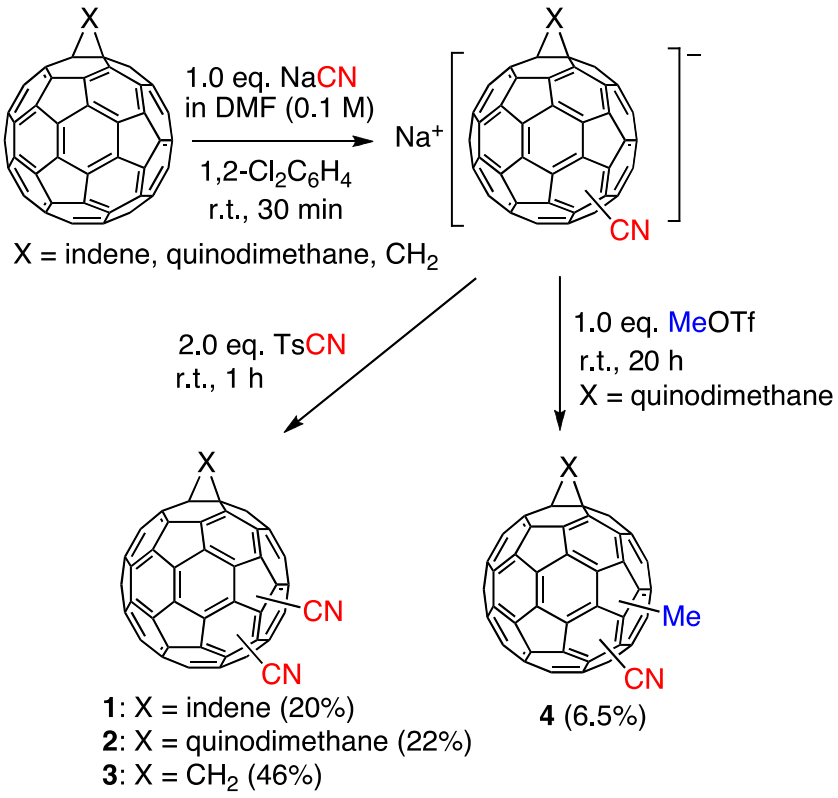

Scheme 1. Synthesis of low-LUMO 56π-electron fullerenes **1**–**4**

4.3 Electrochemical Properties of 56π-Electron Low-LUMO Fullerenes

Next I investigated the electrochemical properties of 56π-electron low-LUMO fullerenes **1**–**4** as well as those of the starting materials and reference compounds (Table 1). Cyclic voltammograms obtained for **1**–**4** exhibited three reversible one-electron reduction waves (Figure 3-6). Reduction potentials for compounds **1**–**3** were positively shifted compared with those for their parent 58π-electron fullerenes, consistent with the introduction of electron-withdrawing cyano groups. I estimated the LUMO levels of compounds **1**–**4** from their first reduction potentials[25] using the equation shown in the footnote of Table 1.[11] The LUMO levels of **1** and **2** (−3.87 and −3.88 eV, respectively) were comparable with that of pristine C_{60} (−3.89 eV). They represent rare examples of raising solubility without changing the LUMO level of fullerene.[21] More interestingly, the dihydromethano dicyano fullerene **3** was found to have a deep LUMO level at −3.96 eV. This LUMO level is lower than that of C_{60}, like the LUMO level of $C_{60}(CN)_2$.[22] Meanwhile, the LUMO level of the methylated compound **4** was high lying (−3.75 eV). This value is comparable with that of SIMEF[11], which is known as a high-LUMO fullerene that gives rise to high open-circuit voltage (V_{OC}).[12, 26, 27] Because electron-withdrawing cyano and electron-donating methyl groups are directly connected to the fullerene core, the LUMO levels of compounds **1**–**4** were widely tunable over a range of 200 meV. This tunability can potentially be exploited in future studies to provide optimum energy levels alignment with a range of electron donors by selecting the fullerene that is most compatible with the donor of choice. The lower LUMO level of the dihydromethano compound **3** compared with those of Ind and QM compounds **1** and **2** is explained by the weaker electron-donating nature of the strained three-membered ring compared with those of the five-membered ring systems.[16]

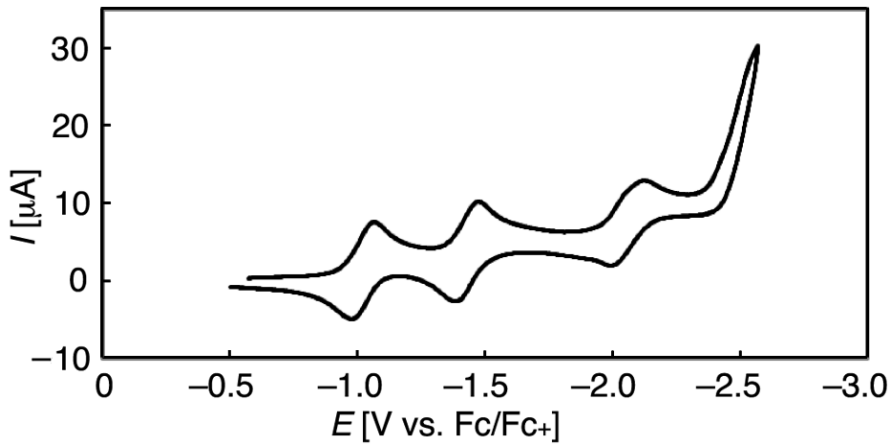

Figure 3. Cyclic voltammogram obtained for **1**

in o-dichlorobenzene/acetonitrile (4/1, v/v).

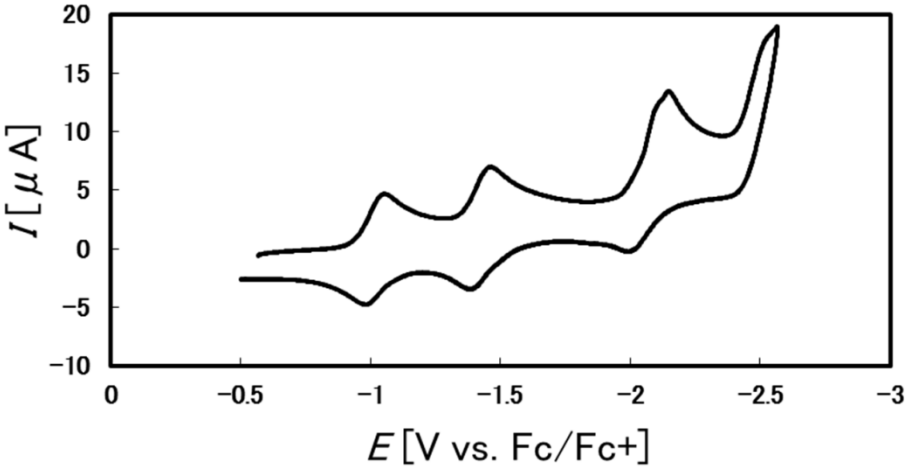

Figure 4. Cyclic voltammogram obtained for **2**

in o-dichlorobenzene/acetonitrile (4/1, v/v).

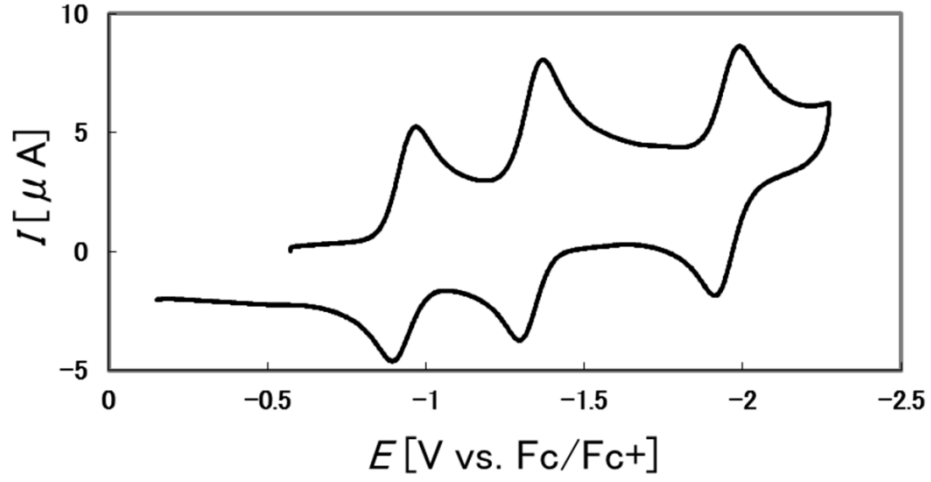

Figure 5. Cyclic voltammogram obtained for **3**

in o-dichlorobenzene/acetonitrile (4/1, v/v).

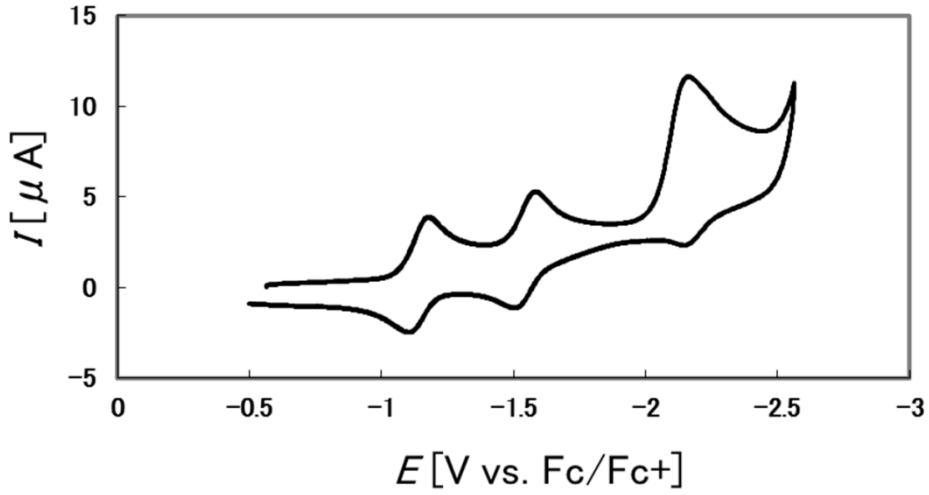

Figure 6. Cyclic voltammogram obtained for **4**

in o-dichlorobenzene/acetonitrile (4/1, v/v).

Table 1. Reduction potentials (V *vs*. Fc/Fc^+) and estimated LUMO levels for **1–4** and reference compounds[a,b]

Compound	$E_{1/2}^{red1}$ [V]	$E_{1/2}^{red2}$ [V]	$E_{1/2}^{red3}$ [V]	LUMO level [eV]
1	−1.02	−1.43	−1.89	−3.87
2	−1.02	−1.42	−1.76	−3.88
3	−0.93	−1.33	−1.95	−3.96
4	−1.14	−1.54	N.A.[d]	−3.75
C_{60}(Ind)	−1.13	−1.53	−2.06	−3.76
C_{60}(QM)	−1.11	−1.51	−1.97	−3.78
$C_{60}(CH_2)$	−1.09	−1.49	−1.99	−3.80
SIMEF[c]	−1.06	−1.63	−2.23	−3.74
PCBM[c]	−1.00	−1.59	−2.19	−3.80
PCBM	–1.09	–1.49	–2.10	–3.80
C_{60}	−1.00	−1.41	−1.87	−3.89

[a] Potential in V *vs*. a ferrocene–ferrocenium couple was measured by cyclic voltammetry in *o*-dichlorobenzene/acetonitrile (4/1, v/v) solution containing $Bu_4N^+PF_6^-$ (0.1 M) as a supporting electrolyte at 25 °C and a scan rate of 0.1 V/s. Glassy-carbon, platinum wire, and Ag/Ag^+ electrodes were used as working, counter, and reference electrodes, respectively. [b] Values for the LUMO level were estimated using the following equation: LUMO level = $-(4.89 + E_{1/2}^{red1})$ [eV]. [c] Potentials were determined in THF containing $Bu_4N^+PF_6^-$ (0.1 M), and LUMO levels were estimated using the following equation: LUMO level = $-(4.80 + E_{1/2}^{red1})$ [eV]. [d] Not available due to irreversible waves.

4.4 OPV Device Performances of 56π-Electron Low-LUMO Fullerenes

I studied the performance of SMOSCs containing InClPc as a low-bandgap small-molecule electron donor and fullerenes **1**–**4** as electron acceptors. Bilayer p-n

heterojunction devices were fabricated with the following configuration: ITO/MoO_3/InClPc/fullerene acceptor/$POPy_2$/Al ($POPy_2$ = phenyl-dipyrenylphosphine oxide). Under optimum conditions, the device containing **1** exhibited a PCE of 2.0% with short-circuit current density (J_{SC}) = 7.05 mA/cm^2, V_{OC} = 0.62 V, and fill factor (FF) = 0.45 (Table 2, Figure 7). This PCE is slightly higher than that of the reference device using PCBM. Comparison of the devices containing **1** and PCBM revealed a large difference in V_{OC} of 120 mV, which was expected because of the low LUMO level of **1**. However, the device containing **1** gave higher J_{SC}, which led to its slightly higher PCE. In general, the use of low-LUMO acceptors such as pristine C_{60} tends to give lower PCE because of the decrease in V_{OC}. However, in the present case, while the device containing **1** did show lower V_{OC} *vs*. that with PCBM, it compensated for the decrease in V_{OC} through an increase in J_{SC}. We thus consider the obtained performance to be respectable, which suggests that compound **1** is a good candidate as an electron acceptor for donor materials with deep HOMO and LUMO levels. Recent development of low-bandgap donor materials is progressing in this direction, so low-LUMO fullerene acceptors will be required to take full advantage of the excellent optoelectronic characteristics of such donors. The relatively high J_{SC} measured for the device containing **1** suggests that these fullerene derivatives could also be used in tandem solar cells to improve the photocurrent generated by the front sub-cell and current matching with the photocurrent from the rear sub-cell.[28,29]

Table 2. Photovoltaic performance of SMOSCs containing a InClPc donor and fullerene acceptors under AM1.5G (100 mA/cm^2) light illumination

acceptor	J_{SC} [mA/cm^2]	V_{OC} [V]	FF [–]	PCE [%]
1	7.05	0.62	0.45	2.0
2	6.24	0.62	0.45	1.8
4	4.67	0.74	0.42	1.5
PCBM	5.46	0.74	0.48	1.9

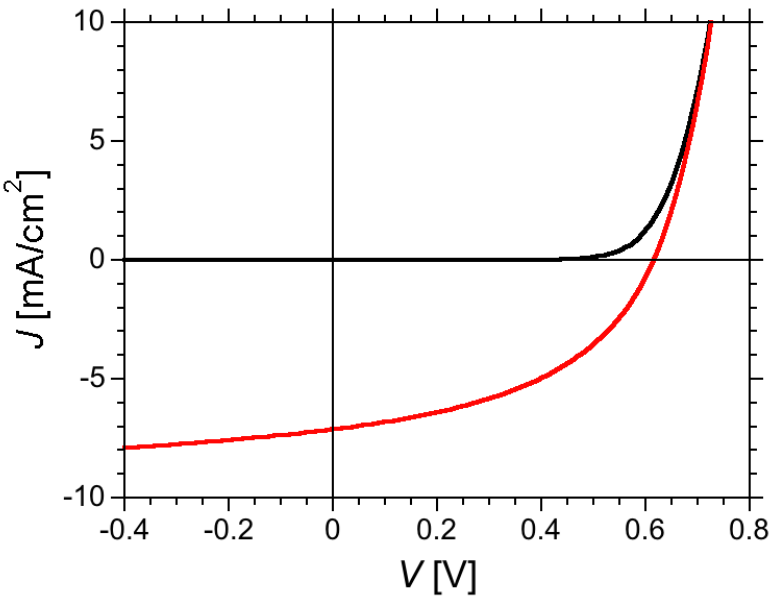

Figure 7. *J*-*V* curves measured for the photocurrent and that in the dark for the device containing **1**.

Turning to devices fabricated with the other low-LUMO fullerene derivatives synthesized, I found that the device with acceptor **2** showed slightly lower PCE compared with that of the device containing **1** because of its lower V_{OC}. The properties of acceptor **3** with the strongest electron-accepting ability of the present four

compounds could not be fairly evaluated because of its low solubility arising from its lack of solubilizing groups. Cyano and dihydromethano groups do not increase solubility markedly. The device containing acceptor **4** showed relatively high V_{OC} because of the larger offset between its LUMO level and the HOMO level of the donor compared with that of the device containing **1**. However, the PCE of the device using **4** was not high. In this work, I fabricated p-n heterojunction SMOSCs because of recent advances in SMOSCs and simple evaluation of systems free from the influence of complex phase separation behavior.[30,31,32] The next stage of research is to investigate the performance of OSCs with various low-bandgap or deep-HOMO polymers and construct ideal phase-separated structures in solution-processed bulk heterojunction[33] and p-i-n junction devices.[12]

4.5 Conclusion

In summary, I synthesized fullerene acceptors with low LUMO levels, which are comparable with or lower than that of pristine C_{60}. Our molecular design relies on electron-withdrawing cyano groups to lower LUMO levels and the presence of regioisomeric mixtures of 56π-electron fullerenes to achieve respectable solubility. Specifically, the low-LUMO 56π-electron fullerenes C_{60}(Ind)$(CN)_2$ (**1**), C_{60}(QM)$(CN)_2$ (**2**) and $C_{60}(CH_2)(CN)_2$ (**3**) presented in this work have LUMO levels of −3.87 to −3.96 eV and solubilities of 0.8 to 1.4 wt% in toluene. These values suggest that the present fullerenes are solution-processable low-LUMO acceptors that can be distinguished from partly-soluble C_{60} and ordinary fullerene derivatives that are soluble but possess high LUMO levels. The performance of these new low-LUMO fullerenes in p-n heterojunction SMOSCs using InClPc as a donor showed that the fullerenes acted as

efficient electron acceptors. The respectable performance obtained for the p-n heterojunction cells indicates that these new fullerenes are promising electron acceptors for low-bandgap organic semiconductors. Moreover, this work contributes to developing design rules to obtain commendable fullerene acceptors for OSCs.

4.6 Experimental Section

4.6.1 Synthesis

General Considerations. All reactions dealing with air- or moisture-sensitive compounds were carried out using standard Schlenk technique or a glove box under an argon or nitrogen atmosphere. HPLC analyses were performed on a LC-2010A HT system equipped with SPD-M10A diode array detector and a Buckyprep column (Nacalai Tesque Inc., 4.6 mm ID x 250 mm). Flash silica gel column chromatography was performed on silica gel 60N (Kanto Chemical, spherical and neutral, 140–325mesh). Gel permeation column chromatography was performed on a Japan Analytical Industry LC-9201 (eluent: $CHCl_3$) with JAIGEL H-40P polystyrene column. NMR spectra were measured with a Bruker AVANCE (400 MHz) spectrometer. Spectra are reported in parts per million from internal tetramethylsilane (δ 0.00 ppm) for ^1H NMR. Mass spectra were measured by APCI using a time-of-flight mass analyzer on a Waters LCT Premier XE (AccuTOF) spectrometer.

Synthesis of C_{60}(Ind)$(CN)_2$ (1). C_{60}(Ind) (92.3 mg, 0.110 mmol) was dissolved in *o*-dichlorobenzene, and the resulting solution was degassed three times. To this solution a 0.1 M DMF solution of NaCN (1.1 mL) was dropped. Color of the solution

was immediately changed from dark red to dark green, indicating formation of the fullerene derivative anion, $C_{60}(Ind)(CN)^-$. After stirring at room temperature at 30 min, an *o*-dichlorobenzene solution of TsCN (40.6 mg, 0.22 mmol, 1.0 mL) to the dark green solution. Immediate color change was again observed from dark green to dark brown. After stirring at room temperature for 1 h, the resulting reaction mixture was subjected a HPLC analysis to monitor the progress of the reaction. Solvent was removed from the resulting solution with a rotary evaporator. The obtained residue was dissolved in toluene, and subjected to silica gel column chromatography separation (eluent, toluene/*n*-hexane 1:4 to 4:1). After the first fraction containing the starting material $C_{60}(Ind)$, the second fraction containing the product **1** was collected. This solution was concentrated with a rotary evaporator, and further purification of the product was carried out with GPC separation. The fraction containing the product **1** was collected and concentrated, then subjected to re-precipitation with methanol. The resulting solid was collected with filtration, and dried in vacuo to obtain **1** as a mixture of regioisomers. Yield, 19.5 mg (20%). ^{1}H NMR (500 MHz, $CDCl_3$): δ 2.67–3.82 (m, 2H, CH_2), 4.59–5.01 (m, 2H, CH), 7.31–7.40 (m, 2H, Ph), 7.47–7.83 (m, 2H, Ph). APCI-MS(–) for $C_{71}H_8N_2$ [M-]: calcd.888; found 888.

Synthesis of $C_{60}(QM)(CN)_2$ (2). $C_{60}(QM)$ (100.0 mg, 0.121 mmol) was dissolved in *o*-dichlorobenzene, and the resulting solution was degassed three times. To this solution a 0.1 M DMF solution of NaCN (1.2 mL) was dropped. Color of the solution was immediately changed from dark red to dark green, indicating formation of the fullerene derivative anion, $C_{60}(QM)(CN)^-$. After stirring at room temperature at 30 min, an *o*-dichlorobenzene solution of TsCN (44.8 mg, 0.247 mmol, 1.0 mL) to the dark

green solution. Immediate color change was again observed from dark green to dark brown. After stirring at room temperature for 1 h, the resulting reaction mixture was subjected a HPLC analysis to monitor the progress of the reaction. Solvent was removed from the resulting solution with a rotary evaporator. The obtained residue was dissolved in toluene, and subjected to silica gel column chromatography separation (eluent, toluene/*n*-hexane 1:4 to 4:1). After the first fraction containing the starting material C_{60}(QM), the second fraction containing the product **2** was collected. This solution was concentrated with a rotary evaporator, and further purification of the product was carried out with GPC separation. The fraction containing the product **2** was collected and concentrated, then subjected to re-precipitation with methanol. The resulting solid was collected with filtration, and dried in vacuo to obtain **2** as a mixture of regioisomers. Yield, 23.0 mg (22%). ^{1}H NMR (500 MHz, $CDCl_3$): δ 4.00–4.81 (m, 4H, CH_2), 7.41–7.63 (m, 4H, Ph). APCI-MS(–) for $C_{70}H_8N_2$ [M-]: calcd.876; found 876.

Synthesis of $C_{60}(CH_2)(CN)_2$ (3). $C_{61}H_2$ (301.6 mg, 0.411 mmol) was dissolved in *o*-dichlorobenzene, and the resulting solution was degassed three times. To this solution a 0.1 M DMF solution of NaCN (4.0 mL) was dropped. Color of the solution was immediately changed from dark red to dark green, indicating formation of the fullerene derivative anion, $C_{61}H_2(CN)^-$. After stirring at room temperature at 15 min, an *o*-dichlorobenzene solution of TsCN (152.9 mg, 0.844 mmol, 5.0 mL) to the dark green solution. Immediate color change was again observed from dark green to dark brown. After stirring at room temperature for 1 h, the resulting reaction mixture was subjected a HPLC analysis to monitor the progress of the reaction. Solvent was removed from the resulting solution with a rotary evaporator. The obtained residue was dissolved in

toluene, and subjected to silica gel column chromatography separation (eluent, toluene/*n*-hexane 1:4 to 4:1). After the first fraction containing the starting material $C_{61}H_2$, the second fraction containing the product **3** was collected. This solution was concentrated with a rotary evaporator, and subjected to re-precipitation with methanol. The resulting solid was collected with filtration, and dried in vacuo to obtain **3** as a mixture of regioisomers. Yield, 150.9 mg (46%). ^{1}H NMR (500 MHz, $CDCl_3$): δ 3.09–3.11 (d, J = 7.2 Hz, 1H, methano-CH_2), 3.48–3.50 (d, J = 6.0 Hz, 2H, methano-CH_2, isomer), 3.70–3.71 (d, J = 6.8 Hz, 1H, methano-CH_2, other isomer), 3.74–3.76 (d, J = 6.8 Hz, 1H, methano-CH_2, other isomer), 4.30-4.32 (d, J = 7.2 Hz, 1H, methano-CH_2). APCI-MS(–) for $C_{63}H_2N_2$ [M-]: calcd.786; found 786.

Synthesis of C_{60}(QM)(CN)(Me) (4). C_{60}(QM) (202.2 mg, 0.245 mmol) was dissolved in *o*-dichlorobenzene, and the resulting solution was degassed three times. To this solution a 0.1 M DMF solution of NaCN (2.5 mL) was dropped. Color of the solution was immediately changed from dark red to dark green, indicating formation of the fullerene derivative anion, $C_{60}(QM)(CN)^-$. After stirring at room temperature at 30 min, MeOTf (203.4 mg, 1.239 mmol) to the dark green solution. The significant color change of solution was not observed. After stirring at room temperature for 20 h, the resulting reaction mixture was subjected a HPLC analysis to monitor the progress of the reaction. The reaction mixture was added with 200 mL MeOH and resulting solid was collected with filtration. The obtained solid was dissolved in CS_2, and subjected to silica gel column chromatography separation (eluent, toluene/*n*-hexane 1:4 to 4:1). After the first fraction containing the starting material C_{60}(QM), the second fraction containing the product **4** and a protonated compound (C_{60}(QM)(CN)H) were collected. This

solution was concentrated with a rotary evaporator, and subjected to GPC separation to obtain **4**. The obtained fraction after recycling several times was concentrated with a rotary evaporator, and subjected to re-precipitation with methanol. The resulting solid was collected with filtration, and dried in vacuo to obtain **4** as a mixture of regioisomers. Yield, 13.7 mg (6.5%). ^{1}H NMR (500 MHz, $CDCl_3$): δ 2.88–3.57 (m, 3H, CH_3), 4.08–4.81 (m, 4H, CH_2), 7.39–7.80 (m, 4H, Ph). APCI-MS(–) for $C_{70}H_{11}N$ [M-]: calcd.865; found 865.

4.6.2 Cyclic Voltammetry

Cyclic voltammetry (CV) was performed using ALS/CHI602C Electrochemical analyzer. All measurements were carried out in a one-compartment cell under Ar gas, equipped with a glassy-carbon working electrode, a platinum wire counter electrode, and an Ag/Ag^+ reference electrode. Measurements were performed in *o*-dichlorobenzene/acetonitrile (4/1, v/v) solution containing tetrabutylammonium perchlorate (0.1 M) as a supporting electrolyte at 25 ºC with a scan rate of 0.1 V/s. All potentials were corrected against Fc/Fc^+.

4.6.3 Fabrication and Characterization of OPVs

Organic solar cells having a p-n heterojunction structure were fabricated as follows. An ITO-coated glass substrate was exposed to UV ozone for 10 min, and then 10-nm-thick MoO_3 (Koujundo Chemical Laboratory Co.) film as a hole transport layer was deposited by vacuum evaporation on the substrate. Then, InClPc was evaporated on the MoO_3 layer at the deposition rate of 0.1 nm/s. The thickness of the InClPc p-layer was 28 nm. On top of the p-layer, a 0.7 wt% solution of fullerene derivatives in toluene

was spin-coated (1000 rpm) as an n-layer. The thickness of the n-layer was approximately 30 nm. After thermal annealing of the p-n film at 120 °C for 10 min on a hot plate, the $POPy_2$/Al electrode ($POPy_2$ = 6 nm; Al = 80 nm) was evaporated onto the film, giving a device with an active area of 0.25 cm^2. Finally, the device was annealed at 120 °C for 5 min.

The current density-voltage (*J-V*) behavior of the encapsulated OPVs was measured under both dark and irradiated conditions with a mask of 0.16 cm^2 aperture. Current-voltage sweeps were obtained with a Keithley 2400 source measurement unit controlled by a computer. The light source for determination of power conversion efficiency was an AM1.5G solar simulator system (Sumitomo Heavy Industries Advanced Machinery) with an intensity of 100 mW/cm^2.

4.7 References and Notes

† This chapter is published on *Org. Electron.* **2013**, *14*, 3306.

(1) S. R. Forrest, *Nature* **2004**, *428*, 911.

(2) Y. Sun, G. C. Welch, W. L. Leong, C. J. Takacs, G. C. Bazan, A. J. Heeger, *Nat. Mater.* **2012**, *11*, 44.

(3) Z. Li, G. He, X. Wan, Y. Liu, J. Zhou, G. Long, Y. Zuo, M. Zhang, Y. Chen, *Adv. Energy Mater.* **2012**, *2*, 74.

(4) J. Y. Zhou, Y. Zuo, X. J. Wan, G. K. Long, Q. Zhang, W. Ni, Y. S. Liu, Z. Li, G. R. He, C. X. Li, B. Kan, M. M. Li, Y. S. Chen, *J. Am. Chem. Soc.* **2013**, *135*, 8484.

(5) J. Roncali, *Acc. Chem. Res.* **2009**, *42*, 1719.

(6) B. Walker, C. Kim, T.-Q. Nguyen, *Chem. Mater.* **2011**, *23*, 470.

(7) P. M. Beaujuge, J. M. J. Fréchet, *J. Am. Chem. Soc.* **2011**, *133*, 20009.

(8) A. Mishra, P. Bäuerle, *Angew. Chem. Int. Ed*. **2012**, *51*, 2020.

(9) J. Hatano, N. Obata, S. Yamaguchi, T. Yasuda, Y. Matsuo, *J. Mater. Chem.* **2012**, *22*, 19258.

(10) T. Yamamoto, J. Hatano, T. Nakagawa, S. Yamaguchi, Y. Matsuo, *Appl. Phys. Lett.* **2013**, *102*, 13305.

(11) Y. Matsuo, A. Iwashita, Y. Abe, C.-Z. Li, K. Matsuo, M. Hashiguchi, E. Nakamura, *J. Am. Chem. Soc.* **2008**, *130*, 15429.

(12) Y. Matsuo, Y. Sato, T. Niinomi, I. Soga, H. Tanaka, E. Nakamura, *J. Am. Chem. Soc.* **2009**, *131*, 16048.

(13) H. Tanaka, Y. Abe, Y. Matsuo, J. Kawai, I. Soga, Y. Sato, E. Nakamura, *Adv. Mater.* **2012**, *24*, 3521.

(14) M. Lenes, G.-J. A. H. Wetzelaer, F. B. Kooistra, S. C. Veenstra, J. C. Hummelen, P. W. M. Blom, *Adv. Mater.* **2008**, *20*, 2116.

(15) Y. He, H.-Y. Chen, J. Hou, Y. Li, *J. Am. Chem. Soc.* **2010**, *132*, 1377.

(16) Y. Zhang, Y. Matsuo, C.-Z. Li, H. Tanaka, E. Nakamura, *J. Am. Chem. Soc.* **2011**, *133*, 8086.

(17) C.-Z. Li, S.-C. Chien, H.-L. Yip, C.-C. Chueh, F.-C. Chen, Y. Matsuo, E. Nakamura, A. K.-Y. Jen, *Chem. Commun.* **2011**, *47*, 10082.

(18) C.-Z. Li, Y. Matsuo, E. Nakamura, *Tetrahedron* **2011**, *67*, 9944.

(19) Y. Matsuo, J. Kawai, H. Inada, T. Nakagawa, H. Ota, S. Otsubo, E. Nakamura, *Adv. Mater.* **2013**, *25*, 6266.

(20) G. Ye, S. Chen, Z. Xiao, Q. Zuo, Q. Wei, L. Ding, *J. Mater. Chem.* **2012**, *22*, 22374.

(21) M. Hashiguchi, N. Obata, M. Maruyama, K. S. Yeo, T. Ueno, T. Ikebe, I.

Takahashi, Y. Matsuo, *Org. Lett.* **2012**, *14*, 3276.

(22) M. Keshavarz-K, B. Knight, G. Srdanov, F. Wudl, *J. Am. Chem. Soc.* **1995**, *117*, 11371.

(23) W. Wang, D. Placencia, N. R. Armstrong, *Org. Electron.* **2011**, *12*, 383.

(24) P. Belik, A. Gügel, J. Spickermann, K. Müllen, *Angew. Chem., Int. Ed. Engl.* **1993**, *32*, 78.

(25) B. W. D'Andrade, S. Datta, S. R. Forrest, P. Djurovich, E. Polikarpov, M. E. Thompson, *Org. Electron.* **2005**, *6*, 11.

(26) Y. Matsuo, J. Hatano, T. Kuwabara, K. Takahashi, *Appl. Phys. Lett.* **2012**, *100,* 063303.

(27) Y. Matsuo, *Chem. Lett.* **2012**, *41*, 754.

(28) J. Y. Kim, K. Lee, N. E. Coates, D. Moses, T.-Q. Nguyen, M. Dante, A. J. Heeger, *Science* **2007**, *317*, 222.

(29) L. Dou, J. You, J. Yang, C.-C. Chen, Y. He, S. Murase, T. Moriarty, K. Emery, G. Li, Y. Yang, *Nat. Photonics* **2012**, *6*, 180.

(30) N. D. Treat, M. A. Brady, G. Smith, M. F. Toney, E. J. Kramer, C. J. Hawker, M. L. Chabinyc, *Adv. Energy Mater.* **2011**, *1*, 82.

(31) W.-R. Wu, U.-S. Jeng, C.-J. Su, K.-H. Wei, M.-S. Su, M.-Y. Chiu, C.-Y. Chen, W.-B. Su, A.-C. Su, *ACS Nano* **2011**, *5*, 6233.

(32) P. Kohn, Z. Rong, K. H. Scherer, A. Sepe, M. Sommer, P. Müller-Buschbaum, R. H. Friend, U. Steiner, S. Hüttner, *Macromolecules* **2013**, *46*, 4002.

(33) G. Yu, J. Gao, J. C. Hummelen, F. Wudl, A. J. Heeger, *Science* **1995**, *270*, 1789.

Chapter 5

56π-Electron Hydrofullerene Derivatives as Electron Acceptors for Organic Solar Cells†

5.1 Introduction

Organic solar cells (OSCs) are expected to become a viable renewable energy source because they have the potential for high cost-performance arising from their inexpensive materials(1) and fabrication processes(2) together with respectable power conversion efficiencies. The molecular engineering of these functional materials holds immense possibilities, so there is considerable potential to improve device performance. To date, research and development of OSCs has been conducted intensely in both academia and industry globally, leading to large improvements in performance, exemplified by the increase in power conversion efficiency (PCE), which can now exceed 10%.(3)

Recently, high-performance OSCs have been achieved using low bandgap polymers and soluble fullerene derivatives as electron-donating and -accepting materials, respectively.(4) While efficiencies have increased in recent years with the development of various low bandgap polymers, the number of fullerene electron acceptors capable of achieving high PCE remains limited. Most studies have used commercially available [6,6]-phenyl-C_{61}-butyric acid methyl ester ($PC_{60}BM$) and $PC_{70}BM$ as acceptors. Emerging high-LUMO 56 π -electron fullerenes,(5,6,7,8,9) as represented by commercially

available $C_{60}(Ind)_2$ (Ind = indene),[6] are not normally effective acceptors for low bandgap polymers due to their low HOMO and LUMO levels[10,11] making exciton dissociation difficult because of the small offset between the low-lying LUMO of the polyners and the high-lying LUMO of such fullerenes.[12] Expanding the repertoire of fullerene acceptors suitable for low bandgap polymers has been anticipated in this field and is needed to further improve the efficiency of OSCs.[13]

The lack of suitable fullerene acceptors may be ascribed to less focus being applied to the discovery of "lead compounds". For instance, little attention has been paid to fullerene derivatives with a hydrogen atom on the fullerene core for OSC applications as fullerene chemists tend to consider such compounds electrochemically unstable.[14] However, an excellent report by Jin, Yamamoto and co-workers debunked this idea by demonstrating that benzylated hydrofullerene $C_{60}(CH_2Ph)H$ can work as an efficient acceptor material, showing a PCE of 3.75% with a standard poly(3-hexylthiophene) donor.[15]

Here I report synthesis of efficient 56π-electron hydrofullerene derivatives through controlled cyanation[16] and subsequent protonation (Scheme 1). I then examine the performance of the obtained hydrofullerene derivative in polymer solar cells containing the low bandgap polymer PTB4 (Figure 1).[17] The present studies will provide important insight into the design of fullerene acceptors.

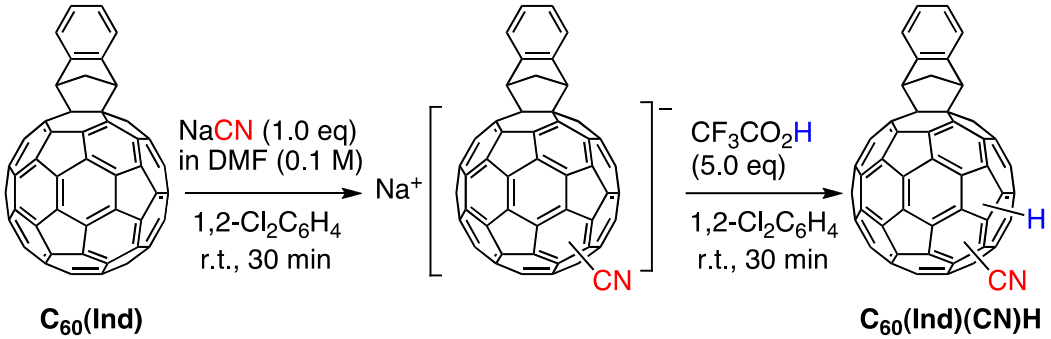

Scheme 1. Synthesis of C_{60}(Ind)(CN)H bearing a hydrogen atom on the fullerene core

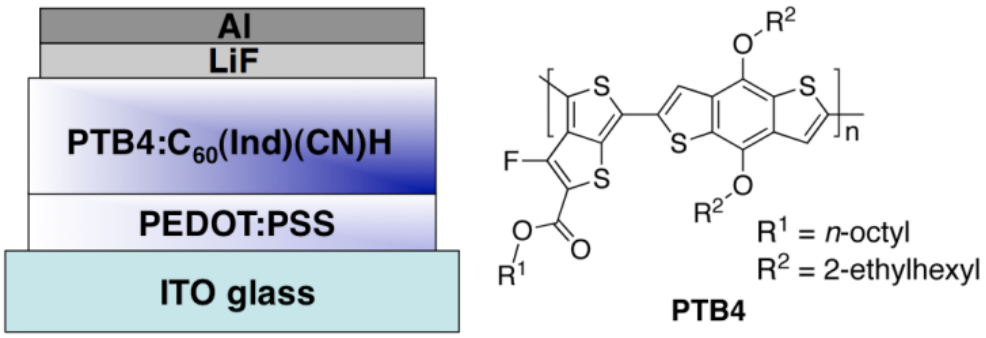

Figure 1. Device configuration and the structure of donor material PTB4.

5.2 Synthesis of 56π-Electron Hydrofullerene Derivatives

I synthesized hydrofullerene derivatives with the aid of a nucleophilic addition of cyanide, which is known as controlled nucleophilic addition among various additions of nucleophiles to C_{60}.[16] The addition of cyanide does not lead to polyaddition, because an intermediate $C_{60}(CN)^-$ is stabilized by the electron-withdrawing cyano group. This intermediate can be protonated by strong acid to produce a hydrogenated compound. In this work, I used 58π-electron fullerenes such as C_{60}(Ind) (Scheme 1) to obtain

56π-electron fullerene derivatives that have sufficient solubility to fabricate thin-film devices by solution-based processes. Treatment of an *o*-dichlorobenzene solution of C_{60}(Ind) with a DMF solution of sodium cyanide at ambient temperature immediately afforded $C_{60}(CN)^-$, which was protonated with trifluoroacetic acid to obtain the crude product containing the desired hydrofullerene product C_{60}(Ind)(CN)H. Separation by silica gel column chromatography using a toluene/*n*-hexane eluent (1/4 to 4/1 v/v) gave analytically pure C_{60}(Ind)(CN)H (8.2%) and the starting material C_{60}(Ind) (32%). The congeners C_{60}(QM)(CN)H and $C_{60}(CH_2)$(CN)H (Figure 2, QM = quinodimethane) were also synthesized following similar procedures using starting materials C_{60}(QM)[18] and $C_{60}(CH_2)$,[7] respectively.

The obtained products were stable in air and soluble in various organic solvents such as toluene, chlorobenzene, and chloroform. The solubility of C_{60}(Ind)(CN)H and C_{60}(QM)(CN)H in toluene was over 1.1 wt%, which is attributed to solubilizing groups such as indene and quinodimethane addends, and to the fact that the products are regioisomeric mixtures of 56π-electron fullerenes. In contrast, the solubility of $C_{60}(CH_2)$(CN)H in toluene was only 0.4 wt%, which is not sufficient for solution-processed polymer solar cells. Thermal stability was examined by thermogravimetry–differential thermal analysis under nitrogen gas flow; all three compounds were found to be stable up to 350 °C.

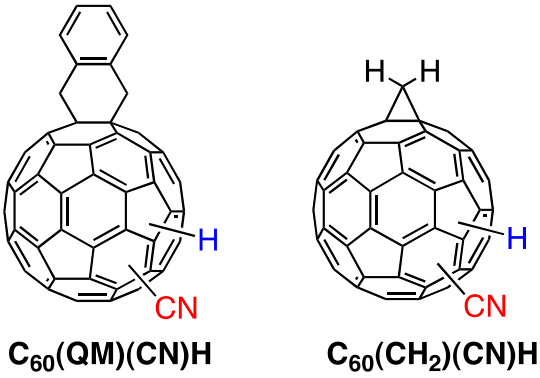

Figure 2. Structures of congeners C_{60}(QM)(CN)H and $C_{60}(CH_2)$(CN)H.

5.3 Electrochemical Properties of 56π-Electron Hydrofullerene Derivatives

I studied the electrochemical properties of C_{60}(Ind)(CN)H, C_{60}(QM)(CN)H and $C_{60}(CH_2)$(CN)H, along with those of reference materials C_{60}(Ind), SIMEF[19,20,21] and PCBM for comparison. Cyclic voltammetry revealed that these hydrofullerene derivatives are electrochemically stable. At least two reversible one-electron reduction waves were observed on the cathodic scan (Figure 3). I ascribe irreversibility of the third step to instability of the fullerene–H bond[14a] and surmise that three-electron reduction does not occur in the thin-film OSCs. I estimated the LUMO levels of the synthesized compounds from their first reduction potentials.[19,22] The LUMO levels of C_{60}(Ind)(CN)H and C_{60}(QM)(CN)H (–3.75 and –3.76 eV, respectively) were comparable to that of C_{60}(Ind) (–3.76 eV) and SIMEF (–3.74 eV), and slightly higher than that of $PC_{60}BM$ (–3.80 eV). Even though the compounds possess an electron-withdrawing cyano group, they possess relatively high-lying LUMO levels. This feature is generally favorable to obtain high open-circuit voltage (V_{OC}) in OSC

devices. The dihydromethano derivative $C_{60}(CH_2)(CN)H$ showed the deepest LUMO level among the tested compounds (–3.84 eV). The low LUMO level of $C_{60}(CH_2)(CN)H$ is explained by the weaker electron-donating ability of the strained three-membered ring than that of the five-membered rings in $C_{60}(Ind)(CN)H$ and $C_{60}(QM)(CN)H$. [7]

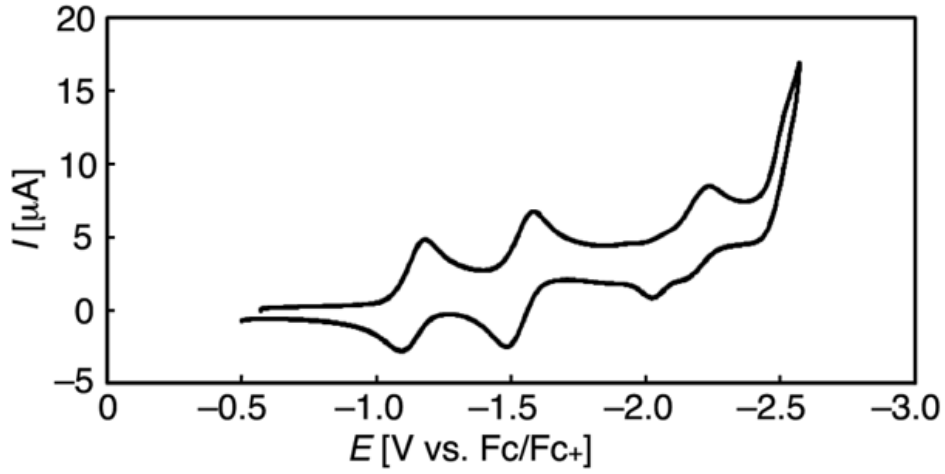

Figure 3. Cyclic voltammogram obtained for $C_{60}(Ind)(CN)H$ in *o*-dichlorobenzene/acetonitrile (4/1, v/v). $E_{1/2}^{red1} = –1.14$ V. $E_{1/2}^{red2} = –1.53$ V.

5.4 OPV Device Performances of 56π-Electron Hydrofullerene Derivative

I investigated the photovoltaic performance of $C_{60}(Ind)(CN)H$ in bulk-heterojunction[23] polymer solar cells using low bandgap polymer PTB4 as the donor (Table 1, Figure 4). The device structure was

ITO/PEDOT:PSS/PTB4:C_{60}(Ind)(CN)H/LiF/Al (Figure 1), where PEDOT:PSS is poly(3,4-ethylenedioxythiophene)–polystyrene sulfonic acid. For the active area, I employed an additive, 1,8-diiodeoctane, and used a mixed solvent of 1,2-dichlorobenzene and 1,8-diiodeoctane (98/2, v/v) for spin-coating. The device exhibited PCE of 5.2% with short-circuit current density (J_{SC}) = 11.1 mA/cm^2, V_{OC} = 0.73 V, and fill factor (FF) = 0.64. Since this performance is respectable, I can conclude that the hydrogen atom on the fullerene core does not adversely affect either charge separation or electron transport. I also studied the effect of changing the additive from aliphatic 1,8-diiodeoctane to aromatic 1-chloronaphthalene. The change in additive led to a decrease in PCE to 2.2%, stemming from a large decrease in J_{SC} and FF, which were derived from poorer intermixing of donor and acceptor materials. However, 1-chloronaphthalene did lead to a slight increase in V_{OC} compared with that of the device using 1,8-diiodeoctane. I attribute relatively high V_{OC} values (0.73–0.75 V) obtained in this work to the slightly higher LUMO level of C_{60}(Ind)(CN)H compared with that of $PC_{60}BM$ and the slightly lower HOMO level of PTB4 than those of other PTB derivatives.[17] The obtained data suggest that fullerene derivatives bearing a hydrogen atom on the C_{60} core are useful electron acceptors for OSCs. They are also potentially interesting materials in view of the small steric demand of the hydrogen atom, which could lead to higher packing density within the fullerene domains and thus higher carrier mobility. [7]

Table 1. Photovoltaic performance of the ITO/PEDOT:PSS/PTB4:C_{60}(Ind)(CN)H/LiF/Al devices under AM1.5G (100 mA/cm^2) light illumination

additive [a]	J_{SC} [mA/cm^2]	V_{OC} [V]	FF [–]	PCE [%]
1,8-diiodooctance	11.1	0.73	0.64	5.2
1-chloronapthalene	6.5	0.75	0.44	2.2

[a] The active layers were spin-coated using a mixtures of dichlorobenzene/additive (98/2, v/v) as a solvent. Donor/acceptor ratio is 1/1.5. The PEDOT:PSS layers were thermally annealed, whereas the active layers were not annealed. Thickness of LiF is 0.6 nm. Detailed procedures for the device fabrication were described in the Electronic Supplementary Information.[24]

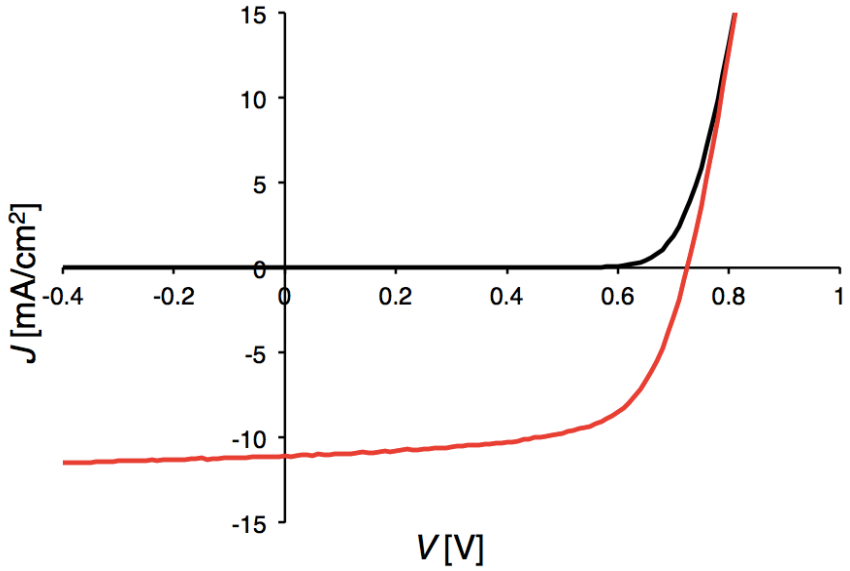

Figure 4. *J-V* curves for the photo and dark currents for the device using 1,8-diiodeoctane as an additive.

5.5 Conclusion

In conclusion, I synthesized fullerene acceptors typified by C_{60}(Ind)(CN)H possessing a hydrogen atom and an electron-withdrawing cyano group on the fullerene core. I found that C_{60}(Ind)(CN)H exhibits a good balance of solubility and LUMO level suitable for solution-processed polymer solar cells with low-bandgap polymers. Importantly, I proved that the presence of a hydrogen atom on the fullerene core does not induce any unfavorable effects, in agreement with the recent report by Jin and Yamamoto *et al*.[15] In addition, the respectable PCE of 5.2% obtained for a polymer solar cell containing C_{60}(Ind)(CN)H reveals the potential of this fullerene acceptor in the development of high-performance OSCs.

5.6 Experimental Section

5.6.1 Synthesis

General Considerations. All reactions dealing with air- or moisture-sensitive compounds were carried out using standard Schlenk technique or a glove box under an argon or nitrogen atmosphere. HPLC analyses were performed on a Shimadzu LC-2010A HT system equipped with SPD-M10A diode array detector and a Buckyprep column (Nacalai Tesque Inc., 4.6 mm ID x 250 mm). Flash silica gel column chromatography was performed on silica gel 60N (Kanto Chemical, spherical and neutral, 140–325mesh). Gel permeation column chromatography was performed on a Japan Analytical Industry LC-9201 (eluent: $CHCl_3$) with JAIGEL H-40P polystyrene column. NMR spectra were measured with a Bruker AVANCE (400 MHz) spectrometer. Spectra are reported in parts per million from internal tetramethylsilane (δ 0.00 ppm) for

^{1}H NMR. Mass spectra were measured by APCI using a time-of-flight mass analyzer on a Waters LCT Premier XE spectrometer.

Synthesis of C_{60}(Ind)(CN)H. C_{60}(Ind) (101.8 mg, 0.122 mmol) was dissolved in *o*-dichlorobenzene, and the resulting solution was degassed three times. To this solution a 0.1 M DMF solution of NaCN (1.0 mL) was dropped. Color of the solution was immediately changed from dark red to dark green, indicating formation of the fullerene derivative anion, $C_{60}(Ind)(CN)^-$. After stirring at room temperature at 30 min, CF_3CO_2H (126 mg, 1.105 mmol) was added to the dark green solution. Immediate color change was again observed from dark green to dark brown. After stirring at room temperature for 30min, the resulting reaction mixture was subjected a HPLC analysis to monitor the progress of the reaction. The reaction mixture was diluted with toluene and subjected to silica gel column chromatography separation (eluent, toluene/*n*-hexane 1:4 to 4:1). After the first fraction containing the starting material C_{60}(Ind), the second fraction containing the title product was collected. This solution was concentrated with a rotary evaporator, then subjected to re-precipitation with methanol. The resulting solid was collected with filtration, and dried in vacuo to obtain the title product as a mixture of regioisomers. Yield, 8.6 mg (8.2%). ^{1}H NMR (400 MHz, $CDCl_3$): δ 2.66–3.85 (m, 2H, CH_2), 4.57–5.15 (m, 2H, CH), 5.90, 6.22, 6.36, 6.61, 6.64, and 6.81 (s, 1H, C_{60}H of regioisomers), 7.30–7.39 (m, 2H, Ph), 7.46–7.81 (m, 2H, Ph). APCI-MS(–) for $C_{70}H_9N$ [M-]: calcd.863; found 863.

Synthesis of C_{60}(QM)(CN)H. Synthesis of C_{60}(QM)(CN)H was performed by employing the procedure of C_{60}(Ind)(CN)H described above using C_{60}(QM) as a

reactant. ^{1}H NMR (400 MHz, $CDCl_3$): δ 4.03–4.52 (m, 4H, CH_2), 6.20, 6.31, 6.60, and 6.80 (s, 1H, $C_{60}H$ of regioisomers), 7.41–7.54 (m, 4H, Ph). APCI-MS(–) for $C_{69}H_9N$ [M-]: calcd.851; found 851.

Synthesis of $C_{60}(CH_2)(CN)H$. Synthesis of $C_{60}(CH_2)(CN)H$ was performed by employing the procedure of **1** described above using $C_{61}H_2$ as a reactant. ^{1}H NMR (400 MHz, $CDCl_3$): δ 2.97–2.98 (d, J = 6.4 Hz, 1H, methano-CH_2), 4.25-4.27 (d, J = 6.4 Hz, 1H, methano-CH_2), 6.93 (s, 1H, $C_{60}H$). APCI-MS(–) for $C_{62}H_3N$ [M-]: calcd.761; found 761.

5.6.2 Cyclic Voltammetry

General procedure. Cyclic voltammetry (CV) was performed using ALS/CHI602C Electrochemical analyzer. All measurements were carried out in a one-compartment cell under Ar gas, equipped with a glassy-carbon working electrode, a platinum wire counter electrode, and an Ag/Ag^+ reference electrode. Measurements were performed in *o*-dichlorobenzene/acetonitrile (4/1, v/v) solution containing tetrabutylammonium perchlorate (0.1 M) as a supporting electrolyte at 25 ºC with a scan rate of 0.1 V/s. All potentials were corrected against Fc/Fc^+ (Table 2).

Table 2. Reduction potentials (V *vs*. Fc/Fc^+) and estimated LUMO levels for the hydrofullerene derivatives[a]

Compound	$E_{1/2}^{red1}$ [V]	$E_{1/2}^{red2}$ [V]	$E_{1/2}^{red3}$ [V]	LUMO level [eV][b]
C_{60}(Ind)(CN)H	–1.14	–1.53	N.A.[c]	–3.75
C_{60}(QM)(CN)H	–1.13	–1.52	N.A.	–3.76
$C_{60}(CH_2)$(CN)H	–1.07	–1.45	–2.03	–3.84

[a] Potential in V *vs*. the ferrocene–ferrocenium couple was measured by cyclic voltammetry in *o*-dichlorobenzene/acetonitrile (4/1, v/v). [b] LUMO levels were estimated using the following equation: LUMO level = $-(4.89 + E_{1/2}^{red1})$ [eV]. [c] Not available due to irreversible waves.

Cyclic voltammograms.

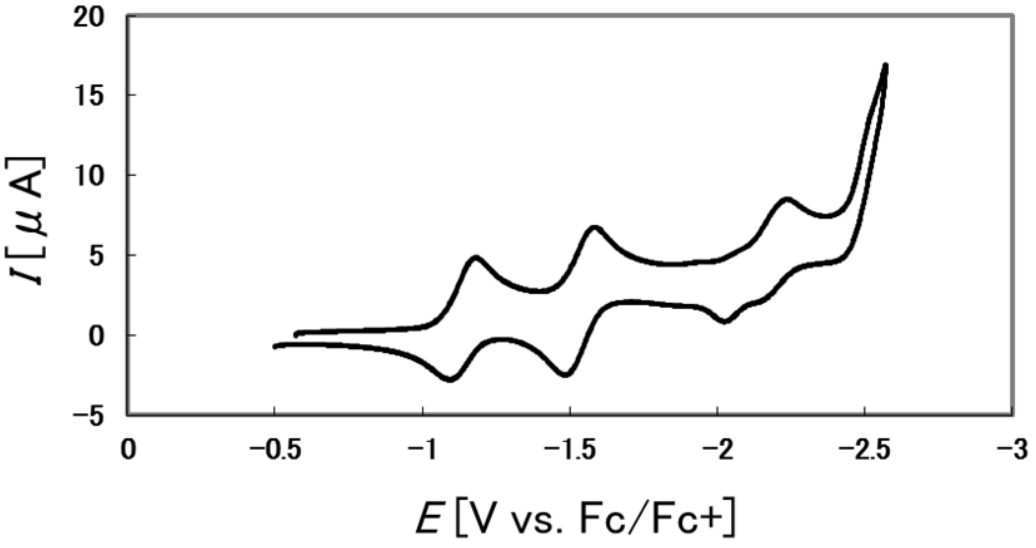

Figure 5. Cyclic voltammogram of C_{60}(Ind)(CN)H.

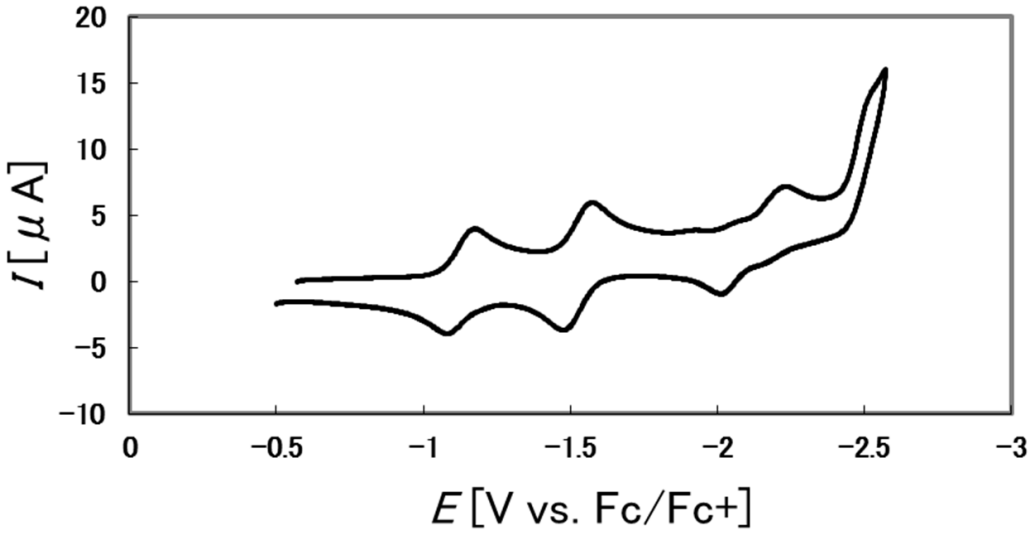

Figure 6. Cyclic voltammogram of C_{60}(QM)(CN)H.

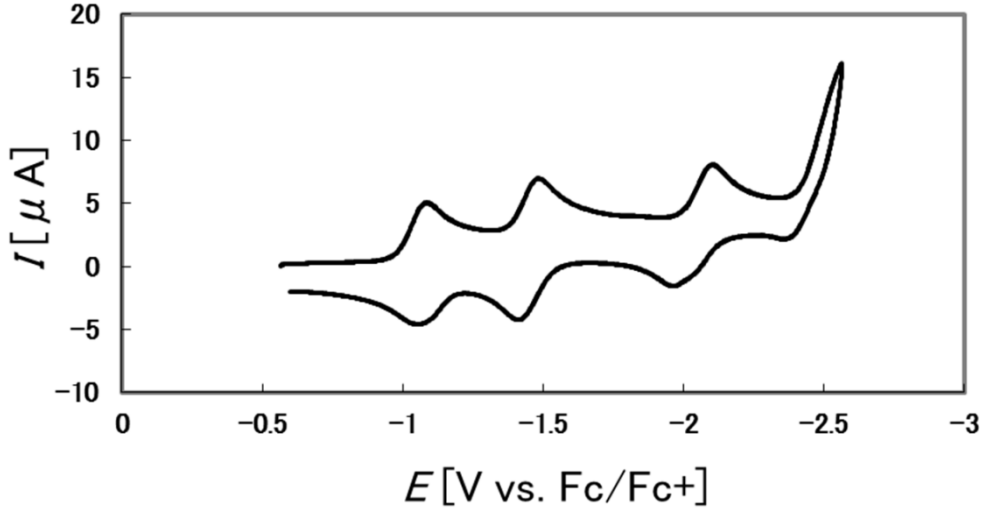

Figure 7. Cyclic voltammogram of $C_{60}(CH_2)$(CN)H.

5.6.3 Device Fabrication Procedures

The structure of the OSC devices was: ITO/PEDOT:PSS/PTB4: C_{60}(Ind)(CN)H/LiF/Al. The devices were fabricated in an N_2-purged glove box. The active area of each device was 0.25 cm^2. An ITO-coated glass substrate was exposed to UV ozone for 10 min. PEDOT:PSS was then spin-coated (4000 rpm) as an hole transport layer and annealed at 120 °C for 10 min. A blend solution (10 mg/mL) of PTB4 and C_{60}(Ind)(CN)H (1/1.5 wt/wt) in 1,2-dichlorobenzene/additive (98/2, v/v) was spin-coated on the hole transport layer. LiF (0.6 nm) was deposited with vacuum deposition, and then Al (80 nm) was deposited under vacuum as a back electrode. Finally, the fabricated OSC cell was encapsulated with a backing glass using a UV-curable resin under N_2 atmosphere. The current density–voltage characteristics under AM 1.5G solar illumination (100 mW/cm^2) with a mask of 0.16 cm^2 aperture was recorded using a Keithley 2400 source-measurement unit.

5.7 References and Notes

† This chapter is published on *Chem. Lett.* **2013**, *42*, 1525.

(1) T. P. Osedach, T. L. Andrew, V. Bulovíc, *Energy Environ. Sci.* **2013**, *6,* 711.

(2) D. Angmo, M. Hösel, F. C. Krebs, *Sol. Energy Mater. Sol. Cells* **2012**, *107*, 329.

(3) M. A. Green, K. Emery, Y. Hishikawa, W. Warta, E. D. Dunlop, *Prog. Photovolt. Res. Appl.* **2012**, *20*, 12.

(4) P.-L. T. Boudreault, A. Najari, M. Leclerc, *Chem. Mater.* **2011**, *23*, 456.

(5) M. Lenes, G.-J. A. H. Wetzelaer, F. B. Kooistra, S. C. Veenstra, J. C. Hummelen, P. W. M. Blom, *Adv. Mater.* **2008**, *20,* 2116.

(6) Y. He, H.-Y. Chen, J. Hou, Y. Li, *J. Am. Chem. Soc.* **2010**, *132*, 1377.

(7) (a) Y. Zhang, Y. Matsuo, C.-Z. Li, H. Tanaka, E. Nakamura, *J. Am. Chem. Soc.* **2011**, *133*, 8086; (b) C.-Z. Li, S.-C. Chien, H.-L. Yip, C.-C. Chueh, F.-C. Chen, Y. Matsuo, E. Nakamura, A. K.-Y. Jen, *Chem. Commun.* **2011**, *47*, 10082; (c) C.-Z. Li, Y. Matsuo, E. Nakamura, *Tetrahedron*, **2011**, *67*, 9944. (d) Y. Matsuo, J. Kawai, H. Inada, T. Nakagawa, H. Ota, S. Otsubo, E. Nakamura, *Adv. Mater.* **2013**, *25*, *6266*.

(8) G. Ye, S. Chen, Z. Xiao, Q. Zuo, Q. Wei, L. Ding, *J. Mater. Chem.* **2012**, *22*, 22374.

(9) Y. Matsuo, *Chem. Lett.* **2012**, *41*, 754.

(10) L. Huo, J. Hou, S. Zhang, H.-Y. Chen, Y. Yang, *Angew. Chem. Int. Ed.* **2010**, *49*, 1500.

(11) H. Zhou, L. Yang, S. C. Price, K. J. Knight, W. You, *Angew. Chem. Int. Ed.* **2010**, *49*, 7992.

(12) M. A Faist, S. Shoaee, S. Tuladhar, G. F. A. Dibb, S. Foster, W. Gong, T. Kirchartz, D. D. C. Bradley, J. R. Durrant, J. Nelson, *Adv. Energy Mater.* **2013**, *3*, 744.

(13) M. Hashiguchi, N. Obata, M. Maruyama, K. S. Yeo, T. Ueno, T. Ikebe, I. Takahashi, Y. Matsuo, *Org. Lett.* **2012**, *14*, 3276.

(14) For instance, (a) H. Iikura, S. Mori, M. Sawamura, E. Nakamura, *J. Org. Chem.* **1997**, *62*, 7912. (b) M. Toganoh, Y. Matsuo, E. Nakamura, *J. Am. Chem. Soc.* **2003**, *125*, 13974. (c) Y. Kuninobu, Y. Matsuo, M. Toganoh, M. Sawamura, E. Nakamura, *Organometallics* **2004**, *23*, 3259. (d) Y. Matsuo, Y. Kuninobu, A. Muramatsu, M. Sawamura, E. Nakamura, *Organometallics* **2008**, *27*, 3403.

(15) S. Lu, T. Jin, T. Yasuda, A. Islam, M. Akhtaruzzaman, L. Han, K. A. Alamry, S. A. Kosa, A. M. Asiri, Y. Yamamoto, *Tetrahedron* **2013**, *69*, 1302.

(16) M. Keshavarz-K, B. Knight, G. Srdanov, F. Wudl, *J. Am. Chem. Soc.* **1995**, *117*, 11371.

(17) Y. Liang, D. Feng, Y. Wu, S.-T. Tsai, G. Li, C. Ray, L. Yu, *J. Am. Chem. Soc.* **2009**, *131*, 7792.

(18) P. Belik, A. Gügel, J. Spickermann, K. Müllen, *Angew. Chem., Int. Ed. Engl.* **1993**, *32*, 78.

(19) Y. Matsuo, A. Iwashita, Y. Abe, C.-Z. Li, K. Matsuo, M. Hashiguchi, E. Nakamura, *J. Am. Chem. Soc.* **2008**, *130*, 15429.

(20) (a) Y. Matsuo, Y. Sato, T. Niinomi, I. Soga, H. Tanaka, E. Nakamura, *J. Am. Chem. Soc.* **2009**, *131*, 16048; (b) H. Tanaka, Y. Abe, Y. Matsuo, J. Kawai, I. Soga, Y. Sato, E. Nakamura, *Adv. Mater.* **2012**, *24*, 3521.

(21) Y. Matsuo, J. Hatano, T. Kuwabara, K. Takahashi, *Appl. Phys. Lett.* **2012**, *100*, 063303.

(22) B. W. D'Andrade, S. Datta, S. R. Forrest, P. Djurovich, E. Polikarpov, M. E. Thompson, *Org. Electron.* **2005**, *6*, 11.

(23) G. Yu, J. Gao, J. C. Hummelen, F. Wudl, A. J. Heeger, *Science* **1995**, *270*, 1789.

Chapter 6

Mobility of Long-lived Fullerene Radical in Solid State and Nonlinear Temperature Dependence[†]

6.1 Introduction

Singly bonded [60]fullerene dimers $(C_{60}R)_2$[1,2,3,4,5] is unique in its ability to reversibly generate two carbon radicals $RC_{60}^{\bullet}$ through thermal homolytic cleavage of the central C–C bond as has so far been studied in solution. In light of the well-known propensity of fullerenes to form plastic crystals[6,7] and to exist in a variety of solid phases, I became interested in the control of the physical properties of the fullerene radicals in solid through temperature-dependent phase transition. I therefore prepared a dimer **2**, $[C_{60}\{CH_2SiMe_2(C_6H_4(2\text{-ethylhexyloxy})\text{-}2)\}]_2$, from a monomer **1** (Scheme 1a),[7] and examined its solid state properties at various temperatures. Herein I report on a striking non-linear temperature dependence of the radical concentration and the electron mobility reflecting the change of a short range orientational order the fullerene moiety without the change of the long range translational order. Heating and cooling of the solid of **2** caused C–C bond cleavage followed by reversible and irreversible reorientation of the fullerene radicals formed in low concentration up to 440K (Scheme 1b). Thus, a microcrystalline powder of the dimer **2** produces a strongly interacting radical pair **3** at <310K, dissociates to a weakly interaction pair **3**, and upon cooling from 440K, a phase transition of the solid causes reorientation of the fullerene radical pair that prevents recombination and hence produces a solid containing a persistent radical. The electron mobility in the field-effect transistor (FET) increased by ten times

while the ESR intensity of the fullerene radical remained almost the same.

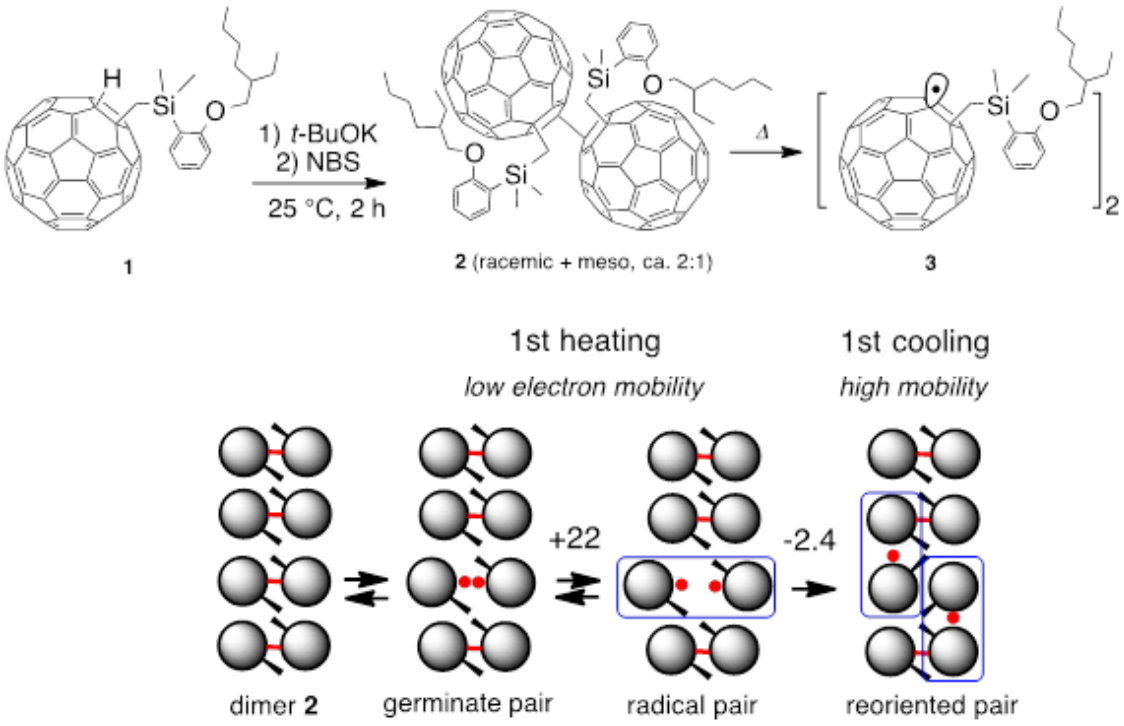

Scheme 1. Synthesis of the singly bonded fullerene dimer **2** and thermal C–C bond dissociation in solid

6.2 Synthesis and Electrochemical Property of the Singly Bonded Fullerene Dimer

The dimer **2**, $[C_{60}\{CH_2SiMe_2(C_6H_4(2\text{-ethylhexyloxy})\text{-}2)\}]_2$ that I examined has two branched alkyl chains that increase the solubility, and was synthesized in 96% yield from hydro(dimethyl(2-ethylhexyloxyphenyl)silylmethyl)[60]fullerene **1** that is readily available in 93% yield from [60]fullerene (Scheme 1).[8] The dimer, especially in its pure recrystallized form, rather insoluble in a variety of solvents, and in solution exists predominantly as aggregates. Dynamic laser light scattering, a 1,2-dicholorobenzene solution revealed the presence of aggregates of several nm and several μm in size which

was dependent on the concentration (3 μM and 3 mM) and temperature (25, 60 and 90°C).

The redox property of the dimer **2** was studied with cyclic voltammetry (Figure 1, Table 1). In the cyclic voltammogram, one cathodic peak, two pairs of reversible redox waves, and one anodic peak for **2** was observed. The cathodic peak at –1.20 V vs. Fc/Fc^+ corresponds to the reduction of the dimer **2** causing dissociation into two molecules of RC_{60}^-. The following two reduction peaks are assigned to RC_{60}^- to RC_{60}^{2-} and RC_{60}^{2-} to RC_{60}^{3-}. On the anodic scan, reversible anodic peaks are oxidation to RC_{60}^-. An irreversible anodic peak at –0.67 V is due to oxidation of RC_{60}^- into $RC_{60}\cdot$, which undergoes rapid recombination to form the dimer **2**. The dimer **2** is regarded to a 1,4-diadduct, whose reduction wave has been observed at a range from $E_{1/2}$ = –1.05 to –1.20 V vs Fc/Fc^+.[8a] Observed cathodic peak potential (–1.20 V) is therefore reasonable. On the other hand, I have observed oxidation from fullerene anions to fullerene radicals in a positive-side region (–0.6 to –0.7 V vs. Fc/Fc^+).[9] I consider that observed anodic peak potential (–0.67 V) is also reasonable. From these potential, I concluded that monomer radical $RC_{60}\cdot$ has much higher electron affinity than the dimer form, and suggests that, if generated in the solid of the dimer, the free radical may act as a dopant and increase the electron mobility of the solid.

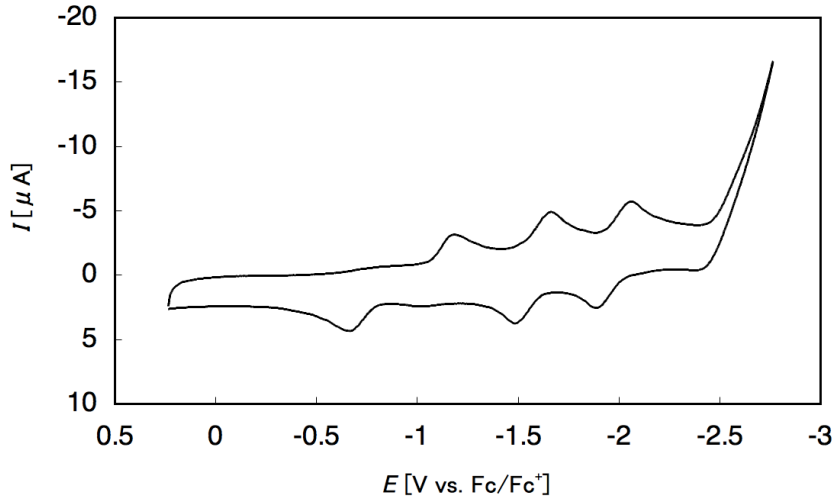

Figure 1. Cyclic voltammogram of **2**. Measurement was performed in a 0.3 mM 1,2-dichlorobenzene solution containing $Bu_4N^+ClO_4^-$ (0.1 M) as a supporting electrolyte at 25ºC with a scan rate of 0.1 Vs^{-1}. Glassy-carbon, platinum wire, and Ag/Ag^+ electrodes were used as working, counter, and reference electrodes, respectively.

Table 1. Electrochemical data for **2**[a]

compound	E_{pa}/V	E_{pc}/V	$E_{1/2}^{red2}$/V	$E_{1/2}^{red3}$/V
2	–0.67	–1.20	–1.57	–1.97

[a] Potential in volts vs ferrocene/ferrocenium measured with cyclic voltammetry(Figure 1).

6.3 Crystal Structure of the Singly Bonded Fullerene Dimer

The structure of the dimer **2** was studied by X-ray crystallographic analysis of single crystals grown in a chloroform solution (Figure 2). The inter-fullerene C–C bond distance is 1.5 Å. Fullerene cores was found to be packed closely with a shortest fullerene(π)–fullerene(π) distance of ca. 3.2 Å. I investigated the thermal property of a

powder sample of the dimer **2** by the XRD analysis and differential scanning calorimeter (DSC). XRD analysis of a powder sample at 298K - 453K, and then at 298K after cooling, showed that molecular packing is not much affected by the temperature change except for a few peaks in small angle region corresponding to the fullerene packing (8.8–17.7 Å) that disappeared upon heating from 298K to 393K (Figure 3).

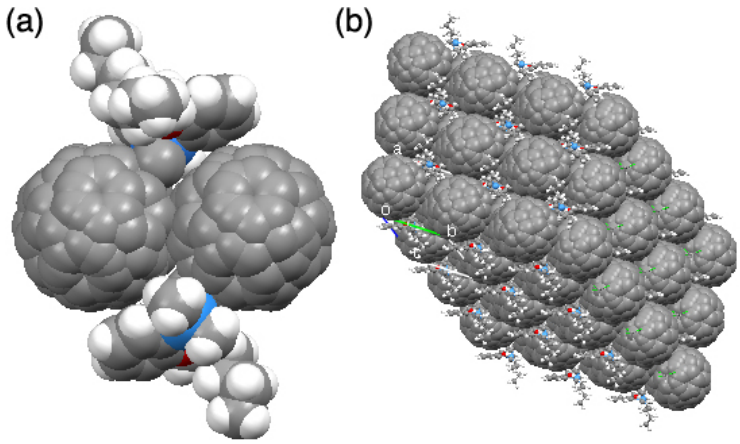

Figure 2. X-ray crystal structure of **2**·($CHCl_3$). (a) Side view of space-filling model. (b) Crystal packing structure. The crystal is triclinic, space group = *P*-1, a = 10.003 Å, b = 15.818 Å, c = 17.837 Å, α = 113.04º, β = 92.89º, γ = 105.44º, V = 2465.1 $Å^3$. Fullerene cores are structurally disordered due to the mixture of *meso* and *racemo* isomers. Chloroform is omitted for clarity.

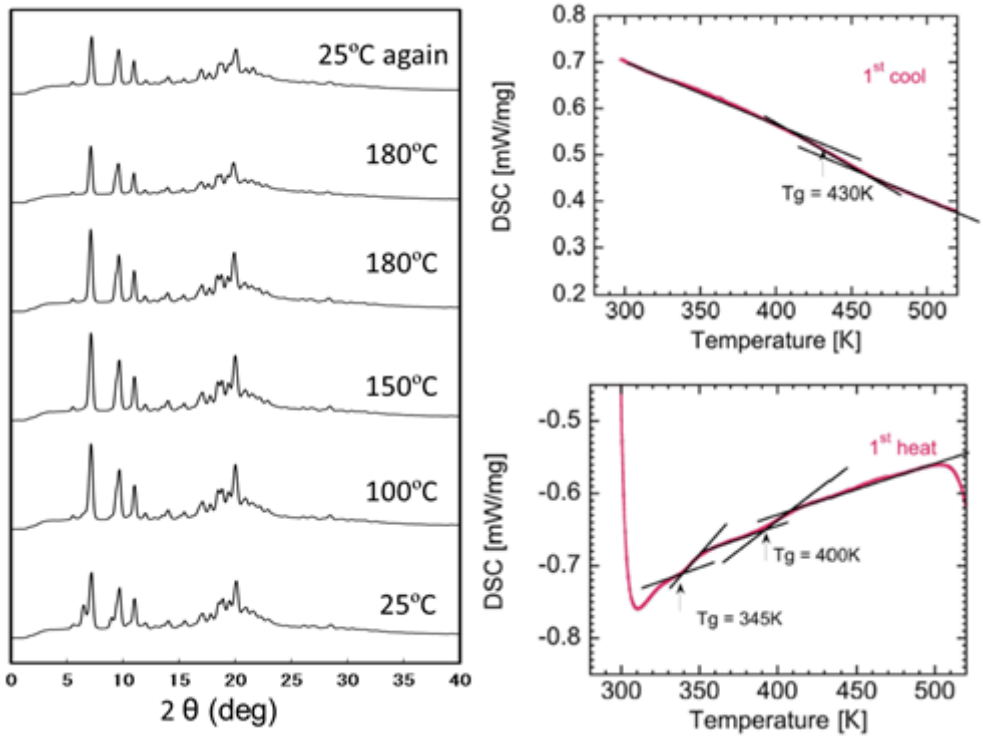

Figure 3. (a) The VT- XRD patterns of **2**. (b) DSC data for **2**.

In agreement with the XRD data, differential scanning calorimetric (DSC) analysis showed subtle signs of thermal events that occur during heating and cooling (Figure 2d). Heating caused two phase transitions at ca. 345 K and ca. 400 K with small exothermicity, and cooling after melting (ca. 540 K) showed a small exothermic phase transition at ca. 430 K.

6.4 ESR Study of the Singly Bonded Fullerene Dimer

The ESR spectra of the dimer **2** in microcrystalline solid showed an intriguing non-linear phenomenon (Figure 4a). The enthalpy of C–C bond dissociation was obtained from the slope of the van't Hoff plot in which ln (*T* x intensity) is plotted against 1000/*T*. The van't Hoff profile of the first heating was very similar to that for

solution, and the ESR signal intensity increased between 300K and 362K with a small slope of the van't Hoff plot (ΔH = 2.3 kcal/mol), and after the phase transition at ca. 360K increased sharply between 362 and 440 K (ΔH = 22.0 kcal/mol). The spin concentration at 400K was essentially the same as that in solution (7.4 x 10^{-8} mol g^{-1}) (Experimental Section). Cooling of the heated sample from 440K to 300K resulted in an unexpected consequence. The spin concentration decreased very slowly (ΔH = 2.4 kcal/mol) and exactly the same profile was traced for the 2nd and the 3rd heating/cooling cycle. Such a small value indicates that the fullerene radical pair generated in the first heating does not recombined in the solid state. The radical concentration after cooling remained constant for well over 1000 min (Figure 4b).

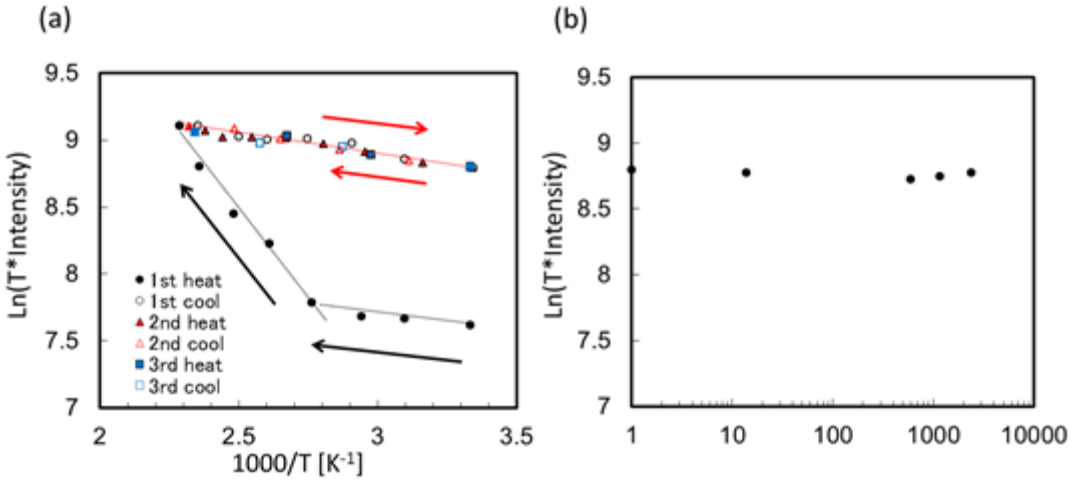

Figure 4. The van't Hoff plot of the ESR signal intensity. (a) The plot of results from a measurement performed for a microscrystalline powder containing toluene. Only the fitting line for the first and the second heating experiments are shown. (b) The radical concentration after cooling.

Taken together the XRD, DSC and ESR temperature dependence of the solid dimer, I consider that the radical pair generated by C–C bond cleavage <310K exist in

low concentration in the solid, maintains strong interaction within the pair till 362K, dissociates into two radical above this temperature, and above 430K the mutual orientation of the two radical changes so much that they never recombine. The phase changes here occur only with the change of a short range orientational order the fullerene moiety without affecting the long range translational order.

The ESR spectra of the dimer **2** in solution (1,2-dichlorobenzene) also showed a similar non-linear behavior that was not described in the literature. As shown in the Figure 5, the intensity of the ESR signal increased between 293K and 340K with a small scope (ΔH = 6.14 kcal/mol) and sharply between 350K and 420 K (ΔH = 28.2 kcal/mol). The spin concentration at 400K was estimated to be 7.2 x 10^{-8} mol g^{-1} by the comparison of the signal intensity of the radical with that of the signal of 4-hydroxy-2,2,6,6-tetramethylpiperidine 1-oxyl (TEMPOL) (Figure 8 in Experimental Section). In light of the DLS information above and the similarity of this ESR profile with that of solid, I consider that the dimer are aggregated in solution and therefore behaves similarly for the temperature range available for the solvent.

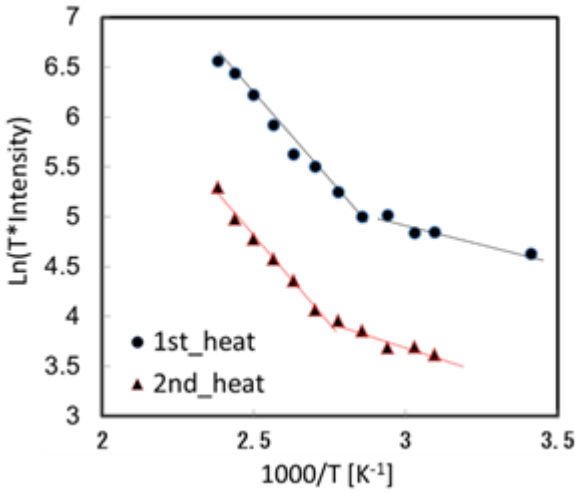

Figure 5. The van't Hoff plot of results from a measurement performed in a 1,2-dichlorobenzene solution.

Table 2. Enthalpies of dimerization (kcal/mol)

state	measurement	–ΔH [kcal/mol]	Temperature [K]
solution	1st heating	6.1	293–340
	1st heating	28.2	350-420
	2nd heating	8.7	293-360
	2nd heating	30.2	370-420
solid	1st heating	2.3	300-362
	1st heating	22.0	362–440
	1st cooling	2.4	440–300
	2nd heating	2.4	300–440
	2nd cooling	2.7	440–300
	3rd heating	2.3	300–440
	3rd cooling	2.1	300–440

6.5 FET Device Performances of the Singly Bonded Fullerene Dimer

The electron mobility of the solid dimer exhibited even more pronounced non-linear temperature dependence than the one found in the van't Hoff plot. The bottom gate FET device made of **2** (spin coated as a CS_2 solution) exhibited a typical

FET property (Figure 6a) The electron mobility on the first heating to 470K remained rather constant being in a 0.1–0.3 x 10^{-3} $cm^2V^{-1}s^{-1}$ range peaking slighly at 330K and 390K. In light of the van't Hoff plot in the same temperature range (Figure 4a), I consider that the low mobility record here is because the radical pairs do not have strong electronic interactions with the neighboring fullerene molecules.

Most remarkably, cooling from 470K to 420K causes an almost ten-fold increase of the mobility to 1.2 x 10^{-3} $cm^2V^{-1}s^{-1}$, and further cooling to room temperature decreased the mobility only to 0.85 x 10^{-3} $cm^2V^{-1}s^{-1}$. Such an increase of the mobility suggests that the fullerene radicals started to affect the bulk property of the solid upon cooling. In light of the van't Hoff plot and the high radical concentration at the first cooling (Figure 4a), I consider that the emergence of the free radical caused by irreversible orientational change of the fullerene moiety is responsible for the increased electron mobility. In the second heating/cooling cycle, the mobility peaked at 1.4 x 10^{-3} $cm^2V^{-1}s^{-1}$. The third heating/cooling process followed similar traces peaking at 1.5 x 10^{-3} cm^2/Vs. In agreement with the ESR evidence of the persisting radical, the second state of the dimer solid is structurally stable and maintains the high level of mobility for >1000 min (the device after the first heating/cooling cycle was kept for 300K (Figure 7).

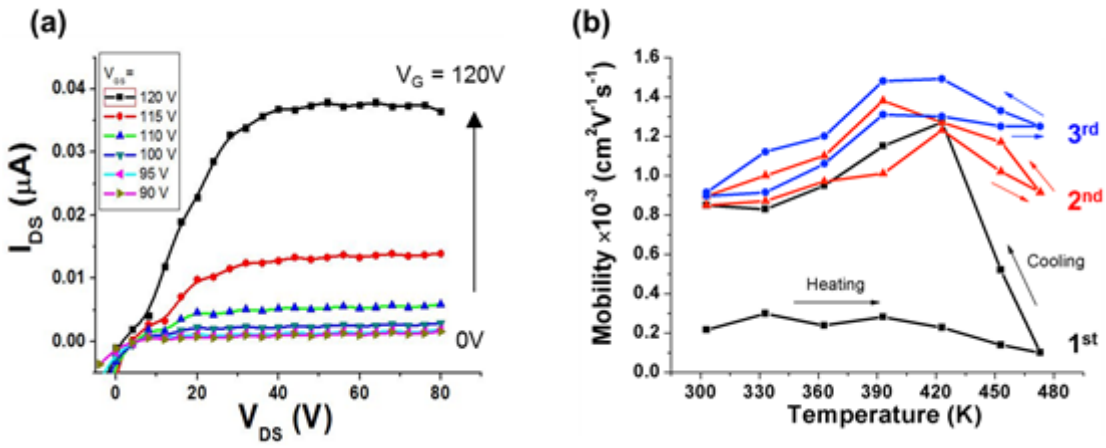

Figure 6. (a) The output curves of the FET devices. (b) Temperature dependency of electron mobility of **2** in the solid state**.**

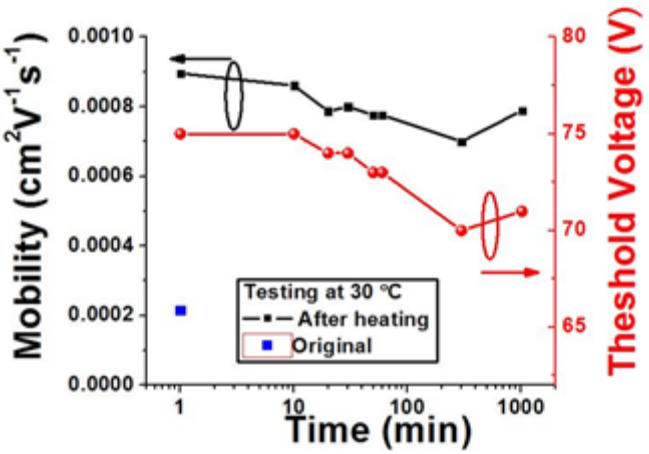

Figure 7. Long-time test of the mobility and threshold voltage of the FET device.

6.6 Conclusion

In summary, I synthesized a new singly bonded fullerene dimer bearing the silylmethyl addend in excellent yield. Electrochemical study of the dimer showed that the monomer radical generating from dissociation of the dimer has higher electron affinity than the dimer itself. Temperature-dependent ESR spectroscopy both in solution and solid was performed to elucidate dissociation dynamics of the dimer. I have found

that thermolysis of the solid fullerene dimer **2** results in reversible and irreversible generation of radicals **3**. The free radicals irreversibly generated by reorientation of fullerene moiety after the first cooling of the solid do not recombine because of the emergence of a second state of molecular packing, which produce a solid containing a long-lived radical. This free radical acts as a dopant for the fullerene solid and increases the electron mobility. On the other, radical pairs which maintain strong interactions with each other do not interact electronically with the neighboring fullerene molecules, and hence do not increase the mobility of the solid. The processes of the formation of the radicals display an unusual non-linear temperature dependence as to the radical concentration and the electron mobility, which can be ascribed to the intrinsic tendency of fullerene molecules to form plastic crystals where the fullerene molelcules can change their orientation with low activation energy without affecting the long range translational order of the crystal.

6.7 Experimental Section

6.7.1 Synthesis

General Considerations. All reactions dealing with air- or moisture-sensitive compounds were carried out using standard Schlenk technique or a glove box under an argon or nitrogen atmosphere. HPLC analyses were performed on a Shimadzu LC-10A system equipped with SPD-M10A diode array detector and a Buckyprep column (NacalaiTesque Inc., 4.6 mm ID x 250 mm). Preparative HPLC was performed on a Buckyprep column (20mm ID × 250 mm) using toluene/2-isopropanol (10/0 – 4/6) as eluents (flow rate 5–15 mL/min, detected at 350 nm with an UV spectrophotometric detector, Shimadzu SPD-6A) and an RP-FULLERENE column (Nomura Chemical, 20

mm ID × 250 mm) using toluene/acetonitrile (7/3 – 4/6) as eluents (flow rate 5–12 mL/min, detected at 350 nm with an UV spectrophotometric detector, Shimadzu SPD-6A). Flash silica gel column chromatography was performed on silica gel 60N (Kanto Chemical, spherical and neutral, 140–325mesh). Gel permeation column chromatography was performed on a Japan Analytical Industry LC-9201 (eluent: toluene) with JAIGEL 2H and 3H polystyrene column. NMR spectra were measured with a JEOL EX-400 (400 MHz) or a JEOL ECA-500 (500 MHz) spectrometer. Spectra are reported in parts per million from internal tetramethylsilane (δ 0.00 ppm) for ^{1}H NMR, from solvent carbon (e.g. δ 77.00 ppm for chloroform) for ^{13}C NMR. High-resolution mass spectra were measured by APCI using a time-of-flight mass analyzer on a JEOL JMS-T100LC (AccuTOF) spectrometer.

Synthesis of the Monoadduct: 1-(dimethyl-*o*-2-ethylhexyloxyphenylsilylmethyl)-1,9-dihydro(C_{60}-I_h)[5,6]fullerene: $C_{60}(CH_2SiMe_2C_6H_4$-*o*-EHO)H (1). To a solution of C_{60} (509 mg, 0.706 mmol) in 1,2-dichlorobenzene (50 mL) containing*N*,*N*-dimethylformamide (1.60 mL, 20.8 mmol) was slowly added a THF solution of $Me_2(C_6H_4$-*o*-EHO)$SiCH_2MgCl$ (2.10 mL, 1.0 M, 2.10 mmol)at 25 °C. After stirring for 60 min, a saturated aqueous NH_4Cl solution (2.0 mL) was added to quench the reaction. The resulting dark-red solution was diluted with toluene, and insoluble products were removed by filtration through a pad of silica gel. Purification of the product was performed by silica gel column chromatography (CS_2/hexane = 1/1). The pure product **1** was obtained after removing the solvent in 65% yield as black crystals.^{1}H NMR (500 MHz, $CDCl_3$): δ 0.832 (s, 6H, CH_2SiCH_3), 0.906 (t, *J* = 7.2 Hz, 3H, EHO), 1.01 (t, *J* = 7.5 Hz, 3H, EHO), 1.36–1.42 (m, 4H, EHO), 1.53

(m, 2H, EHO), 1.66–1.74 (m, 2H, EHO), 1.96 (q, 1H, EHO), 3.25 (s, 2H, CH_2), 3.97 (d, J = 5.7 Hz, 2H, OCH_2), 6.52 (s, 1H, $C_{60}H$), 6.86 (d, J = 8.1 Hz, 1H, C_6H_4), 6.99 (t, J = 7.4 Hz, 1H, C_6H_4), 7.34–7.37 (m, 1H, C_6H_4), 7.67 (d, J = 7.2 Hz, 1H, C_6H_4); ^{13}C NMR (125MHz, $CDCl_3$) all signals represent C (C_{60}, sp^2) except as being noted. δ –0.2223 (1C, SiCH$_3$), –0.2080 (1C, SiCH$_3$), 11.31 (1C, EHO), 14.26 (1C, EHO), 23.21 (1C, EHO), 24.33 (1C, EHO), 29.33 (1C, EHO), 31.10 (1C, EHO), 36.78 (SiCH$_2$), 40.41 (1C, EHO), 61.43 (1C, $C_{60}H$), 62.50 (1C, CCH$_2$), 70.01 (1C, OCH$_2$), 110.08 (1C, C_6H_4), 120.69 (1C, C_6H_4), 125.21 (1C, C_6H_4), 131.91 (1C, C_6H_4), 134.88 (1C, C_6H_4), 136.26, 136.56, 139.88, 139.96, 141.55, 141.57, 141.86, 141.96, 141.98, 142.02, 142.49, 143.22, 144.66, 144.67, 145.14, 145.29, 145.35, 145.81, 145.90, 146.12, 146.16, 146.23, 146.36, 146.97, 147.28, 154.19, 157.98, 164.17 (1C, C_6H_4). APCI-HRMS (-): m/z calcd for $C_{77}H_{29}OSi$ (M-H$^+$), 997.1988; found, 997.2032.

Synthesis of the dimer: (C_{60}($CH_2SiMe_2C_6H_4$-*o*-EHO))$_2$ (2). To a solution of **1** (301m g, 0.300 mmol) in 1,2-dichlorobenzene was added a THF solution of KO^{t}Bu (0.360 mL, 1.0 M, 0.360 mmol) at 25 °C. A dark green solution of potassium salt of C_{60}($CH_2SiMe_2C_6H_4$-*o*-EHO)$^-$ was obtained immediately. After stirring for 45 min, *N*-bromosuccinimide (165 mg, 0.926 mmol) was added to the solution. Then, the reaction mixture was stirred for 2 h at 25 °C. The resulting dark red solution was diluted with toluene, and passed through a pad of silica gel to remove potassium salts. The toluene solution was evaporated to obtain concentrated solution containing the product, which was reprecipitated by addition of methanol (ca. 50~100 mL). The product **2** (96% HPLC purity) was obtained after removing the solvent in 98% yield (288.8mg) as dark brown powder. ^{1}H NMR (500 MHz, $CDCl_3$): δ 0.500 (d, 6H, CH_2SiCH_3, racemic),

0.536–0.546 (dd, 6H, CH_2SiCH_3, meso), 0.606–0.628 (dd, 6H, CH_2SiCH_3, meso),0.652–0.673 (dd, 6H, CH_2SiCH_3, racemic),0.845–0.933 (m, 12H, EHO), 1.26–1.29 (m, 8H, EHO), 1.43–1.61 (m, 8H, EHO), 1.81–1.83 (m, 2H, EHO), 2.85–3.07 (m, 4H, CH_2), 3.63–3.77 (m, 4H, OCH_2), 6.62 (d, J = 8.3Hz, 2H, C_6H_4), 6.81–6.84 (m, 2H, C_6H_4), 7.20–7.25 (m, 2H, C_6H_4), 7.39–7.43 (m, 2H, C_6H_4); ^{13}C NMR (125 MHz,$CDCl_3$): ^{13}C NMR (125 MHz, $CDCl_3$) all signals represent C (C_{60}, sp^2) except as being noted. δ –0.33 ($SiCH_3$), 11.01–11.12 (EHO), 14.22–14.24 (EHO), 23.11–23.16 (EHO), 24.14–24.18 (EHO), 29.16–29.24 (EHO), 29.70–29.80 (EHO), 30.77–30.89 (EHO), 39.53–39.78 ($SiCH_2$), 57.31 (C_{60}, sp^3), 66.85 (C_{60}, pivot), 69.77 (OCH_2), 109.62 (C_6H_4), 120.25 (C_6H_4), 125.05, 127.70 (C_6H_4), 130.53 (C_6H_4), 131.72 (C_6H_4), 136.06, 136.10, 138.80, 139.89, 140.11, 142.14, 142.21, 142.23, 142.30, 143.22, 143.27, 143.31, 143.35, 143.37, 143.52, 143.65, 143.73, 143.86, 144.30, 144.34, 144.43, 144.52, 144.66, 144.74, 145.60, 145.64, 145.72, 145.75, 146.66, 146.86, 146.98, 147.03, 147.10, 147.16, 147.83, 147.97, 148.49, 148.88, 151.87, 151.96, 154.43, 159.54, 164.17 (C_6H_4). Elemental analysis: $C_{154}H_{58}O_2Si_2$▪$0.034CH_3OH$ calcd, C 91.12 %, H 3.25 % ; found, C 91.38 %, H 3.25 %.

6.7.2 Dynamic Light Scattering (DLS)

1,2-Dichrolobenzene (ODCB) solution of dimer **2** (3 mM and 3μM) was filtrated through a PTFE membrane filter (pore size is 0.2 μm). DLS machine was Zetasizer Nano ZS equipped with an He-Ne laser operating at 4 mW power of 633 nm wavelength, and a computer-controlled correlator, at a 173° accumulation angle by Malvern Corp., USA. Size measurement was carried out at 25 °C, 60 °C, 90 °C respectively in a quartz cuvette. The data were processed using dispersion technology

software version 5.10 to give Z-average particle size and polydispersity index (PDI) value by cumulant analysis, and particle size distribution through general analysis. 5 continuous measurements were executed to ensure reproducibility and stability of samples.

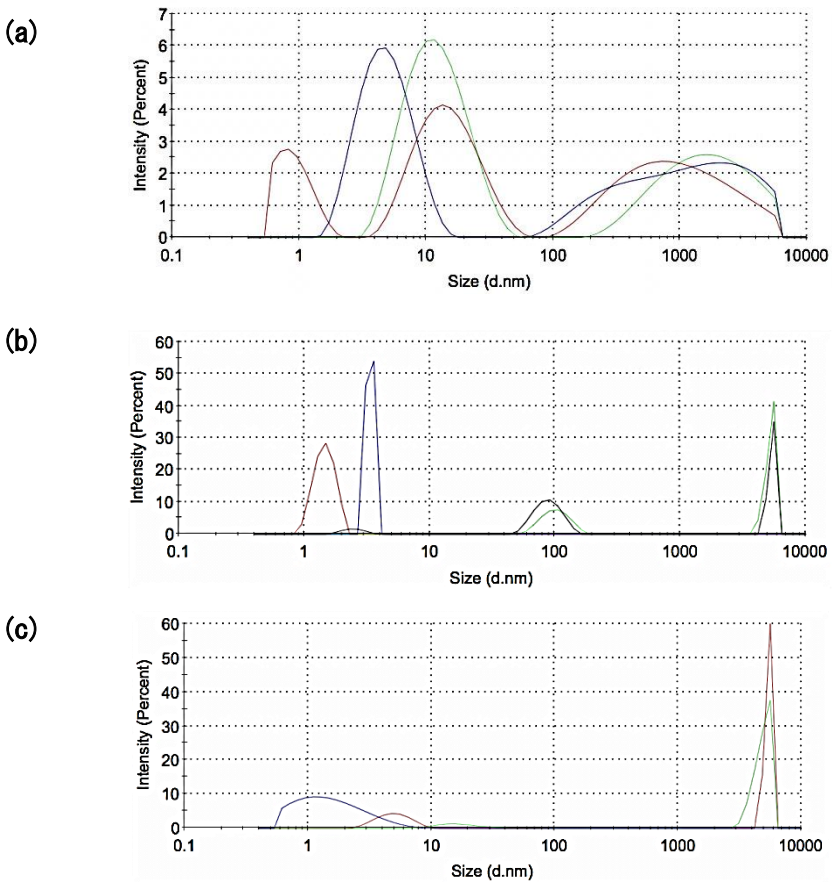

Figure 8. DLS profile of dimer **2** in ODCB solution. (a) 3mM solution at 25 ºC, (b) 3μM solution at 25 ºC, (c) 3μM solution at 90 ºC

6.7.3 Cyclic Voltammetry

Cyclic voltammetry (CV) was performed using HOKUTO DENKO HZ-5000 voltammetric analyzer. A measurement was carried out in a one-compartment cell under Ar gas, equipped with a glassy-carbon working electrode, a platinum wire counter

electrode, and an Ag/Ag^+ reference electrode. The measurement was performed in 1,2-dichrolobenzene solution containing tetrabutylammonium perchlorate (0.1 M) as a supporting electrolyte at 25 ºC with a scan rate of 0.1 V/s. All potentials were corrected against Fc/Fc^+.

6.7.4 Differential Scanning Calorimetry (DSC)

Differential scanning calorimetry (DSC) was performed on a NETZSCH thermal analyzer (DSC 204/F1). Samples (~5 mg) were placed in aluminum pans and heated at 10 ºC/min, under N_2 gas.

6.7.5 Powder X-ray diffraction analysis

Powder X-ray diffraction study was carried out on a Rigaku R-AXIS RAPID II imaging plate diffractometer using Cu-Kα radiation. The measurement temperatures were varied using the temperature controller Rigaku CGD-4 under N_2 gas. Sample was obtained by reprecipitation of toluene solution of dimer **2** with MeOH. Sample was grinded down and packed into glass capillaries, and annealed for 1 hour at the target temperature before measurement.

6.7.6 Single-Crystal X-ray Structure

Table 3. Crystal and refinement data for **2**

Empirical formula	$[C_{60}(CH_2Si(CH_3)_2C_6H_4$-*o*-$OCH_2CH(C_2H_5)C_4H_9)]_2 \cdot 2CHCl_3$
Formula weight	2235.06
Temperature	153(2) K
Radiation	Cu$K\alpha$ (λ = 1.54180 Å)
Crystal system	Triclinic
Space group	*P*-1
Unit cell dimensions	a = 10.003 Å
	b = 15.818 Å
	c = 17.837Å
	α = 113.04 °
	β = 92.89°
	γ = 105.44°
V (Å^3)	2465.1
Z	1
Density ρ calc (g·cm^{-3})	1.522
Absorption coefficient (mm^{-1})	2.362
F(000)	1154
Crystal dimensions (mm^3)	0.3 · 0.1 · 0.1
range for data collection	3.19 ≤ θ≤ 68.23°
Index ranges	–12 ≤ h ≤ 12
	–18 ≤ k ≤ 19
	–21 ≤ l ≤ 21
Reflections collected / unique	29134 / 8808 (R_{int} = 0.1082)
Refinement method	Full-matrix least-squares on F^2
Data / restraints / parameters	8808 / 13 / 714
Goodness-of-fit on F^2	1.078
Final R indices [I>2σ(I)][a), b)]	R1 = 0.1366, wR2 = 0.3477
R indices (all data)[a), b)]	R1 = 0.2565, wR2 = 0.4407
Largest diff. peak and hole (e·Å^3)	0.591 / –0.409

[a)] $\Sigma(||Fo| - |Fc||)/\Sigma|Fo|$

[b)] $wR2 = [\Sigma\omega(|Fo^2| - |Fc^2|)^2 / \Sigma(\omega Fo^4)]^{1/2}$

6.7.7 ESR Study

In a measurement in solution, 4-hydroxy-2,2,6,6-tetramethylpiperidine 1-oxyl (TEMPOL) was added to a solution of dimer **2** in 1,2-dichrolobenzene(2.9×10^{-2} M) in a sample tube of an inner diameter of about 1mm. The sample was degassed by the Freeze and Thaw method, and sealed with dry nitrogen gas. The variable temperature measurement was performed from 293 K to 420 K with 10 K interval, and then cooled. This cycle was repeated for 2 times. In a measurement in solid, 12 mg of dimer **2** in a sample tube of an inner diameter of about 4.5mm was degassed and sealed with dry nitrogen gas. The variable temperature measurement was performed from 300 K to 440 K, and then cooled from 440 K to 300 K, with 20 K interval. This cycle was repeated for 3 times. Measurements were performed 10 minutes after reaching the desired temperature. All measurements were performed using JEOL FA300 ESR analyzer being equipped with the usual devices for temperature, microwave frequency, and magnetic field.

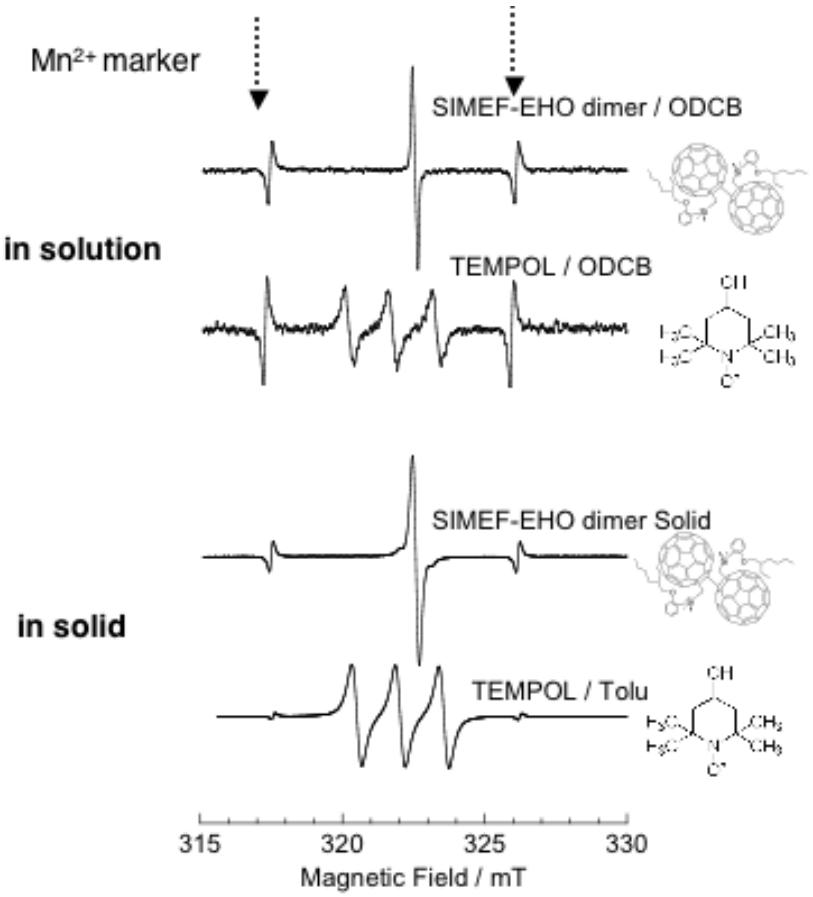

Figure 9. ESR spectra of the radical formed by the dissociation of dimer **2** in ODCB solution and in solid with the comparison of the signal intensity of the radical of TEMPOL as standard reagent. g = 2.0023 (in solution) and 2.0025 (in solid).

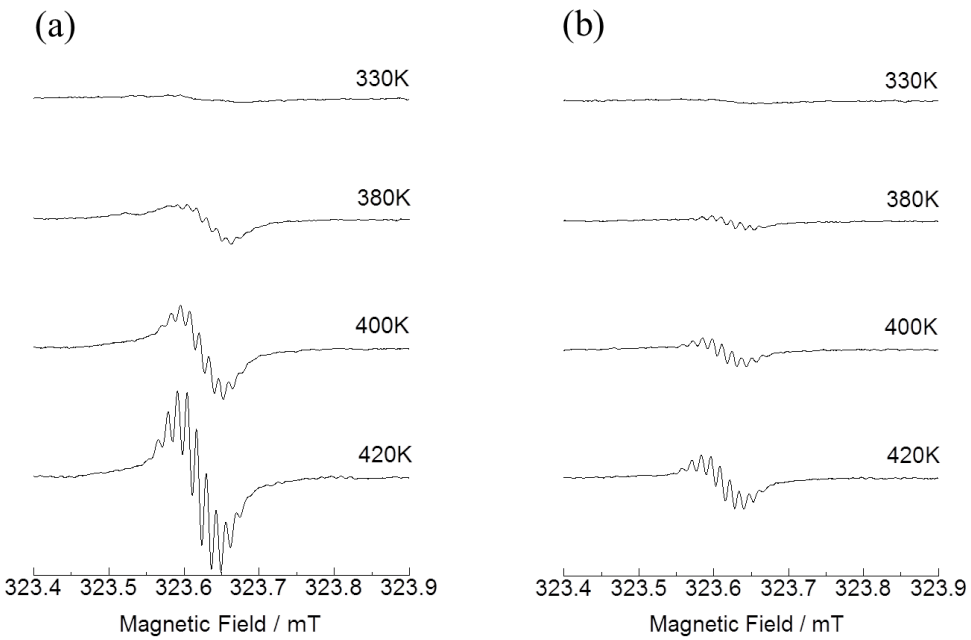

Figure 10. The set of ESR spectra of variable temperature measurement in solution. (a) 1st heating process. (b) 2nd heating process.

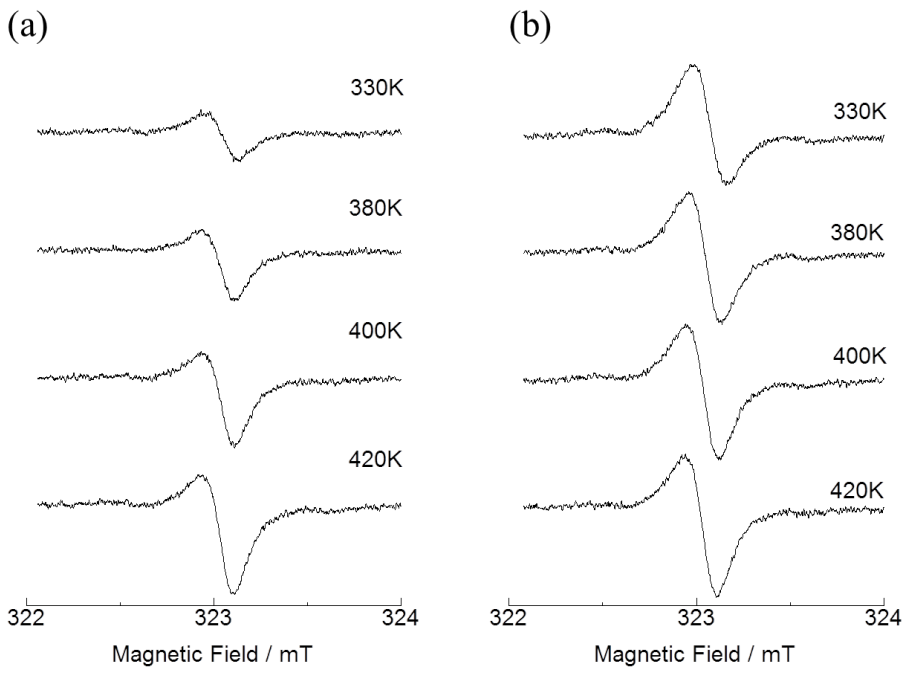

Figure 11. The set of ESR spectra of variable temperature measurement in solid. (a) 1st heating process. (b) 2nd heating process.

6.7.8 Organic Field Effect Transistor (OFET)

Fabrication of Field-Effect Transistors (FETs). Bottom-gate/bottom-contact FETs were fabricated. An n-doped Si substrate with 300 nm SiO_2 (capacitance C_i=11.5nF cm^{-2}) was used as gate electrode and gate dielectric layer, respectively. The source and drain electrode (Au/Cr) were prepared by photolithography. The channel width and length were 325 μm and 10 μm, respectively. The thin film was formed by drop-casting process with 0.25 wt% dimer **2** in CS_2. The electrical characteristics of the OFETs were measured by a Keithley 4200 SCS semiconductor parameter analyzer in vacuum chamber (<2Pa). The mobility of the OFETs in the saturation region was extracted from the following equation:

$$I_{DS}= (W/2L)\ \mu C_i(V_{GS}-V_{th})^2 \qquad (1)$$

where I_{DS} is the drain electrode collected current, V_{th} is the threshold voltage. The V_{th} of the device was determined by extrapolating the $(|I_{DS}|)1/2$ vs. V_{GS} plot to I_{DS} = 0.

Variable Temperature Measurement. A device fabricated in the same procedure as described above was placed in a micro chamber under N_2 gas. The temperature variable measurement was performed with heating at 20 °C/min from 30 °C to 200 °C under vacuum condition, and then cooled from 200 °C to 30 °C at the same rate as heating process. FET measurements were performed 5 minutes after reaching the desired temperature.

6.8 References and Notes

† This chapter is published on *J. Am. Chem. Soc.* in press [DOI:10.1021/ja500340f].

(1) (a) F. Cheng, Y. Murata, K. Komatsu, *Org. Lett.* **2002**, *4*, 2541. (b) G.-W. Wang, C.-Z. Wang, S.-E. Zhua, Y. Murata, *Chem. Commun.* **2011**, *47*, 6111.

(2) S. Lu, T. Jin, E. Kwon, M. Bao, Y. Yamamoto, *Angew. Chem. Int. Ed.* **2012**, *51*, 802.

(3) (a) J. R. Morton, K. F. Preston, P. J. Krusic, E. Wasserman, *J. Chem. Soc., Perkin Trans.2* **1992**, 1425. (b) J. R. Morton, K. F. Preston, P. J. Krusic, S. A. Hill, E. Wasserman, *J. Am. Chem. Soc.* **1992**, *114*, 5454. (c) P. J. Fagan, P. J. Krusic, C. N. McEwen, J. Lazar, D. H. Parker, N. Horrn, E. Wasserman, *Science* **1993**, *262*, 404.

(4) J. L. Segura, N. Martin, *Chem. Soc. Rev.* **2000**, *29*, 13.

(5) (a) D. V. Konarev, S. S. Khasanov, A. Otsuka, G. Saito, *J. Am. Chem. Soc.* **2002**, *124*, 8520. (b) Y. Matsuo, E. Nakamura, *J. Am. Chem. Soc.* **2005**, *127*, 8457.

(6) *Carbon Molecules and Materials*, Ralph Setton, Patrick Bernier, Serge Lefrant, Editors, Taylor & Francis, New York, 2002.

(7) C.-Z. Li, Y. Matsuo, E. Nakamura, *J. Am. Chem. Soc.* **2010**, *132*, 15514.

(8) (a) Y. Matsuo, A. Iwashita, Y. Abe, C. –Z. Li, K. Matsuo, M. Hashiguchi, E. Nakamura, *J. Am. Chem. Soc.* **2008**, *130*, 15429. (b) Y. Matsuo, Y. Sato, T. Niinomi, I. Soga, H. Tanaka, E. Nakamura, *J. Am. Chem. Soc.* **2009**, *131*, 16048. (c) H. Tanaka, Y. Abe, Y. Matsuo, J. Kawai, I. Soga, Y. Sato, E. Nakamura, *Adv. Mater.* **2012**, *24*, 3521. (d) Y. Matsuo, H. Oyama, I. Soga, T. Okamoto, H. Tanaka, A. Saeki, S. Seki, E. Nakamura, *Chem. Asian J.* **2013**, *8*, 121.

(9) Y. Matsuo, Y. Kuninobu, A. Muramatsu, M. Sawamura, E. Nakamura, *Organometallics* **2008**, *27*, 3403.

Chapter 7

Conclusion

This chapter described work on the development of new acceptor materials for organic thin film devices. First, I examined the crystal structures and thermotropic properties of three electron accepting silylmethyl[60]fullerene derivatives, as well as their photovoltaic performance in combination with a benzoporphyrin electron donor. Thermal annealing of a p-i-n organic photovoltaic device containing a crystalline benzoporphyrin donor and solvated crystals of a silylmethylfullerene acceptor increased device performance when applied at a temperature where partial desolvation of the acceptor occurred, in other words, where an "amorphous mesophase" and enhanced the PCE of the device.

Next, I investigated the complexation of a singly bonded fullerene dimer $[C_{60}(CH_2SiMe_2O^iPr)]_2$ and 1,8-diazabicyclo[5.4.0]undec-7-ene (DBU) in order to develop facile separation of a fullerene derivative from the mixture of fullerene and its derivatives without the use of time consuming and expensive chromatographic techniques. Addition of DBU to a 1,2,4-trimethylbenzene solution of C_{60} and $[C_{60}(CH_2SiMe_2O^iPr)]_2$ afforded complexation only with $[C_{60}(CH_2SiMe_2O^iPr)]_2$, leading to precipitation of the $[C_{60}(CH_2SiMe_2O^iPr)]_2$-DBU complex. Decomplexation with 1,2-dichlorobenzene gave $[C_{60}(CH_2SiMe_2O^iPr)]_2$ in 56% recovery. In addition, the $[C_{60}(CH_2SiMe_2O^iPr)]_2$-DBU complex could be used for the synthesis of dihydromethano[60]fullerene $C_{61}H_2$.

Further, I developed 56π-electron fullerene derivatives with electron-withdrawing cyano groups. I synthesized 56π-electron fullerene derivatives

with electron-withdrawing cyano groups by reaction of 58π-electron fullerenes with NaCN, followed by in situ treatment with TsCN or MeOTf. The fullerene derivatives have low-lying LUMO levels, which are comparable with or lower than that of pristine C_{60}. The derivatives were used as solution-processable electron acceptors in small-molecule organic solar cells that showed a maximum PCE of 2.0% (short-circuit current, 7.05 mA/cm^2; open-circuit voltage, 0.62 V; and fill factor = 0.45) using chloroindium phthalocyanine as electron donor. Also, 56π-electron fullerene derivatives possessing both a hydrogen and an electron-withdrawing cyano group were synthesized by reaction of 58π-electron fullerene with NaCN and subsequent protonation. The LUMO levels of these derivatives were found to be comparable to or slightly higher than those of 58π-electron fullerene derivatives such as PCBM. I tested the derivatives as acceptors in bulk heterojunction solar cells containing a low-bandgap polymer donor, and the device showed PCE of 5.2%.

Furthermore, to expand the variation of n-type organic materials for organic FETs, I efficiently synthesized a singly bonded fullerene dimer $[C_{60}R]_2$ (R = CH_2SiMe_2{C_6H_4(2-ethylhexyloxy)-2}) through high-yielding preparation of a silylmethyl fullerene ($C_{60}RH$) and oxidation of $C_{60}R^-$ with *N*-bromosuccinimide. I found a unique function where heating the fullerene dimer in the solid phase caused C–C bond cleavage and thus generated a long-lived fullerene radical pair. Upon cooling from 470 K, the solid underwent a rapid phase transition to generate a radical-containing solid that was more stable by only about 2 kcal/mol and had a lifetime of over 17 h. This phase change accompanied an abrupt increase of electron mobility by a factor of 10 to become 1.2×10^{-3} cm^2/Vs; the mobility remained in this range after repeated heating and cooling between 300 and 470 K.

In conclusion, I synthesized a variety of organic acceptor materials for organic thin film electronics and studied their function in devices. Unless development of donor and acceptor materials is done in tandem, the performance of organic thin film devices seems unlikely to surpass that of inorganic devices. I am confident that the performance of organic thin film devices will be further improved by expanding the variety of fullerene derivatives that function well as organic acceptor materials.

List of Publications

Chapter 2

(1) An Amorphous Mesophase Generated by Thermal Annealing for High-Performance Organic Photovoltaic Devices

H. Tanaka, Y. Abe, Y. Matsuo, J. Kawai, I. Soga, Y. Sato, E. Nakamura, *Adv. Mater.* **2012**, *24*, 3521.

Chapter 3

(2) 1,8-Diazabicycloundecene-mediated Separation of Singly bonded Fullerene Dimer and Application to Facile Preparation of $C_{61}H_2$

Y. Abe, Y. Matsuo, *Fullerenes, Nanotubes and Carbon Nanostructures* in press.

Chapter 4

(3) Low-LUMO 56π-Electron Fullerene Acceptors Bearing Electron-withdrawing Cyano Groups for Small-Molecule Organic Solar Cells

Y. Abe, T. Yokoyama, Y. Matsuo, *Org. Electron.* **2013**, *14*, 3306.

Chapter 5

(4) 56π-Electron Hydrofullerene Derivatives as Electron Acceptors for Organic Solar Cells

Y. Abe, R. Hata, Y. Matsuo, *Chem. Lett.* **2013**, *42*, 1525.

Chapter 6

(5) Mobility of Long-lived Fullerene Radical in Solid State and Nonlinear Temperature Dependence

Y. Abe, H. Tanaka, Y. Guo, Y. Matsuo, E. Nakamura, *J. Am. Chem. Soc.* in press [DOI:10.1021/ja500340f].

Acknowledgment

The studies presented in this thesis are the summaries of the author's work carried on during 2007-2009 at the University of Tokyo, and 2010 at Mitsubishi Chemical Corporation.

First the author would like to express her deepest gratitude to Professor Yutaka Matsuo for continuous guidance, hearty encouragement, informative suggestion and fruitful discussion during the course of this study.

The author wishes to express her sincerest gratitude to Professor Eiichi Nakamura for his continuous advice, exciting discussion and sincerely support throughout this work.

The author would like to express her deeply gratitude to Dr. Yoshiharu Sato, Mr. Takaaki Niinomi, Dr. Iwao Soga, Dr. Naoki Obata, and Mr. Masahiko Hashiguchi at Mitsubishi Chemical Corporation for helpful discussion and support.

The author would like to express her deep gratitude to Dr. Hideyuki Tanaka, Dr. Toshihiro Okamoto and Dr. Hiroshi Okada for helpful discussion and support.

The author would like to appreciate Professor Masahiro Ehara and Professor Michinori Suginome their kind support.

The author is grateful to Dr. Hayato Tsuji, Dr. Laurean Ilies, Dr. Koji Harano, and all members of Nakamura's and Matsuo's group for helpful suggestion and friendship. The author is also grateful to Mr. Hiroaki Yamaoka, Dr. Toshihiro Kobayashi, Dr. Junya Kawai, Dr. Takamichi Yokoyama, Ms. Rieko Hata, Ms. Misako Okabe, and all members of Photovoltaics Project at Mitsubishi Chemical Corporation. It is great

pleasure to thank Mr. Iwao Yamamoto, Dr. Hisao Urata, Dr. Masaru Utsunomiya, Mr. Kazuaki Kanno, Mr. Akira Ohno and Dr. Yoshimasa Sakai for fruitful suggestions and kind support.

Finally, the author would like to thank her parents, Hiroshi and Machiko, her grandmothers, Fusako and Tsuya, her sister, Motomi, and her brother-in-law, Masahiro, for their continuous understanding and indispensable support.

February 2014 Yoko Abe